COMPOSITE SKID LANDING GEAR DESIGN INVESTIGATION

A Thesis
Presented to
The Academic Faculty

by

Kshitij Shrotri

In Partial Fulfillment
of the Requirements for the Degree
Doctor of Philosophy in Aerospace Engineering

School of Aerospace Engineering
Georgia Institute of Technology
August 2008

COMPOSITE SKID LANDING GEAR DESIGN INVESTIGATION

Approved by:

Prof. Daniel Schrage, Advisor
School of Aerospace Engineering
Georgia Institute of Technology

Prof. Andrew Makeev
School of Aerospace Engineering
Georgia Institute of Technology

Prof. Olivier Bauchau
School of Aerospace Engineering
Georgia Institute of Technology

Mr. Robert Meissbach
Director of Engineering and Integration
MD Helicopter Inc, Mesa, AZ

Prof. Sathyanarayan Hanagud
School of Aerospace Engineering
Georgia Institute of Technology

Date Approved: April 2008

Dedicated to my parents

Dr. Nishikant Shrotri and Dr. Mrs. Aparna Shrotri

whose blessings, upbringing and prayers

brought me this far

TABLE OF CONTENTS

LIST OF TABLES

LIST OF FIGURES

LIST OF SYMBOLS AND ABBREVIATIONS

W_G	Rotorcraft Gross Weight
W_E	Rotorcraft Empty Weight
V_f	Fiber Volume Fraction
ρ	Density (kg/m^3)
h	Landing Gear drop height
d	Maximum center of gravity displacement during landing analyses
L	Ratio of assumed rotor lift to rotorcraft gross weight
n	limit inertia load factor
n_j	Load factor developed during impact on the mass used in the drop test
E_1	Young's Modulus along the longitudinal or fiber direction
E_2	Young's Modulus along the transverse or matrix direction
G_{12}	In-plane Shear Modulus
G_{13}	Out-of-plane Shear Modulus
G_{23}	Out-of-plane Shear Modulus
ν_{12}	In-plane Poisson's Ratio
θ	Fiber orientation angle
σ_{11}	Normal stress along the fiber/longitudinal direction
σ_{22}	Normal stress along the matrix/transverse direction
σ_{12}	In-plane Shear stress
ε_{11}	Normal strain along the fiber/longitudinal direction
ε_{22}	Normal strain along the matrix/transverse direction
γ_{12}	In-plane Shear strain

σ_{33}	Out-of-plane normal stress
τ_{13}	Out-of-plane transverse shear stress
τ_{23}	Out-of-plane transverse shear stress
S4R	Four node quadrilateral Shell element with reduced integration
S3R	Three node triangular Shell element with reduced integration
$\mu\varepsilon$	Microstrains (10^{-6} m)
NE11	ABAQUS Nominal Normal Strain along the fiber direction
NE22	ABAQUS Nominal Normal Strain along the matrix direction
NE12	ABAQUS In-plane Nominal Shear Strain
NE33	ABAQUS Nominal Normal Out-of-plane Strain
S11	ABAQUS Nominal Normal Stress along the fiber direction
S22	ABAQUS Nominal Normal Stress along the matrix direction
S33	ABAQUS Out-of-Plane Nominal Normal Stress
S12	ABAQUS In-Plane Nominal Shear Stress
TSHR13	ABAQUS Transverse Shear Stress
TSHR23	ABAQUS Transverse Shear Stress
X_T	Longitudinal Tensile Strength
X_C	Longitudinal Compressive Strength
Y_T	Transverse Tensile Strength
Y_C	Transverse Compressive Strength
S_L	In-Plane Shear Strength
G_{IC}	Mode I Fracture Toughness
G_{IIC}	Mode II Fracture Toughness
g	Ratio of the fracture toughness of modes I and II
τ_e	Effective Shear Stress defined with respect to the angle between the plane

	perpendicular to the laminate mid-plane and the fracture plane
m	Fiber misalignment angle
<x>	Macaulay Bracket operator such that x = (x + |x|)/2
η_L	Coefficient of Influence relating the in-plane shear strength to longitudinal compressive strength
R	ABAQUS Failure theory scalar parameter indicating failure when ≥ 1.0
TSAIW	Tsai-Wu Failure Criterion
ILSS	Inter-laminar shear strength
C3D8R	ABAQUS Continuum 3- D deformable eight node quadrilateral solid element
COH3D8	ABAQUS Cohesive 3- D deformable eight node quadrilateral solid element
MISESMAX	ABAQUS Equivalent Von Mises Stress output variable
S,MISES	ABAQUS Von Mises Stress Output Variable
MPC	Multi point constraint
σ^T_Y	Yield Stress in tension
σ^C_Y	Yield Stress in compression
MPa	Mega Pascal (10^6 N/m^2)
Δv	Change in velocity
GPa	Giga Pascal (10^9 N/m^2)
SEA	Specific Energy Absorption in kJ/kg
FAR	Federal Aviation Regulations
MIL STD	Military Standard
DGW	Design Gross Weight
KE	Kinetic Energy
Al 7075	Aluminum alloy
Ke49	Kevlar Aramid Fiber of 768 filament yarn

IM7	HexTow (HS-CP-6000) carbon fiber 6000 filament tow
AS4	HexTow AS4 carbon fiber 6000 filament tow
T700S	Torayca T700S carbon fiber
8552	HexPly 8552 amine cured, toughened epoxy resin
977-3	Cycom 350º F toughened epoxy resin
PEEK	Thermoplastic poly-ether-ether-ketone resin
E-Glass	Electrical glass fiber
S-Glass	Structural glass fiber
MMC	Metal Matrix Composite
MaDyAc	Multibody analysis tool developed by Politecnico di Milano
STA	Station Line
BL	Butt Line
WL	Water Line
ALLFD	ABAQUS All Friction Energy Dissipation History Output Variable
ALLPD	ABAQUS All Plastic Energy Dissipation History Output Variable
ALLDMD	ABAQUS All Damage Energy Dissipation History Output Variable
mil	thickness (1 mil = 0.01 inches = 0.0000254 m)
HSNMCCRT	ABAQUS Hashin Matrix Damage Initiation Criteria
CFAMC	Carbon Fiber Aluminum Matrix Composite

SUMMARY

A Composite Skid Landing Gear Design investigation has been conducted. Limit Drop Test as per Federal Aviation Regulations (FAR) Part 27.725 was simulated using ABAQUS^{TM} to evaluate performance of multiple composite fiber-matrix systems under limit loads. Load factor developed during multiple landing scenarios was computed and strength as well as stiffness based constraints were imposed. Generalized Tsai-Wu and LaRC04 physics and strength based failure criteria were used to evaluate designs. LaRC04 predicts that failures will be initiated as matrix cracking under compression and fiber kinking under in-plane shear and longitudinal compression.

Initial results indicate that an all composite skid landing gear may not be feasible due to strength concerns in the cross member bends. Hybridization of multiple composites with elasto-plastic aluminum 7075 showed proof of strength under limit loads. Laminate tailoring for load factor optimization under limit loads was done by parameterization of a single variable fiber orientation angle for multiple laminate families. Tsai-Wu failure criterion was used to impose strength constraints. A quasi-isotropic N = 4 (π/4) 48 ply IM7/8552 laminate was shown to be the optimal solution with a load factor under level landing condition equaling 4.17g's. All failures under limit loads being reported in the metal-composite hybrid joint region, the joint was simulated by adhesive bonding and filament winding, separately. Simply adhesive bonding the metal and composite regions does not meet strength requirements. A filament wound metal-composite beam shows the desired proof of strength. Filament wound metal-composite bolted to the metal cross members is the final joining methodology.

Finally, crash analysis was conducted as per requirements from MIL STD 1290A (AV). Crash at 42 ft/sec with 1 design gross weight (DGW) lift was simulated using ABAQUS. Plastic and friction energy dissipation in the reference aluminum skid landing gear was compared with plastic, friction and damage energy dissipation in the hybrid composite design. Damage in composites was modeled as progressive damage with Hashin's damage initiation criteria and an energy based damage evolution law. The latter meets requirements of aircraft kinetic energy dissipation up to 20 ft/sec (67.6 kJ) as per MIL STD 1290A (AV). Weight saving possibility of up to 49% over conventional metal skid landing gear is reported.

The final design recommended includes Ke49/PEEK skids, 48 ply IM7/8552 (or IM7/PEEK) cross member tapered beams and Al 7075 cross member bend radii, the latter bolted to the filament wound composite-metal tapered beam. Concerns in composite skid landing gear designs, testing requirements and future opportunities are addressed.

CHAPTER 1

INTRODUCTION

Rotary winged aircraft traditionally use one of two types of landing gear systems. The oleo-strut landing gear with wheels offers advantages of initial taxi and take-off run capability but at the cost of design complexity. Skid landing gears on the other hand offer simplicity in design and reduction in empty weight (W_E). Currently skid landing gears are manufactured from metal alloys such as Aluminum 7075. The elasto-plastic properties of such metals offer significant energy dissipation capabilities during plastic bending. FAR Part 27[1] regulations permit yielding of the landing gear under limit load conditions. When subjected to crash loads, metal plastically deforms, absorbing energy and allowing the fuselage underbelly to crash in a controlled crashworthy manner.

Reduction in gross weight (W_G) and empty weight (W_E) are two primary performance concerns for a designer. Light weight design, corrosion resistance concerns in metals, as well as fatigue performance can be adequately addressed with usage of composites. Composites offer other advantages such as increased Specific Energy Absorption (SEA) under crushing loads[2]. Literature search reveals that a composite skid landing gear design would be a novel idea. The first step in designing such a landing gear would require performance evaluation under limit loads as per FAR Part 27.725. Material selection, particularly for the composite fiber, will be necessary. Upon successful design under limit loads, crashworthiness will have to be addressed. Crash requirements as per MIL STD 1290A (AV)[3] will have to be met. This thesis outlines the objective, hypothesis, results of composite skid landing gear design feasibility, material selection followed by composite skid landing gear performance under limit loads, load factor optimization under limit loads, metal-composite hybrid joint and finally crash analysis.

- Chapter II elaborates on research motivation.

- Chapter III reports findings of the literature survey.
- Chapter IV defines the research objective, puts forth questions and describes the proposed methodology.
- Chapter V details the results of composite skid landing gear design feasibility, including material system evaluations and load factor computations.
- Chapter VI includes the final composite fiber selection followed by load factor optimization under limit loads and metal-composite joint analysis.
- Chapter VII discusses crashworthiness results.
- Chapter VIII outlines the future recommendations.

CHAPTER 2

MOTIVATION

2.1 Rotorcraft Design

A rotorcraft possesses the unique ability to efficiently hover. However, the complex nature of the rotor's oscillatory loads and vibration characteristics induced on each sub system make successful rotorcraft design a challenge to accomplish. Rotary winged aircraft are used extensively in both civil and military missions on a regular basis. One of the major challenges associated with the rotorcraft design process is minimizing the gross weight (W_G) and empty weight (W_E).

Rotorcraft have been extensively used in transportation of military personnel and attack missions, as well as civil training, transportation and rescue and reconnaissance missions. The one unique drawback of such an aircraft is the inability of the pilot and crew to eject with a parachute analogous to that from a fixed winged aircraft. While a rotorcraft does possess the equally unique ability to autorotate, autorotation is inevitably dangerous and dictated by pilot skill, split second decisions and importantly the height-velocity (H-V) bounds within which only can autorotation be successfully implemented.

Some helicopters are very unforgiving in the event of a pilot error and also do not autorotate well. Additionally, a tail rotor system strike resulting in loss of yaw control can cause it to crash if appropriate procedures are not correctly and immediately implemented. A number of accidents and hostile incidences in the Iraq war have proved this with respect to the UH-60 Black Hawk and CH-47 Chinook helicopters. It is therefore imperative that not only should a rotorcraft be crashworthy, but it should also have as low an empty weight (W_E) as possible in order to hover efficiently at higher altitudes and temperatures, as well as have increased performance during cruise. Thus, reduction in weight and crashworthiness are two major objectives for rotorcraft design.

2.2 Rotorcraft Sub-Systems

A rotorcraft consists of the following major sub-systems:

1. Fuselage
2. Transmission
3. Rotor Hub
4. Rotor Blades
5. Propulsion Systems (Main Engine, Auxiliary Engine)
6. Empennage (Horizontal and Vertical Stabilizers)
7. Tail Rotor
8. Landing Gear
9. Fuel Tanks

Each of these sub-systems account for a portion of the empty weight (W_E) and plays a distinct role in the performance of the rotorcraft. Figure 1 shows a typical rotorcraft with the sub-systems identified.

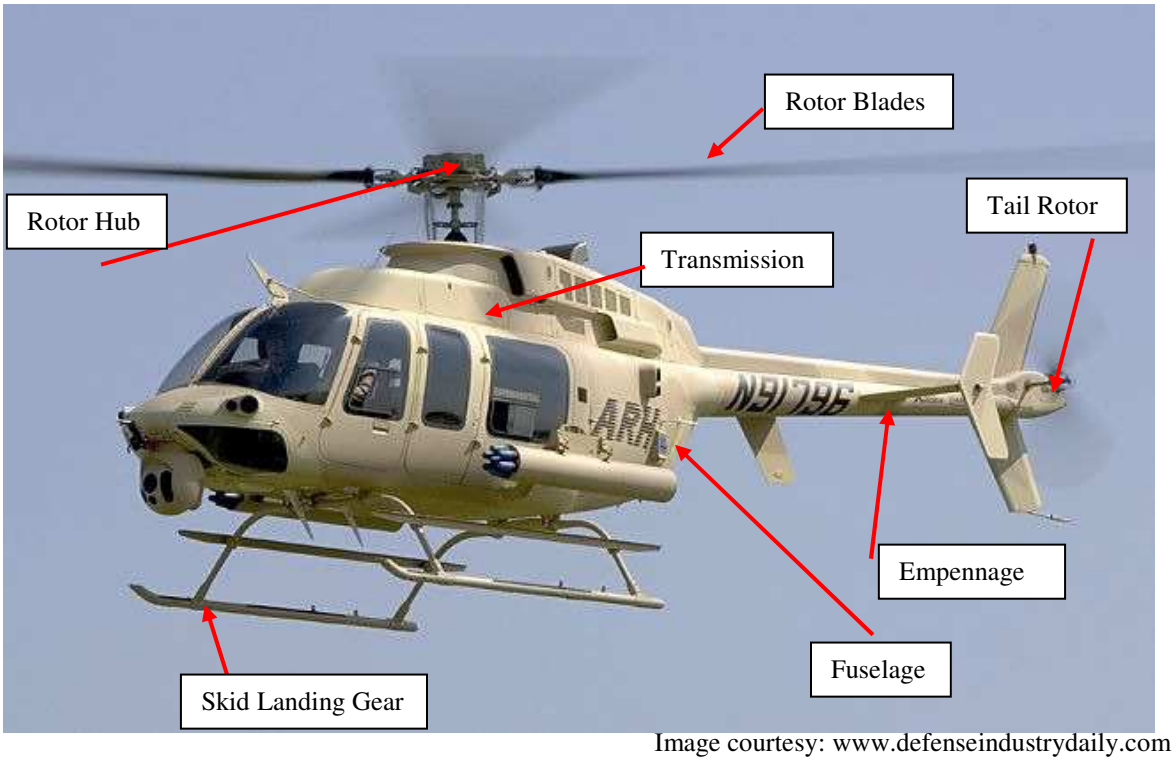

Image courtesy: www.defenseindustrydaily.com

Figure 1. Rotorcraft Sub-Systems

2.3 Rotorcraft Crashworthiness

Federal Aviation Regulations (FARs) require a rotorcraft to be designed for crash loads so as to protect the occupant from injury. Much research and technology development work has been done on crashworthiness of rotorcraft and has been focused on landing systems, fuselage and seats for the cabin and crew. The landing gear is the first sub-system that generally hits the impact surface. Hence, this sub-system is critically important for crashworthiness. Current crashworthiness requirements[3,44,45] state that the landing gear must dissipate kinetic energy of the entire aircraft which is equivalent to 20 ft/sec of crash velocity, with the vertical impact velocity being 42 ft/sec.

While significant amount of work has been done on crashworthy fuselage design by Cronkhite[5] et al, for both metal and composite designs, not much attention has been given to the possibility of using composite materials in the landing gear systems. Traditionally, two types of landing gear systems have been used. The wheeled landing gear allows for initial taxi and take-off run but with added design complexity and weight while a skid landing gear simplifies the design and reduces weight. The latter is very commonly used on Bell, Robinson, MD helicopters and Agusta Westland rotorcraft.

2.4 Skid Landing Gears

A typical skid landing gear is shown in Figure 2. The primary components of this landing gear are the two skid tubes and the two cross members on which the fuselage rests. Dampers on the landing gear are placed at appropriate locations to account for potential ground resonance instability issues. Wheels can be separately added on if desired. Currently, skid landing gears are fabricated from metal alloys such as Aluminum 7075. The motivation in this research lies in investigating if composite materials can be used for skid landing gear design.

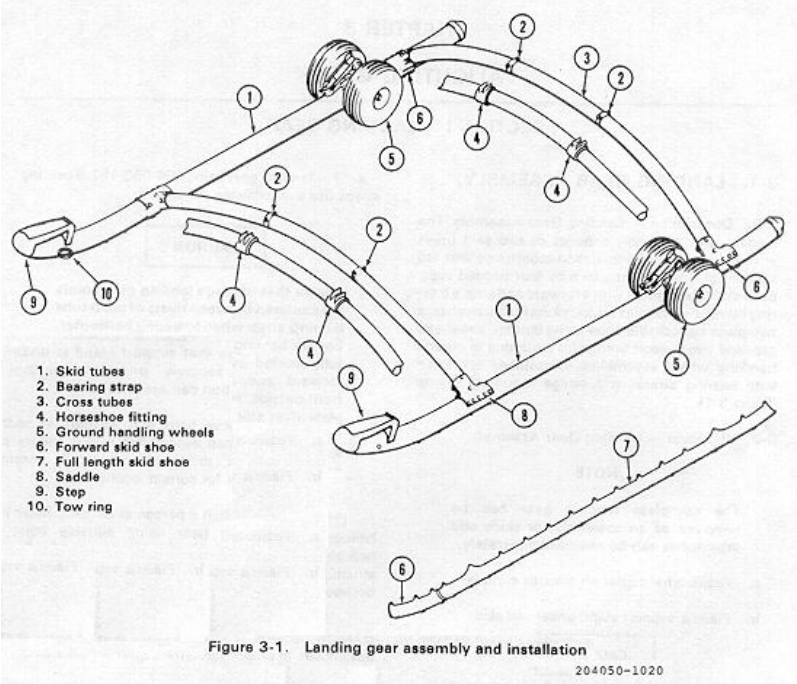

HTTP://INCOLOR.INEBRASKA.COM

Figure 2. Typical Skid Landing Gear

2.5 Motivation

The practical motivation comes from the possibility of being able to use light weight composite materials for fabrication of part or all of the skid landing gear. If this were to be successful, a significant amount of weight savings could be obtained, thus reducing the empty weight (W_E). In addition, a successful design under limit load conditions, as is required by FAR Part 27.725, would provide motivation for further research in making it a crashworthy design. Composite columns and tubes, if triggered to crush under compressive loads, can dissipate high amounts of energy and enhance Specific Energy Absorption (SEA). As quoted by Mamalis[2], SEA as high as 180 kJ/kg can be obtained by crushing some composite columns. Hence, it is desired to investigate the usage of composite materials in skid landing gear design and serves as a motivation for research that could lead to weight reduction, better performance and possibly crashworthy design.

CHAPTER 3

LITERATURE SURVEY

3.1 Composite Structures in Rotorcraft Design

Composite structures offer very high performance capabilities at reduced weights. They are also excellent in fatigue performance and do not have the same concerns associated with corrosion which metals have. Cronkhite[5] has shown that composite fuselages can be designed and fabricated for crashworthiness. Carbon Fiber Reinforced Polymer (CFRP) composites and NOMEX honeycomb structures have been used for the composite fuselage as well as outer protective shell. Fasanella[6] et al have shown that a concept for a fuselage with an external and internal composite shell and composite floor, all with foam sandwiched in between the outer and inner composite shells, shows no damage in terms of sub-floor crushing but causes significant damage to the outer skin. Figure 3 shows the concept that they have developed. While research continues on crashworthy fuselage designs using composites, such as for the V22-Osprey tilt rotor aircraft, industries are already using composites in their fuselage designs.

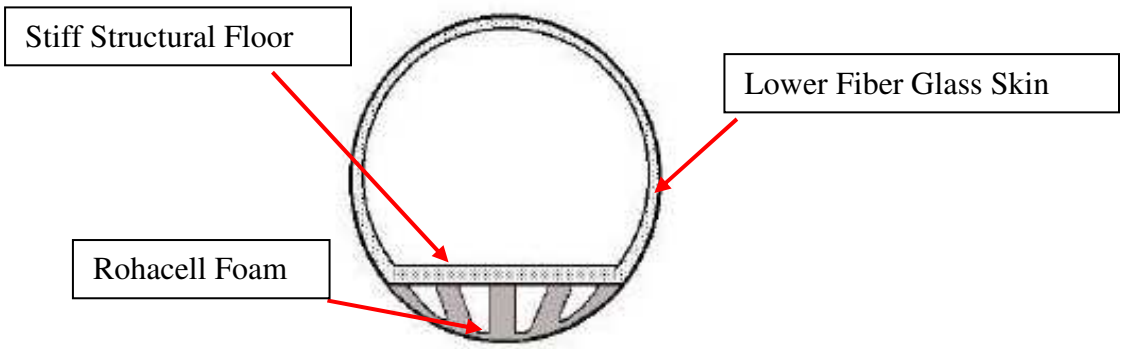

Figure 3. Energy Absorbing Composite Fuselage Design

Composite materials have also been used significantly in rotor blades since the 1970s. Aeroelastic tailoring of rotor blades is an active area of research. The Longbow helicopter currently uses an advanced metallic blade and has tested an advanced composite rotor blade. Materials such as glass/epoxy and carbon or graphite fiber and epoxy resin for spars, Kevlar/epoxy for skins and Nomex honeycomb as a filler material for sandwich construction are being used consistently. Figure 4 below shows a cross section of a rotor blade used by the Istanbul Technical University (ITU) Light Combat Helicopter (LCH) project. Composites are also being used in the empennage tail boom, vertical and horizontal stabilizer sections and other regions of the rotorcraft.

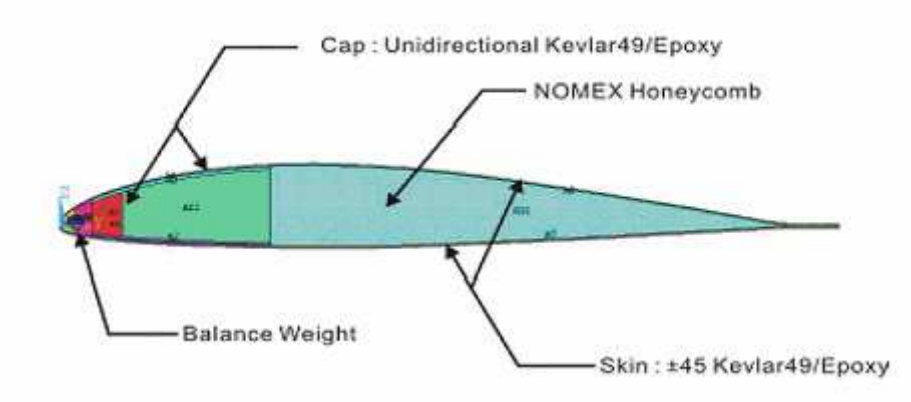

Figure 4. Composite Rotor Blade Airfoil Section

3.2 Landing Gear Designs

Typically, one of two types of landing gear systems is used on rotorcraft. The wheeled type of landing gear is complex and heavy. The design features include, tires, wheels, braking devices, oleo struts and other hydraulic equipment. Energy absorption takes place through brakes and shock absorbers. These types of landing gears also have to accommodate retracting mechanisms which further complicate the design. Macy[7] et al have shown that a titanium metal matrix composite (MMC) is a possible landing gear material for portions of the landing gear. The other type used commonly is the skid landing gear, which was shown earlier in Figure 2. Literature survey has revealed that

there has been no work done on skid landing gear design that is fabricated in part or whole using composite materials.

Skid landing gears have a unique way of being crashworthy. The metal alloys that are used for the skids and cross members exhibit elasto-plastic stress-strain behavior. FAR Part 27 permits yielding of the landing gear when subjected to limit loads. The design accommodates large strain producing ability. The skids slide, and also plastically deform, on the ground while the cross member radii bends undergo plastic deformation. This results in significant energy dissipation and thus reduces the velocities of impact on the fuselage underbelly from 42 ft/sec to approximately 30-35 ft/sec.

Several designs for skid landing gear cross members have been researched. The cross member horizontal beam regions generally incorporate a taper to enhance performance during bending. Some designs incorporate I-beam sections within the components while some incorporate rectangular cross sections for the cross member beams. A standard methodology for skid landing gear design has been established based on FAR Part 27. While sizing varies from design to design as per the requirements, performance in certain landing scenarios, such as rolled attitude landing, are required in all cases to design a skid landing gear.

3.3 Skid Landing Gear Design Optimization

Airoldi and Janszen[8] and Caprile et al[9] have conducted multi-body analyses on skid landing gear design and performance using MaDyAc. Further analysis and optimization of the skid landing gear design using multi-body analysis and genetic algorithm was done by Airoldi and Lanzi[10,11,12]. The optimization methodology involved optimizing the load factor developed during limit loads under multiple landing scenarios. The objective function was either the load factor or the gradient of the bending strain in the cross member beams, which was minimized. Cozzone's[13] plasticity model was incorporated in the analysis. The metal skid landing gear was fabricated from Aluminum

7075. This work provides a methodology for optimizing and simultaneously analyzing metal skid landing gears.

However, no such work has been done on skid landing gears using composite materials. Literature search revealed no documented work on a composite skid landing gear in the public domain. Thus, though literature survey revealed a lot for composite materials, composite material failure criteria and composite structures in rotorcraft designs, none of the work was pertinent to skid landing gears. Thus, it is perceived that composite skid landing gear design research would be a novel idea.

3.4 Composite Failure Criteria

The major difference between composite materials and metals lies in the inherent anisotropy in the former. As a result, the failure modes and criteria are still not well understood and established. There are scores of failure theories that have been tested, modeled and developed, which are specific to either the type of composite material, the type of loading conditions, the stacking sequence or the thickness of the laminate. Failure theories are classified into two types, namely those which distinguish the failure mode and those which do not. Some commonly used theories are Maximum stress/strain theories, Tsai-Wu[13], Hill[14], Hashin-Rotem[15], Hashin[16], Hoffman[17], Puck[18], Christensen[19], Yeh-Stratton[20], Chang-Lessard[21], Tsai-Azzi[22] and Davila-Camanho[23] criteria.

Appropriate failure criteria will need to be either established based on testing or selected based on previous work or other reasons, such as physics based fracture prediction. Literature survey indicates that these failure criteria consider failure modes such as fiber/matrix tensile failure, matrix cracking under compression, fiber kinks and buckling under compression, fiber/matrix shear failure and delamination due to inter-laminar stresses. After establishing the same, the skid landing gear will have to demonstrate proof of strength under limit loads and crashworthiness during crash.

CHAPTER 4

QUESTIONS, HYPOTHESES AND PROPOSED METHODOLOGY

Previous sections detailed motivation for research and literature survey pertinent to the topic in question. While there are reasons for which composite materials may not have been used thus far in skid landing gear designs, many questions remain unanswered. Some of these questions were answered based on hypotheses and some based on preliminary and/or final results.

4.1 Hypotheses

i) ***An all composite and/or hybrid metal-composite skid landing gear can be designed for sufficient stiffness to sustain large deformations without critical structural damage, and with acceptable load factors, under limit load conditions.***

ii) ***Given that the above hypothesis is accurate, it would be worthwhile to explore crashworthiness, such as by allowing progressive damage or triggering crush in composite regions for crashworthiness enhancement, during crash landing.***

4.2 Research Objective

The research objective is to conduct a composite skid landing gear design investigation.

The following concerns will have to be resolved for a feasible and successful design.

Limit Load Performance

Federal Aviation Regulation (FAR) Part 27.725 quotes the following:

The limit drop test must be conducted as follows:

(a) The drop height must be --

(1) 13 inches from the lowest point of the landing gear to the ground; or

(2) Any lesser height, not less than eight inches, resulting in a drop contact velocity equal to the greatest probable sinking speed likely to occur at ground contact in normal power-off landings.

(b) If considered, the rotor lift specified in § 27.473(a) must be introduced into the drop test by appropriate energy absorbing devices or by the use of an effective mass.

(c) Each landing gear unit must be tested in the attitude simulating the landing condition that is most critical from the standpoint of the energy to be absorbed by it.

(d) When an effective mass is used in showing compliance with paragraph (b) of this section, the following formula may be used instead of more rational computations:

$$W_e = W \times \frac{h + (1 - L)d}{h + d} \tag{1}$$

$$n = (n_j \times \frac{W_e}{W}) + L \tag{2}$$

where: W_e=the effective weight to be used in the drop test (lbs.);

W= W_M for main gear units (lbs.), equal to the static reaction on the particular unit with the rotorcraft in the most critical attitude. A rational method may be used in computing a main gear static reaction, taking into consideration the moment arm between the main wheel reaction and the rotorcraft center of gravity.

W= W_N for nose gear units (lbs.), equal to the vertical component of the static reaction that would exist at the nose wheel, assuming that the mass of the rotorcraft acts at the center of gravity and exerts a force of 1.0 g downward and 0.25 g forward.

W= W_T for tail wheel units (lbs.), equal to whichever of the following is critical:

(1) The static weight on the tail wheel with the rotorcraft resting on all wheels; or

(2) The vertical component of the ground reaction that would occur at the tail wheel, assuming that the mass of the rotorcraft acts at the center of gravity and exerts a force of 1 g downward with the rotorcraft in the maximum nose-up attitude considered in the nose-up landing conditions.

h = specified free drop height (inches).

L = ratio of assumed rotor lift to the rotorcraft weight.

n = limit inertia load factor.

n_j = the load factor developed, during impact, on the mass used in the drop test (i.e., the acceleration dv/dt in g 's recorded in the drop test plus 1.0)

Note: d = maximum center of gravity displacement during Landing analysis as reported by Tho[24] et al.

The composite skid landing gear will have to produce load factors which are acceptable and also maintain structural integrity during limit drop tests. Composite materials typically do not yield. Hence, first ply failure and gross damage are of concern. The latter should not occur and the former should be manageable. Multiple landing scenarios are of concern. However, Airoldi and Janszen[8] and Tho[24] et al have shown that typically three landing scenarios, namely, level landing, level landing with drag (run-on) condition and rolled attitude landing, are critical for limit load design. MIL STD 1290A (AV)[3] further details a pitch-roll envelope as discussed in Chapter VIII on Crashworthiness, every maneuver within which must meet crash requirements. Thus, desirable or acceptable load factors must be obtained for a successful hypothesis.

Structural Strength

Under limit loads, metal alloy skid landing gears are permitted to yield as per FAR Part 27. However, composites typically do not yield. Hence, adequate strength must be displayed during all drop scenarios. Suitable failure theory would have to be established. Maximum strain theory is a widely accepted theory for design and is

commonly used for composite structures. Initially, it was thought that maximum strain theory would be suitable for the design. However, results in Chapter V show that strength criteria predict very less failures. Without experimental testing, as the failure mechanism will not be certain, considering the complexity and general nature of this problem, Tsai-Wu[13] generalized theory for anisotropic materials was considered as most suitable for failure identification. However, the fracture modes are not predicted by Tsai-Wu criterion. Hence, LaRC04[25] criteria published by Davila and Camanho in 2006, was considered in addition to Tsai-Wu criterion for fracture mode prediction.

Weight Saving

The composite and/or hybrid metal-composite design should result in sufficient weight savings. This is imperative as, if weight saving is negligible and crashworthiness were to prove to be just equal or marginally better than the metal skid landing gear, then a composite skid landing gear design would not be worthwhile.

Crashworthiness

Finally, the last concern is crashworthiness. Fleming and Vizzini[26] report that composite columns under off-axis loads greater than 10º do not exhibit favorable Specific Energy Absorption (SEA). Thus, attention would need to be given to the cross member inclined beams, which are typically greater than 45º to the vertical. While crashworthiness is necessary for any skid landing gear design, successfully meeting proof of strength requirements and acceptable load factors under limit loads is a prerequisite. Crash requirements from MIL STD 1290A $(AV)^3$ will have to be met and are addressed in subsequent chapters.

4.3 Research Questions

i) Would it be possible to have a laminate with a thickness which is the equivalent of a ¼" aluminum wall thickness and which results in satisfactory performance under limit loads?

Answer: Results from dynamic explicit FEA show this to be feasible. However, failure stresses and strains are observed in the cross member radii bends.

ii) Would the above be feasible, if so better or not, with hybrid metal-composite skid landing gears?

Answer: It is feasible. Hybrid metal-composite design would be most desirable.

iii) Would it be possible to locally stiffen the cross member beams by ply drop methodology to decrease the strains in these localized regions?

Answer: Local stiffening is generally possible by reinforcements. However, any stiffening effect could also adversely affect the load factor being produced.

iv) Would fabricating the radius bends of the cross members out of an elasto-plastic metal alloy result in sufficient strain relief along the cross member beams?

Answer: Results from Chapters V, VI and VII show this to be true and it is most desirable from the crashworthiness perspective as well.

v) Would optimization of volume fraction of metal and composite be useful?

Answer: Results in Chapter V show that hybridization benefits are region based and not volume fraction based.

vi) Would the first-ply failures result in damage which, though not a complete structural collapse could be of concern (example: excessive delamination)?

Answer: While this would be best answered by mechanical testing, computational analysis shows that gross damage does not necessarily occur.

vii) Would it be possible to trigger crushing mechanism in the composite beam region of the cross member, should the connecting radii bends be fabricated from metal? If not, are there other ways to make the design crashworthy?

Answer: Triggering crush needs to be addressed experimentally. Modeling progressive damage in composites shows damage dissipation energy, which when combined with plastic dissipation of metal and friction dissipation, meets crashworthiness requirements. However, only damage dissipation energy is not sufficient.

viii) Would optimization of the composite lay-up help in maintaining the load factor to less than 4g's and yet have a wall thickness equivalent to ¼"?

Answer: It is possible to reduce the load factor significantly by laminate tailoring, and is discussed in Chapter VI. However, metal-composite joining in the cross members, size of the metal cross member bend radii and material non-linearity play a more significant role in load factor reduction than fiber orientation.

ix) What failure criteria should be used?

Answer: LaRC04 physics-based criteria for limit loads and point stress failure criterion for ultimate loads would be appropriate. Generalized anisotropic Tsai-Wu failure criterion is suitable for initial design, but could be more conservative, compared to LaRC04. Hashin's criteria can be used for progressive damage modeling, which includes the necessary fracture mechanisms similar to LaRC04.

4.4 Methodology

The methodology was based on extensive computational modeling, simulation and analysis using ABAQUS^{TM} FEA and supported by experimental test data for the failure criteria for composites. Figure 5 shows a flow chart of the proposed methodology. Rotorcraft Identification, Material Comparison and Selection, Laminate Tailoring for

Load factor optimization under Limit loads, metal-composite joining and crash analysis would be the key elements of the design process. Limit load design and optimization of load factor under limit loads was the initial focus. Crashworthiness has been addressed based on progressive damage modeling in composites and energy dissipation.

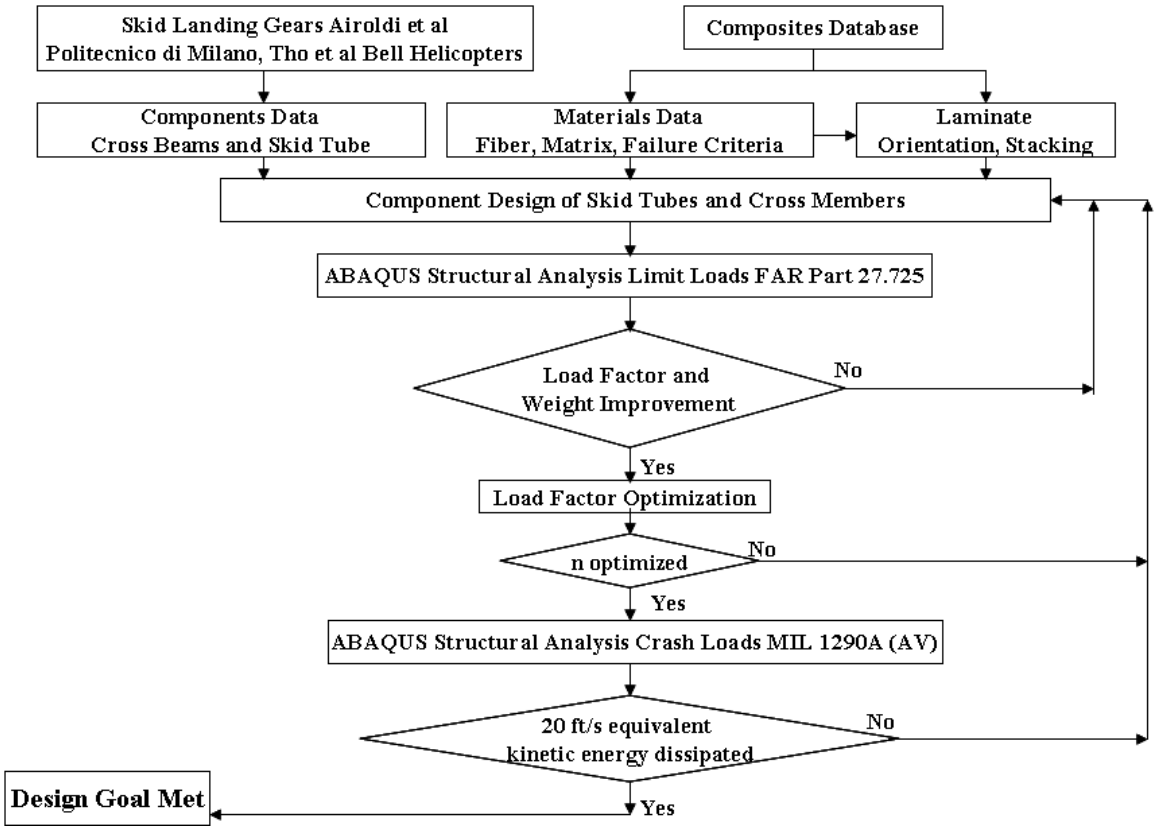

Figure 5. Research Proposed Methodology

CHAPTER 5

COMPOSTE SKID LANDING GEAR DESIGN FEASIBILITY

5.1 Rotorcraft Identification

The design process began with an identified rotorcraft configuration with available specifications from NASA TM 84281[27]. An AH-1S Cobra Helicopter was used for the analysis. Skid landing gear dimensions were based off partially available data for the AH-1S Cobra and the dimensions listed in the work done by Airoldi and Janszen[8] and Monterrubio and Scharf[28]. The landing gear was modeled in ABAQUS™ and dynamic explicit FEA was conducted under limit loads first. Table 1 lists helicopter specifications.

Table 1. AH-1S Cobra Specifications

Design Parameter	Metric value
Rotorcraft Mass	3636.36 kg
Fuselage Rolling Inertia (I_{xx})	3660.7 kg-m^2
Fuselage Pitching Inertia (I_{zz})	17354 kg-m^2
Fuselage Yawing Inertia (I_{yy})	14643 kg-m^2
Landing Gear Damper Coefficient	60 N-m-s**
CG STA location	0.770 m from rear cross member*
CG BL location	0 mm
CG WL location	1854.2 mm

* Dimension based off Airoldi and Janszen's[8] work due to lack of available data.

** Landing Gear Damper Coefficient taken from Monterubbio and Scharf's[28] work.

5.2 Material Selection

Al 7075 has been used for the reference landing gear for comparison of results. 7 fibers and 2 matrix systems were initially considered for comparison of load factors and strain limits. Fiber properties[29,30,31,32] are shown in Table 2. 8552 356º F epoxy resin matrix properties are also included in the table, as it was used in the later stage of the analysis

which is discussed in subsequent chapters. S-Glass, E-Glass and Boron were eliminated due to densities similar to Al, which hinder weight saving. Elastic properties for unidirectional lamina have been calculated in Matlab© V 7.0 using rule of mixtures. All fibers are transversely isotropic and matrices are isotropic. Table 3 lists the fiber and matrix properties[29,30,31,32,33]. Table 4 lists comparison of IM7/977-3 lamina properties with experimental results for a 65% fiber volume fraction laminate published by Kulkarni[34] in his Master's thesis. Results match within 13% for all moduli values. Table 5 lists lamina properties for all the composites. An N = 4 (π/4) 48-ply quasi-isotropic $[(45/-45/0/90)_6]_s$ laminate with ply thickness of 5 mils (0.127 mm) was used. Equivalent laminate properties were computed using Matlab© V 7.0 and are listed in Table 6. To eliminate testing of all materials, a simple linear spring-mass model was used for load factor comparison. The material with lowest stiffness has the lowest load factor. An energy based equation of equilibrium was written to compute load factors as a function of the equivalent spring stiffness. However, on conducting static analysis and computing the equivalent stiffness as the ratio of the reaction force to a prescribed unit displacement it was found that the equilibrium spring-mass model based on conservation of energy for the linear elastic case, did not capture the load factors accurately, though they were within ball park range of 3-4 g's. To impose a lower bound on stiffness, based on strains, static analysis was done. Ke49 fiber was eliminated due to low stiffness. Dynamic drop analysis was done for the remaining fibers and matrices. Thermoplastic PEEK and 977-3 epoxy resin (350º F cure) were used.

Table 2. Composite Fibers

Fiber	E (GPa)	ρ (kg/m^3)
E-Glass	77	2540
S-Glass	85	2480
AS4	231	1790
IM7	292	1790
T700S	230	1800
Boron	385	2650
Kevlar49	130	1450

Table 3. Fiber/Matrix and Al 7075 Properties

Fiber	**E_1**	**E_2**	**G_{12}**	**ν_{12}**	**ρ**
IM7	292	19.5	70	0.2	1790
AS4	231	14	14		1790
T700S	230	23.2*	95.8*		1800
Ke49	130	13*	13*		1450
Matrix	**E_1**	**E_2**	**G_{12}**	**ν_{12}**	**ρ**
977-3	3.45	3.45	1.23	0.32	1300
PEEK	4	4	1.42	0.4	1309
8552	4.67	4.67	1.73	0.35	1301
Metal	**E_1**	**E_2**	**G_{12}**	**ν_{12}**	**ρ**
Al 7075	72	72	27.03	0.33	2700

* approximated.IM7 fiber G_{23} = 5.74 GPa. All Moduli are in GPa and density in kg/m^3

Table 4. Rule of Mixtures Property Comparison

Property	IM7/977-3	Kulkarni's Thesis
E_1 (GPa)	191	180 (-6%)
E_2 (GPa)	9.5	9.7 (+1%)
ν_{12}	0.24	0.33 (+27%)
G_{12} (GPa)	5.3	6.1 (+13%)
ρ (kg/m^3)	1621.7	---

Table 5. Lamina Properties (65% V_f)

Laminate	E_1 (GPa)	E_2 (GPa)	G_{12} (GPa)	ν_{12}	ρ (kg/m^3)
IM7/977-3	191	9.5	5.3	0.24	1622
IM7/PEEK	191.2	10.7	5.76	0.25	1619
AS4/977-3	151.4	8.2	4.17	0.23	1622
AS4/PEEK	151.6	9.1	4.45	0.26	1619
T700S/977-3	150.7	10.2	5.40	0.23	1628
T700S/PEEK	150.9	11.1	6.21	0.23	1625
Ke49/977-3	85.7	7.9	4.09	0.23	1401
Ke49/PEEK	85.9	8.7	4.36	0.26	1398

Table 6. Equivalent Laminate Properties

Laminate	Equivalent Laminate Property		
	E (GPa)	G (GPa)	ν_{12}
IM7/977-3	71.177	27.213	0.3078
IM7/PEEK	72.022	27.53	0.3079
AS4/977-3	56.587	21.611	0.3092
AS4/PEEK	57.183	21.809	0.311
T700S/977-3	58.037	22.295	0.3016
T700S/PEEK	59.086	22.796	0.2960
Ke49/977-3	35.086	13.529	0.2937
Ke49/PEEK	34.519	13.342	0.2937

Aluminum 7075 with a piece-wise elasto-plastic stress strain law was modeled for the reference skid landing gear and for the metal regions in the hybrid configurations. The true stress-logarithmic strain data is shown in Table 7 and was taken from Dowling's[35] textbook. Aluminum elastic properties are listed in Table 3 along with the unidirectional composite lamina properties.

Table 7. Aluminum 7075 Elasto-Plastic Stress-Strain Law

True Stress (σ) MPa	True Strain (ε)
326	0
417.5	0.00603
476.325	0.007
509.02	0.007938
532.02	0.009485
548.55	0.012017

5.3 Finite Element Analysis

Dynamic Explicit FEA was conducted using ABAQUS/EXPLICIT V 6.7-1. The skid tubes and cross members were modeled using S4R shell elements. The fuselage is represented by a rigid reference node with prescribed mass and inertia properties as listed in Table 1. Rigid beam connectors connect the fuselage at two locations on both cross members. Two dampers have been modeled on the rear cross member. A single R3D4

Discrete Rigid Element with a central reference node, whose translational and rotational degrees of freedom are fully constrained using the Encastre boundary condition, represents the ground. Master-Slave contact has been specified with the ground as the Master surface and the skid landing gear as the contacting Slave surface. Penalty Contact friction algorithm has been prescribed with a coefficient of friction of 0.35. A piece-wise elasto-plastic[36] stress-strain law for Al 7075 with yield at 326 MPa and 1.2% plastic strain at 542 MPa was modeled. 1g load was applied. Total step time varied from 0.6-1 s.

Landing analysis was first conducted by introducing rotor lift equaling 2/3rd of the helicopter gross weight (W_G). Vertical CG displacements of the fuselage CG after impact computed from ABAQUS (shown in displacement plots ahead) were used for equivalent drop weight (W_e) calculation. A single ply laminate with equivalent properties as listed in Table 6 was used for these analyses to reduce computational time. CG displacement depends on the drop mass and the landing gear stiffness. Hence an equivalent stiffness approach was considered satisfactory. Drop test analysis was conducted by prescribing only 1g gravity load. CG maximum vertical acceleration developed at the fuselage CG after impact was computed and used in load factor calculation. Maximum bending strains were observed in the cross member tapered sections. Hence, only these critical regions were modeled with 48 plies. The remaining structure was modeled with a single ply laminate or aluminum as per the configuration. Figure 6 depicts the mesh (3538 shell elements). All shells were modeled as mid-plane surfaces. Composite lay-up was modeled as a conventional shell with local cylindrical co-ordinates. Table 8 and Table 9 show typical allowable strains and stresses. Typical tensile and compressive allowable for σ_{11} and a range of absolute values for the remaining stresses, was considered.

Table 8. Typical Laminate Strain Allowable

Fiber Angle	Strains (10^6 με)			
	ε_{11}	ε_{22}	ε_{33}	γ_{12}
0^o	14	8	15	12
90^o	10	8	15	12
+/-45^o	6	8	15	12

Table 9. Typical Laminate Stress Allowable

Fiber Angle	Stresses (MPa)			
	$\sigma_{11}^{T/C}$	σ_{22}	σ_{33}	σ_{12}
All	2200 /1500	80 /135	80 /135	100 /150

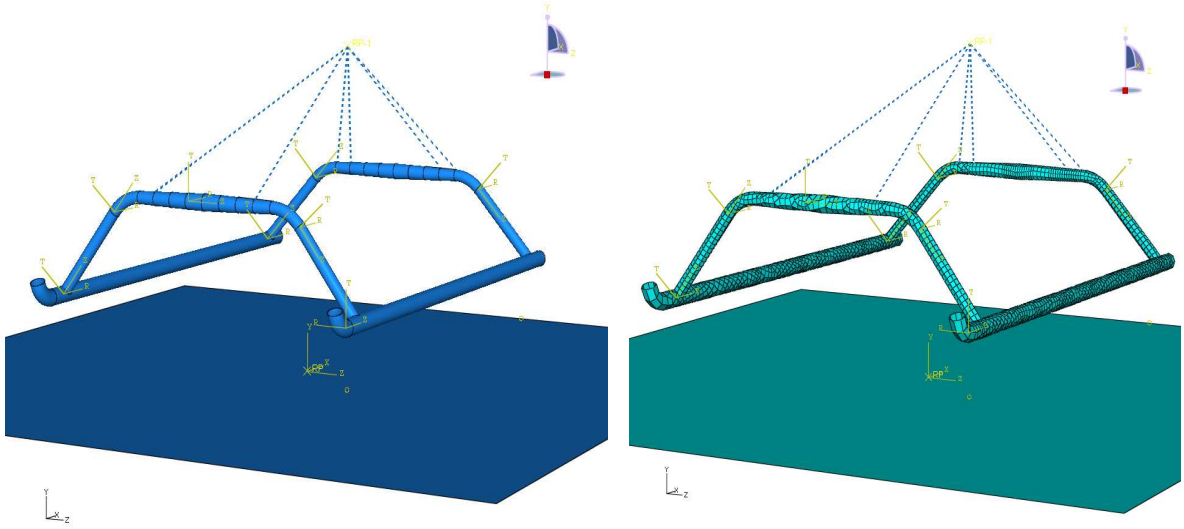

(a) FE Model **b) FE Mesh**

Figure 6. ABAQUS FE Modeling

5.4 Maximum Stress and Strain Theories

Maximum strain theory was used initially to evaluate the strains in the individual plies, along the fiber directions, in the critical cross member beam regions. Allowable strains were considered to be within the allowable values shown in Table 8. Analyses, as depicted in figures ahead, showed that strength based failure criteria predict much lower failures and maximum strain theory may be very conservative.

5.5 Design Feasibility Results

Level Landing – Aluminum Skid Landing Gear

Figure 7 shows CG displacement and acceleration plots during landing and drop analyses. The point of minima on the displacement plots indicates the commencement of the landing gear rebound. Load factor is 3.59, which agrees with typical published load factors. Figure 8 shows maximum Mises stress as 548 MPa, less than UTS of 571 MPa.

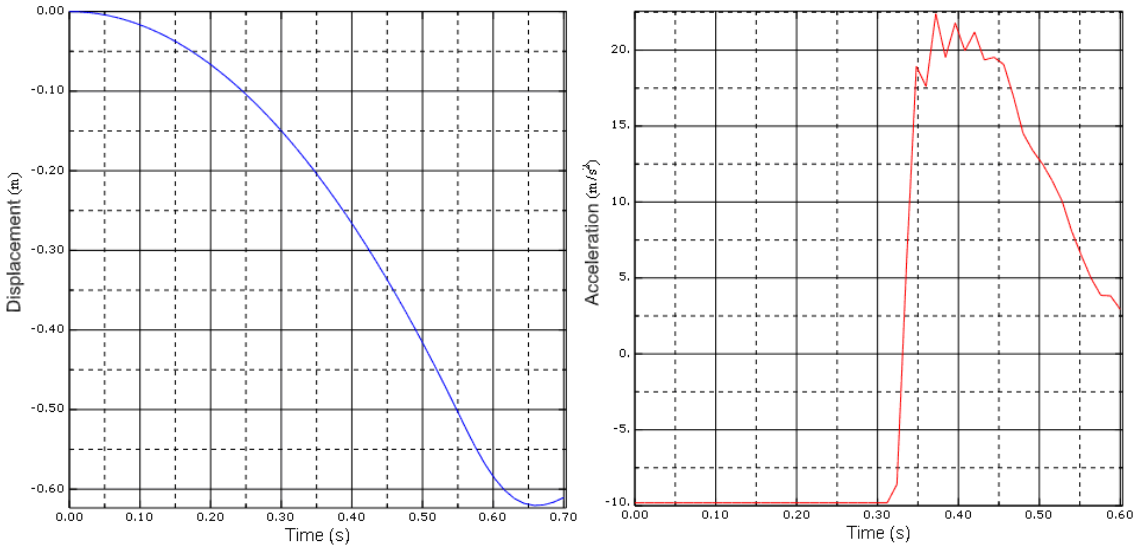

Figure 7. CG Vertical Displacement and Acceleration -Al 7075

Sample Load Factor Computation

Maximum CG displacement from landing analysis: **611.38 – 508 = 103.38 mm**

Equivalent Drop Mass (W_e):

$$\mathbf{3636.36 \times [(508 + (1\text{-}0.67) \times 103.38) \div (508 + 103.38)] = 3221.81\ kg}$$

Maximum CG acceleration from drop analysis: **22.49 m/s^2**

Load Factor (n_j):

$$\mathbf{[[(22.49 \div 9.81) + 1] \times (3221.81 \div 3636.36)] + 0.67 = 3.59g}$$

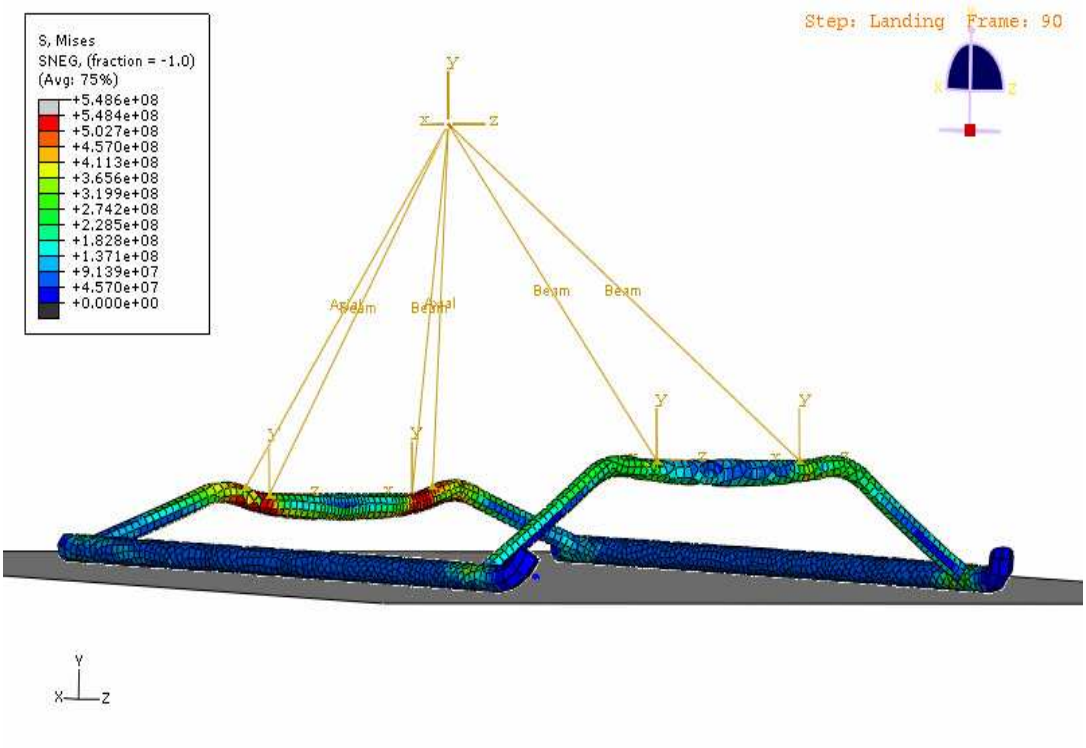

Figure 8. Mises Stress – Al 7075 Reference Configuration

Level Landing – Composite Skid Landing Gears

Figure 9 and Figure 10 shows normal and shear stresses are greater than 3000 MPa and 124 MPa, in the 0º and 45º fibers, and exceed allowable values. Figure 11 shows CG displacements and accelerations of the 48 ply all composite IM7/977-3, T700S/977-3, AS4/977-3 and IM7/PEEK skid landing gears. As expected, acceleration's are higher than for the metal landing gear. Highest load factors computed are 5.75 and 5.73 for IM7/PEEK and IM7/977-3 designs. Figures 12 through 19 show normal strains along the 0º fiber in ply 46 and shear strains along the 45º fiber in ply 48, along cross member outer diameters. Most of the IM7 fiber cross member beam produces strains within +/- 3000-6000 με. Ply strains are high in regions close to radius bends on the rear cross member. Local stiffening or plasticity induced strain relief may be required. Shear strains are as high as +/- 10000-30000με in the rear cross member.

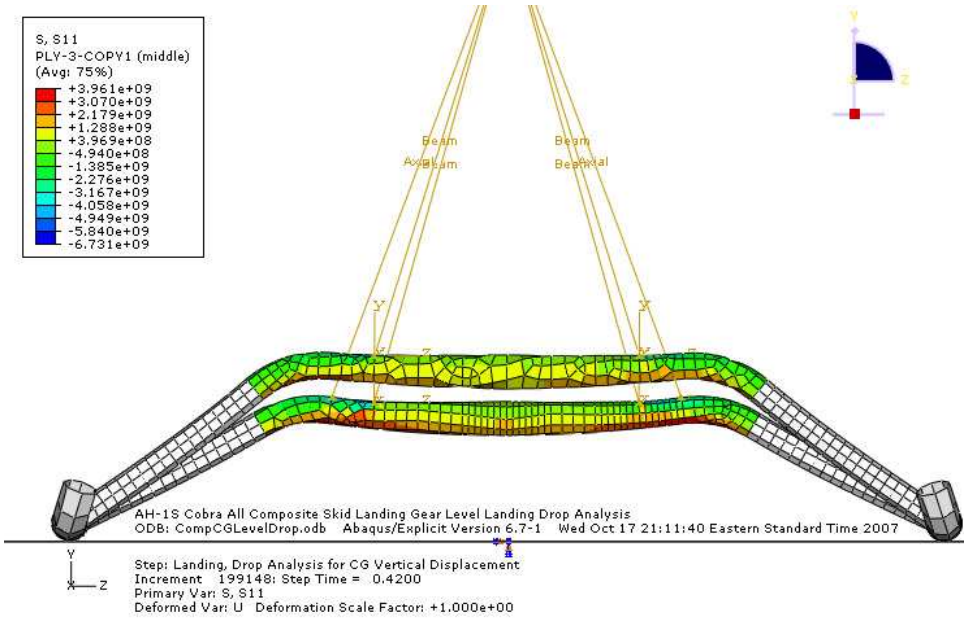

Figure 9. Ply 46 (0º) σ_{11} – IM7/977-3

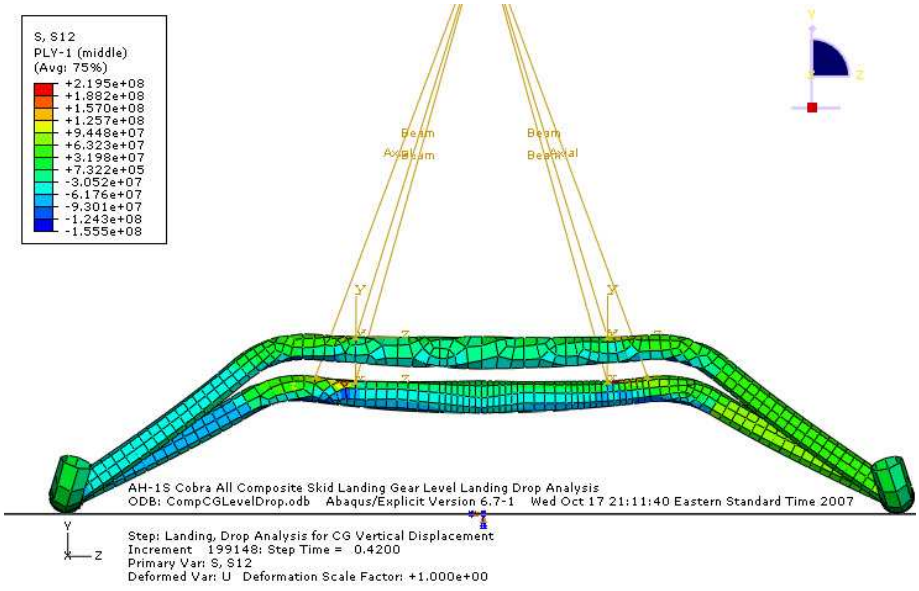

Figure 10. Ply 48 (45º) σ_{12} – IM7/977-3

Both strains increase with decreasing fiber stiffness. Thus, it can be said that high stiffness IM7 fiber shows better performance in the cross member regions for a single composite configuration. It is to be noted though that the skids do not produce much

strains. Hence, low stiffness yet high impact resistant Ke49 fiber may be used in this region. A key point to be noted is the absence of plasticity and non-linearity in the stress-strain law prescribed for the composites. Hybridization of multiple composites and metal was analyzed to study the effect on load factor and strength.

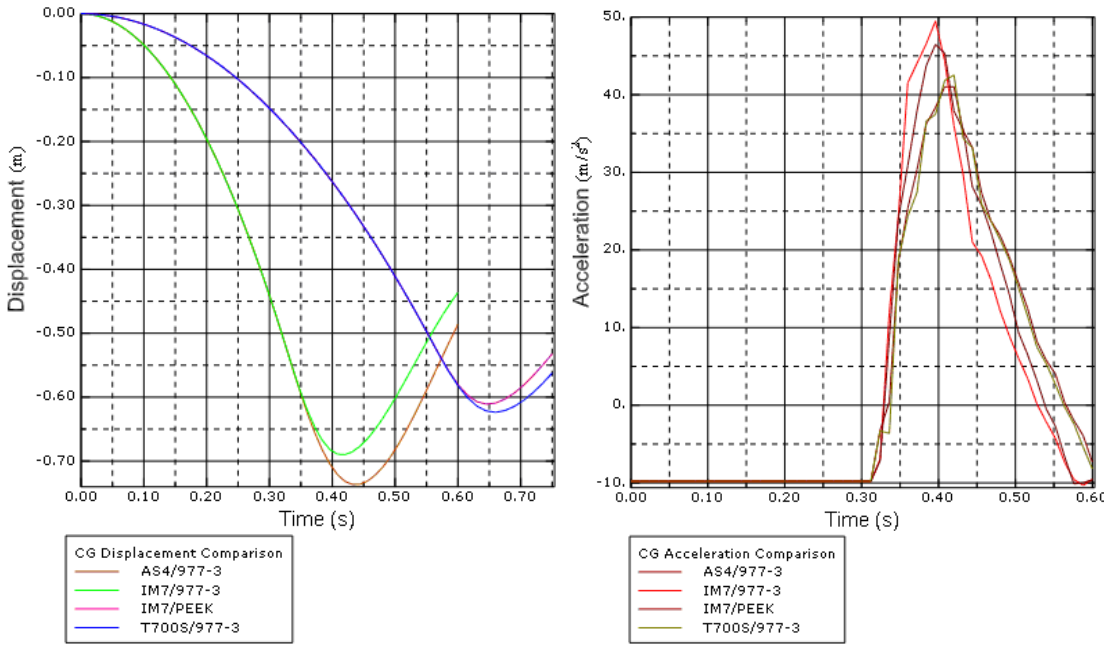

Figure 11: CG Vertical Displacement and Accelerations – Composites

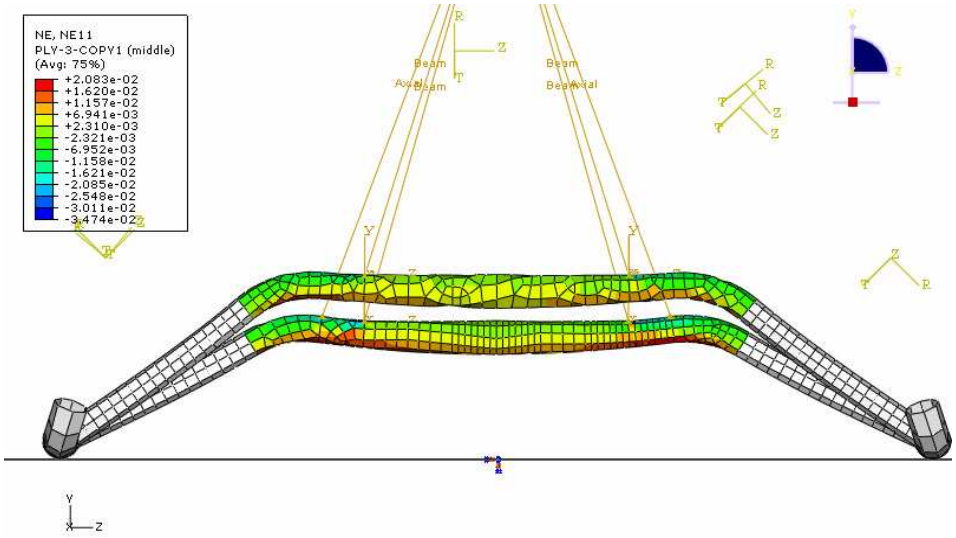

Figure 12. Ply 46 (0°) ε_{11} – IM7/977-3

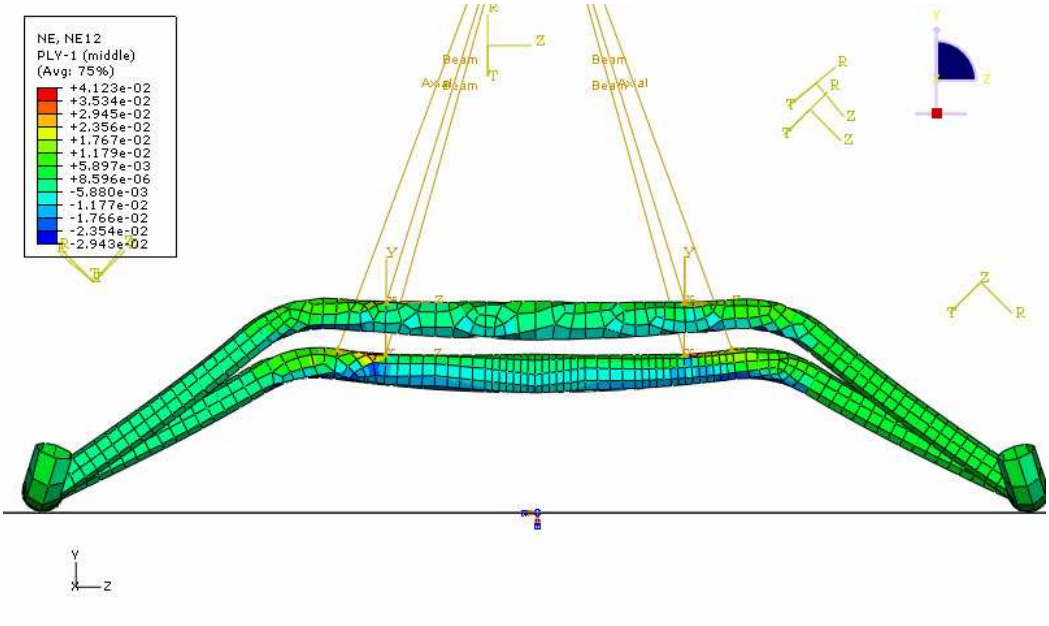

Figure 13. Ply 48 (45°) γ_{12} – IM7/977-3

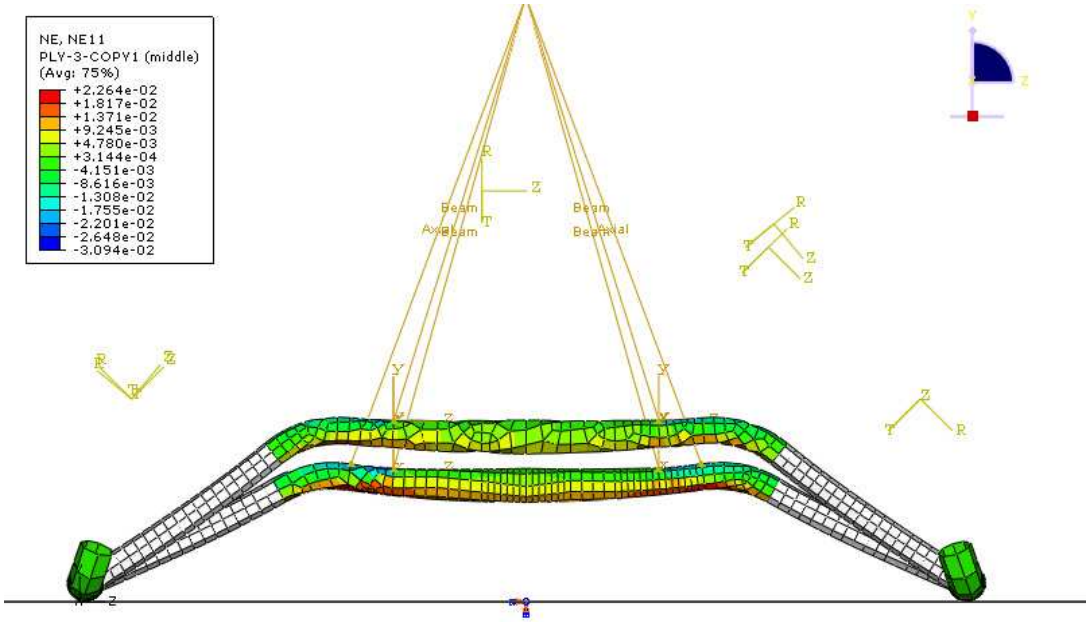

Figure 14. Ply 46 (0°) ε_{11} - IM7/PEEK

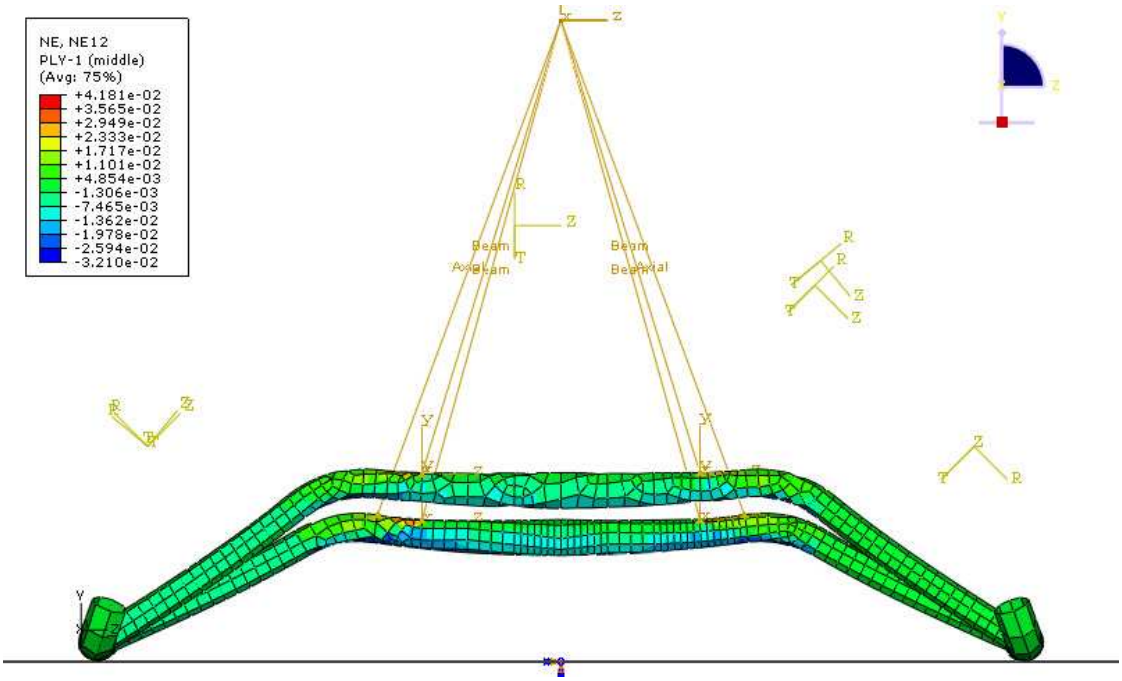

Figure 15. Ply 48 (45º) γ_{12} - IM7/PEEK

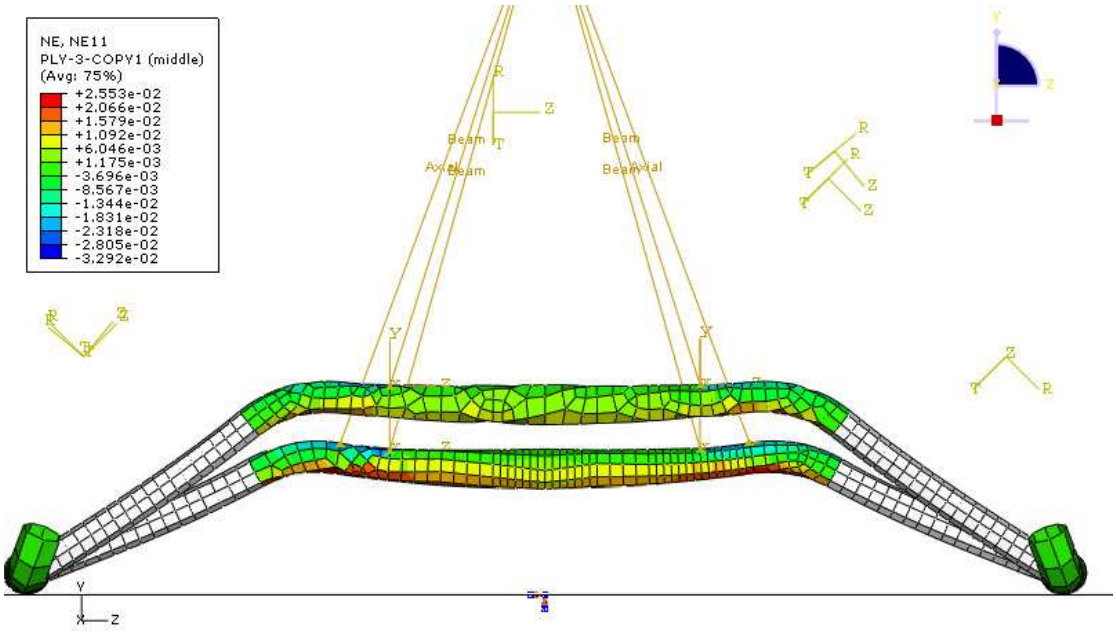

Figure 16. Ply 46 (0º) ε_{11} – T700S/977-3

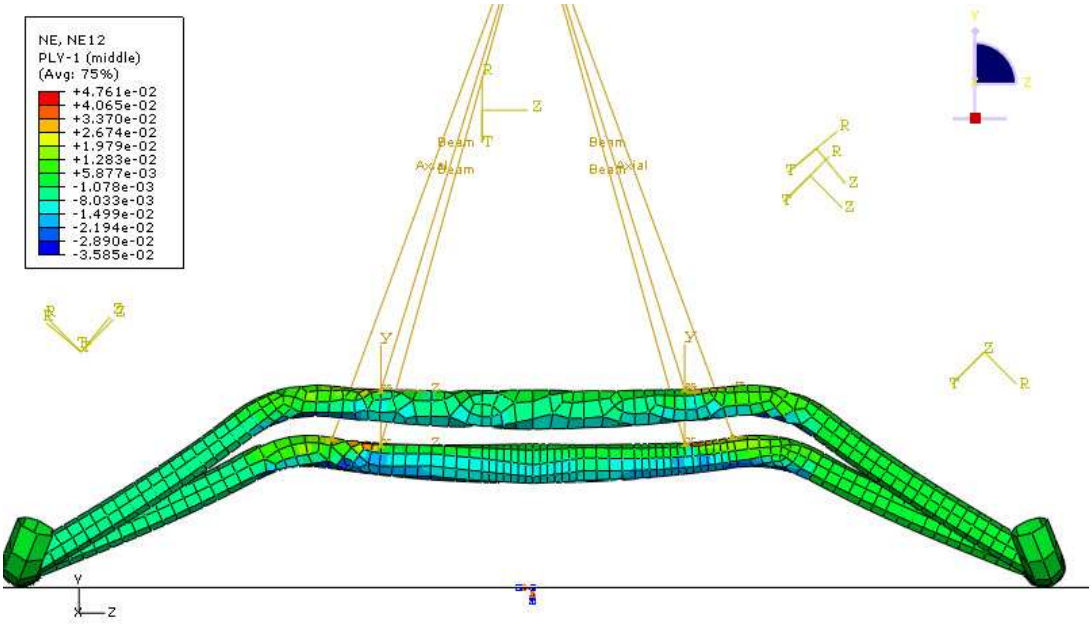

Figure 17. Ply 48 (45º) γ_{12} – T700S/977-3

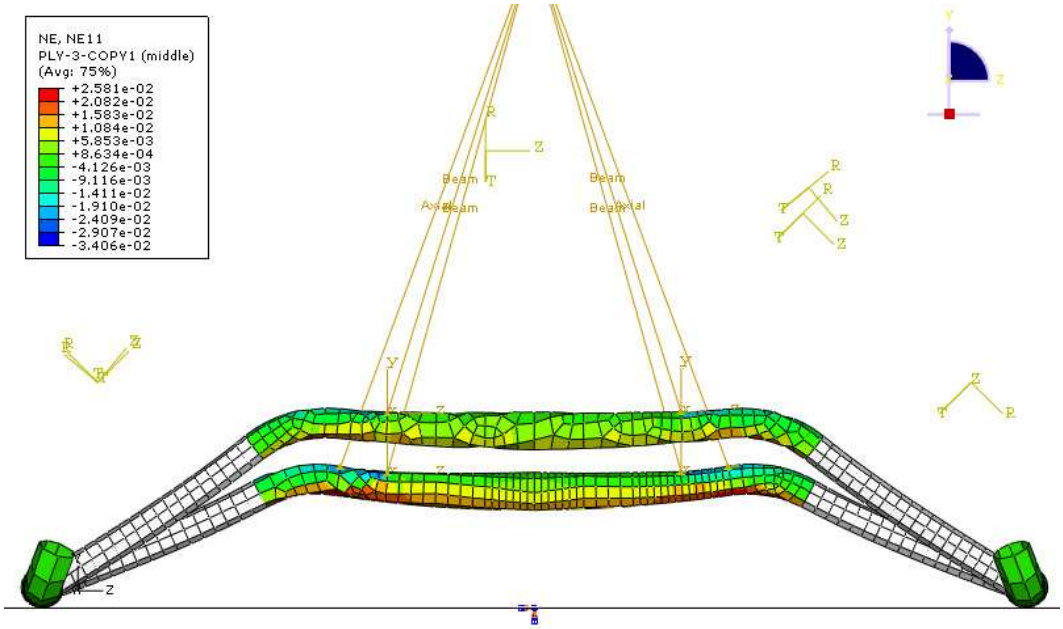

Figure 18. Ply 46 (0º) ε_{11}– AS4/977-3

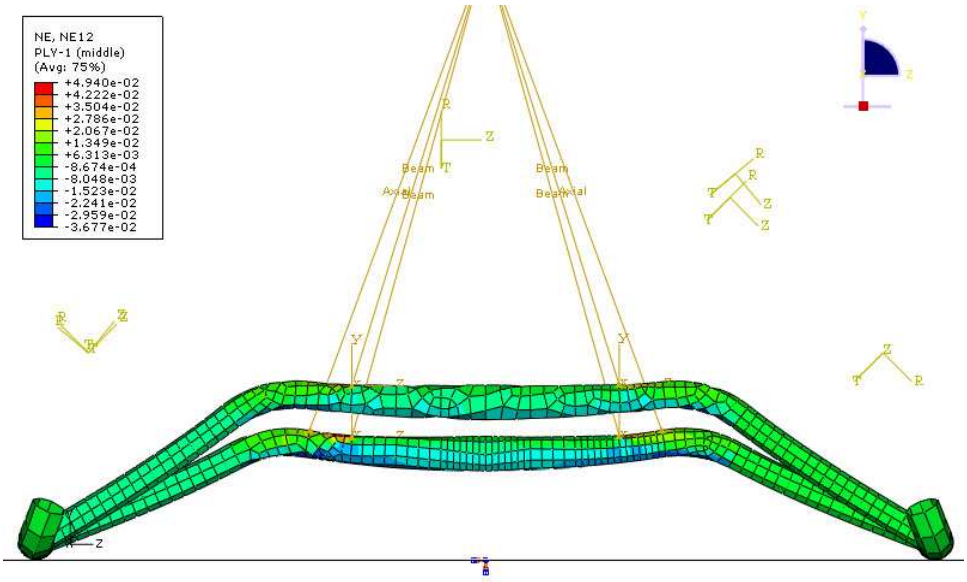

Figure 19. Ply 48 (45°) γ_{12} – AS4/977-3

Level Landing – Hybrid Skid Landing Gears

From previous results it can be noted that strains are large in regions close to the bend radii of the cross members. Also, the skids do not undergo significant straining. Ke49 fiber can be used for the skids leaving the remainder with high stiffness fibers. To alleviate strains in the cross members, the radii bends were assigned Al 7075 elasto-plastic properties. Thus, a combination of metal plasticity with non-linear constitutive stress-strain law and linear composite stress-strain law was prescribed. Several configurations, with both PEEK and 977-3, were analyzed to understand the amount of strain relief as well as the volume fraction dependence of metal in the design. Figure 20 depicts the CG displacements and accelerations of the hybrid designs. It can be inferred that metal plasticity in the bends alleviates the load factors significantly without adding much weight. The lowest load factor with acceptable strains is obtained for a design with Ke49/PEEK skids, Al 7075 cross member bends and rest IM7/977-3. As the elastic

properties of PEEK are very nearly similar to those of 977-3, it is projected that replacing IM7/977-3 with IM7/PEEK in any configuration should result in near identical performance. Figures 21-40 show normal strains, normal stresses, shear strains and shear stresses in the 0º and 45º fibers in plies 46 and 48 along the outer diameters of the rear cross member. Figure 41 shows out-of-plane strains. IM7 produces 7000 με in the 0º fiber and 9000-12000 με along +/- 45º in shear. AS4 and T700S produce marginally higher strains. Both, normal and shear strains are high. The strength based theory shows that any of the three fibers is acceptable provided the regions close to the cross member bend radii are metallic. While IM7 fiber shows the most desired performance, stress based allowable show that any of the fibers can be used in conjunction with metal plasticity in the bend regions. Hence, AS4 and IM7 fiber, with high SEA values[37] are recommended. It can be concluded that metal plasticity aids significantly in lowering the load factor. Thus, it may be possible to use either of the fibers in conjunction with 977-3 or PEEK or a similar matrix, for the hybrid metal composite design. The configuration with Al cross member bends and skids and the rest made of IM7/977-3 has a load factor of 4.40 while that with only Al Bends and rest of IM7/977- 3 is 4.14. Weight saving as compared to an Al skid landing gear of ¼" wall thickness is 41.77% for the latter and 13.73% for the former. Thus, usage of metal in regions other than the bends adversely affects weight saving. Metal-composite hybridization is not a function of volume fraction and is only dependent on the cross member bend radii. Fabricating skids from Ke49/PEEK increases weight saving to 49%. A design with Ke49/PEEK skids, Al 7075 cross member bends and the rest of the landing gear fabricated from AS4 or IM7/PEEK is the recommended design. The choice for PEEK over 977-3 comes from benefits of

high fracture toughness. PEEK has interlaminar fracture toughness an order of magnitude higher than that for 977-3. Elastic properties being similar, both result in similar performance under limit loads.

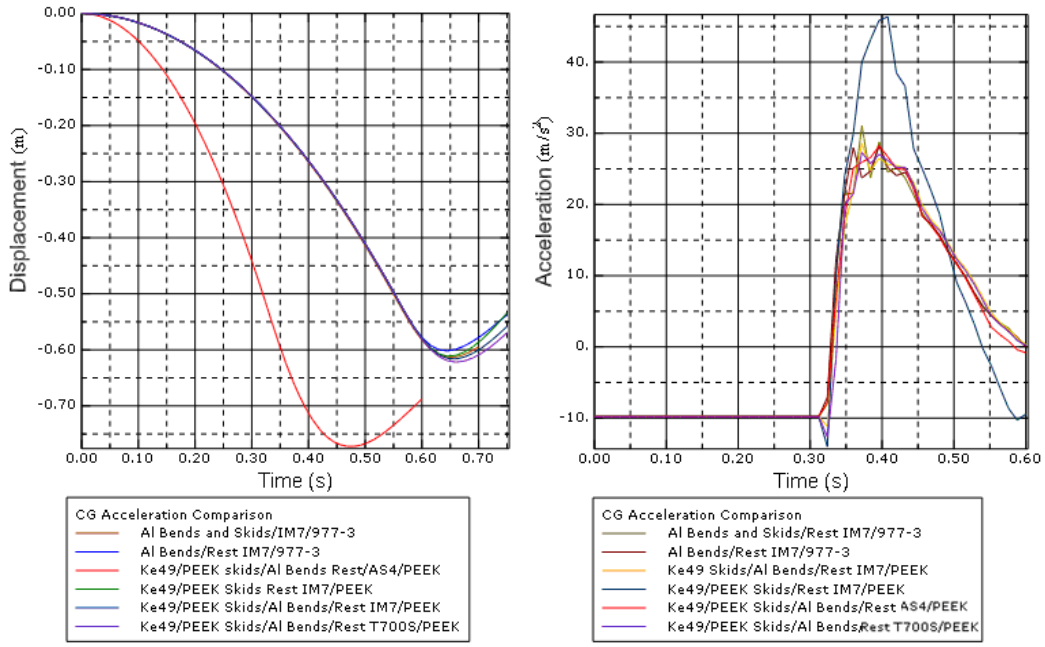

Figure 20. CG Vertical Displacements and Accelerations – Hybrid Design

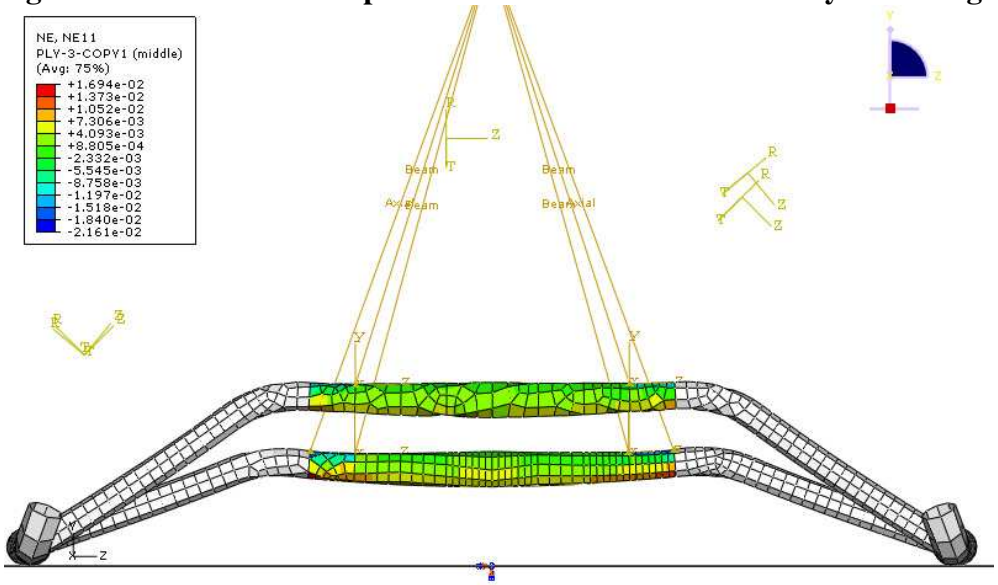

Figure 21. Ply 46 (0°) ε_{11} – Al Bends/IM7/977-3

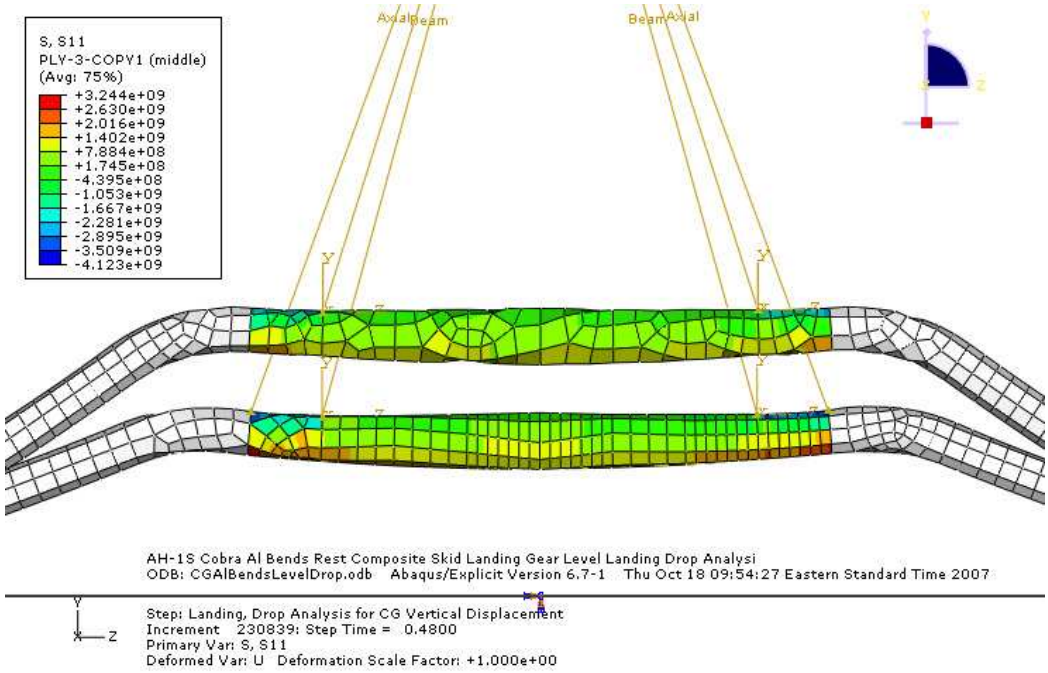

Figure 22. Ply 46 (0°) σ_{11} – Al Bends/IM7/977-3

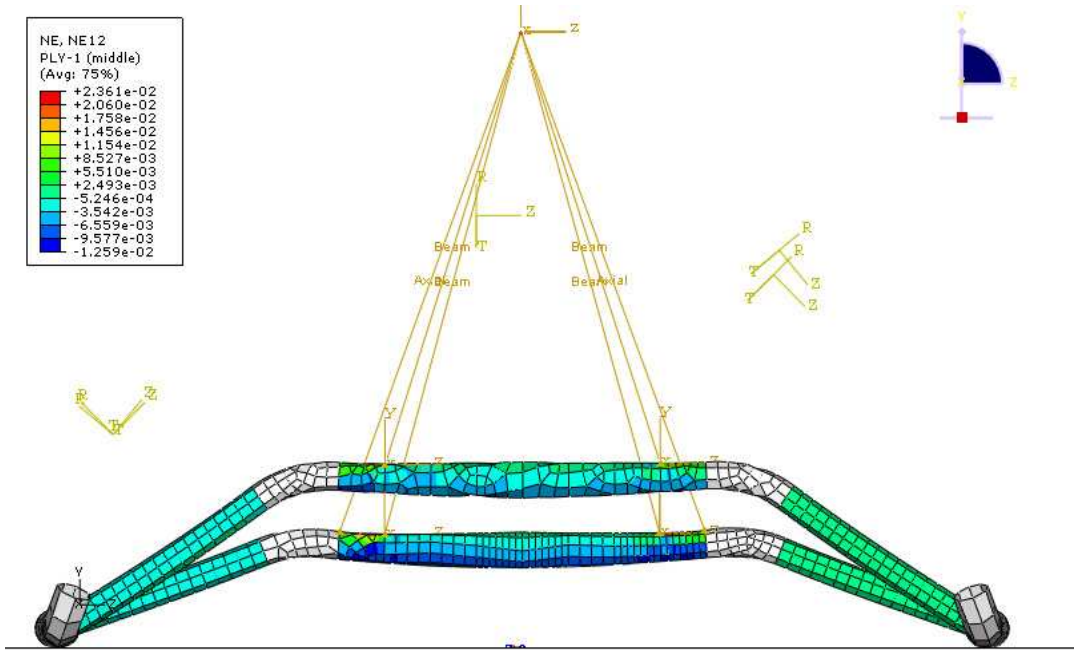

Figure 23. Ply 48 (45°) γ_{12} – Al Bends/IM7/977-3

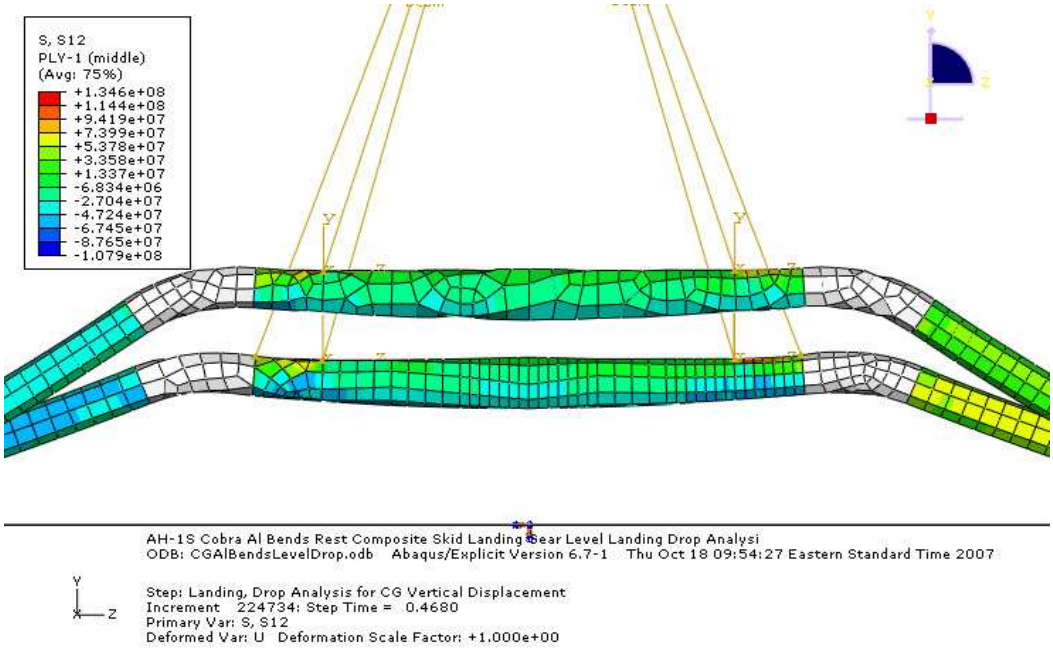

Figure 24. Ply 48 (45º) σ_{12} – Al Bends/IM7/977-3

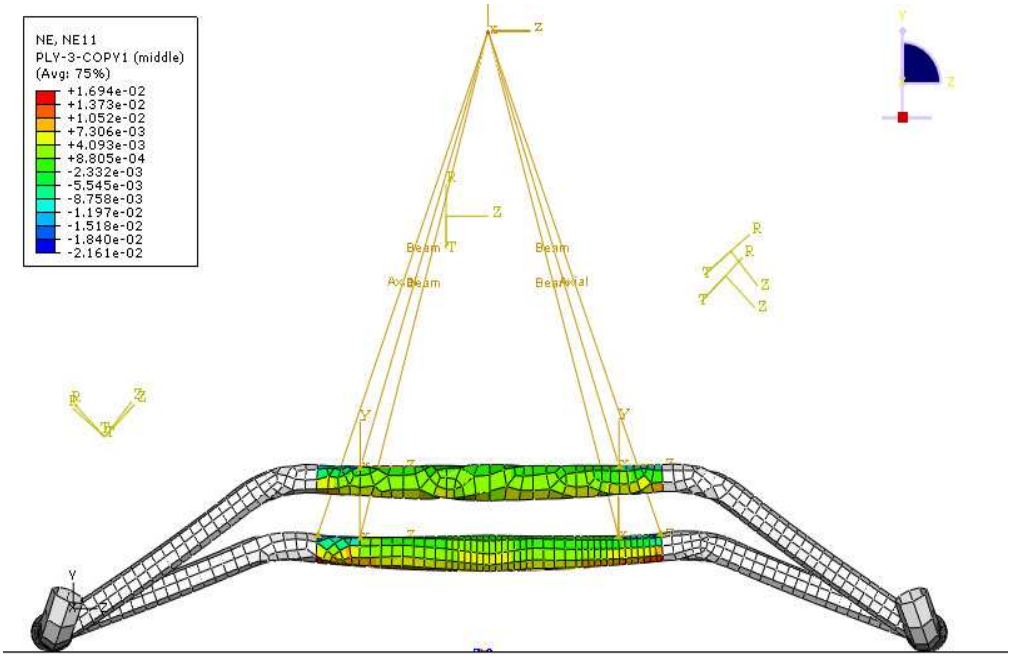

Figure 25. Ply 46 (0º) ε_{11} - Al Bends & Skids/Rest IM7/977-3

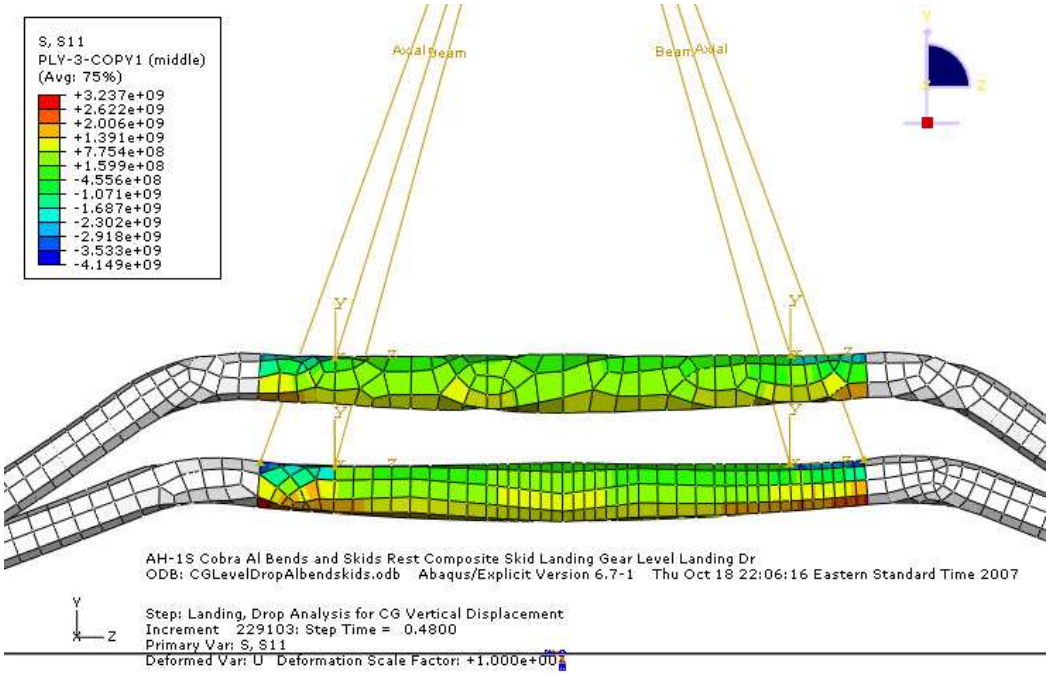

Figure 26. Ply 46 (0°) σ_{11} - Al Bends & Skids/Rest IM7/977-3

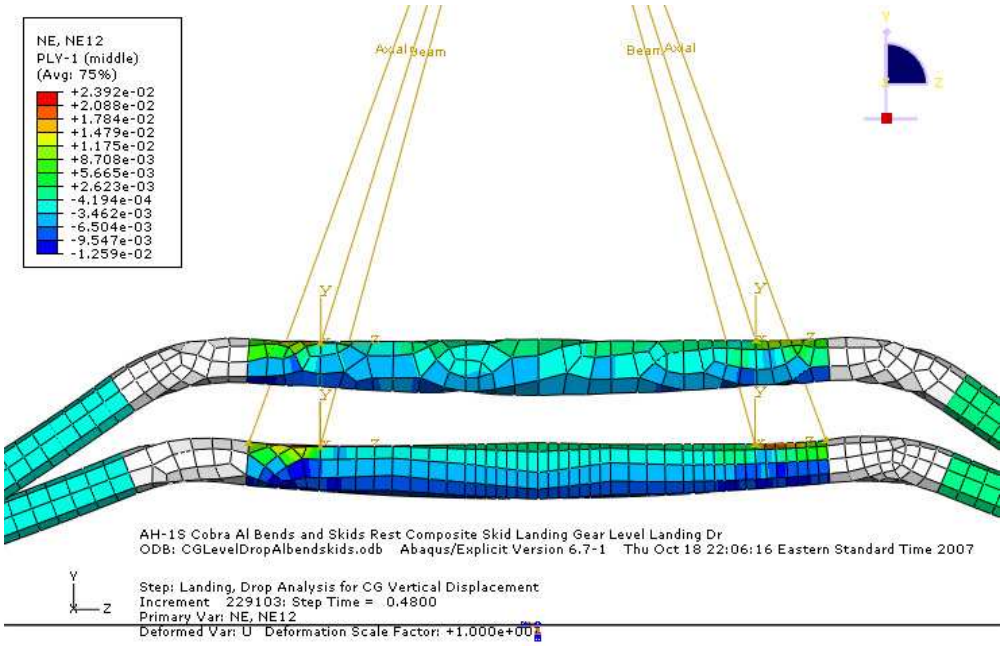

Figure 27. Ply 48 (45°) γ_{12} - Al Bends & Skids/Rest IM7/977-3

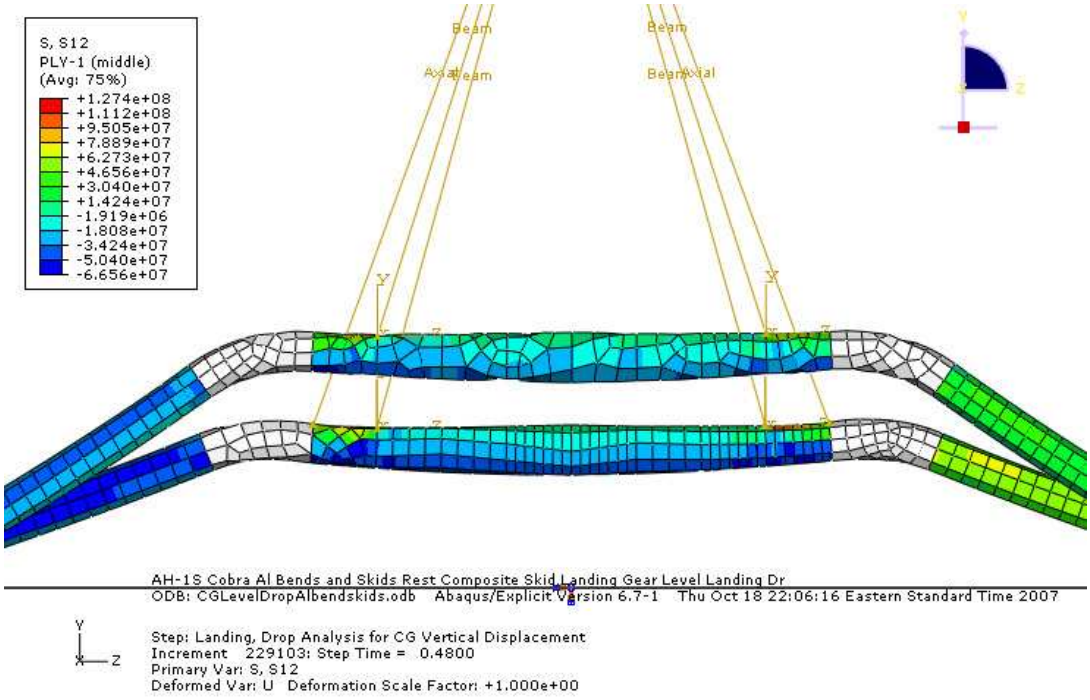

Figure 28. Ply 48 (45°) σ_{12} - Al Bends & Skids/Rest IM7/977-3

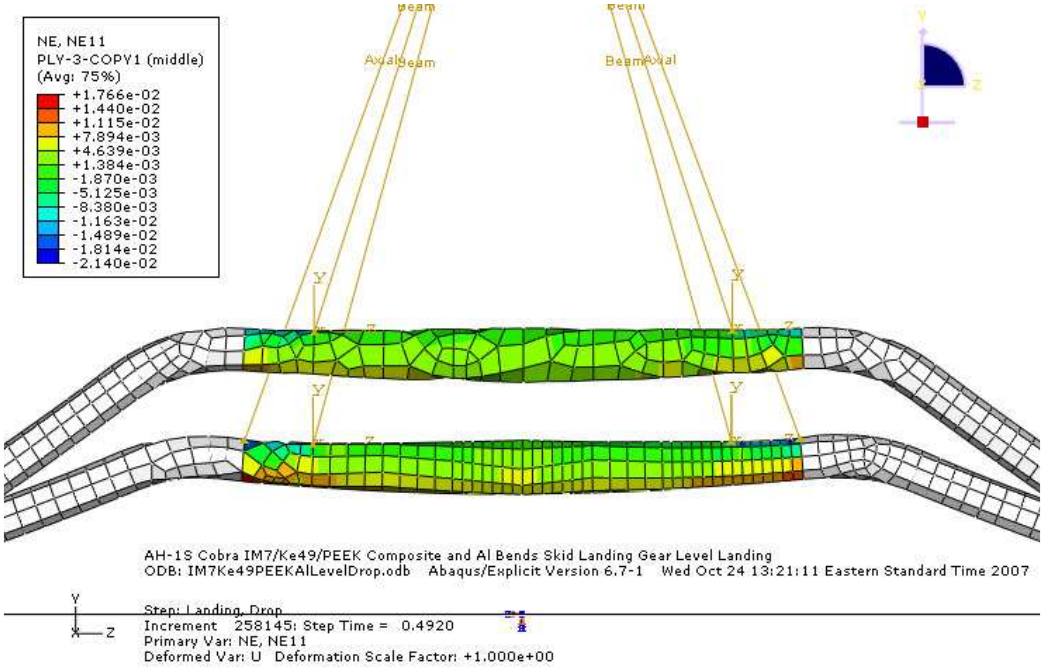

Figure 29. Ply 46 (0°) ε_{11}– Ke49/IM7/PEEK/ Al Bends

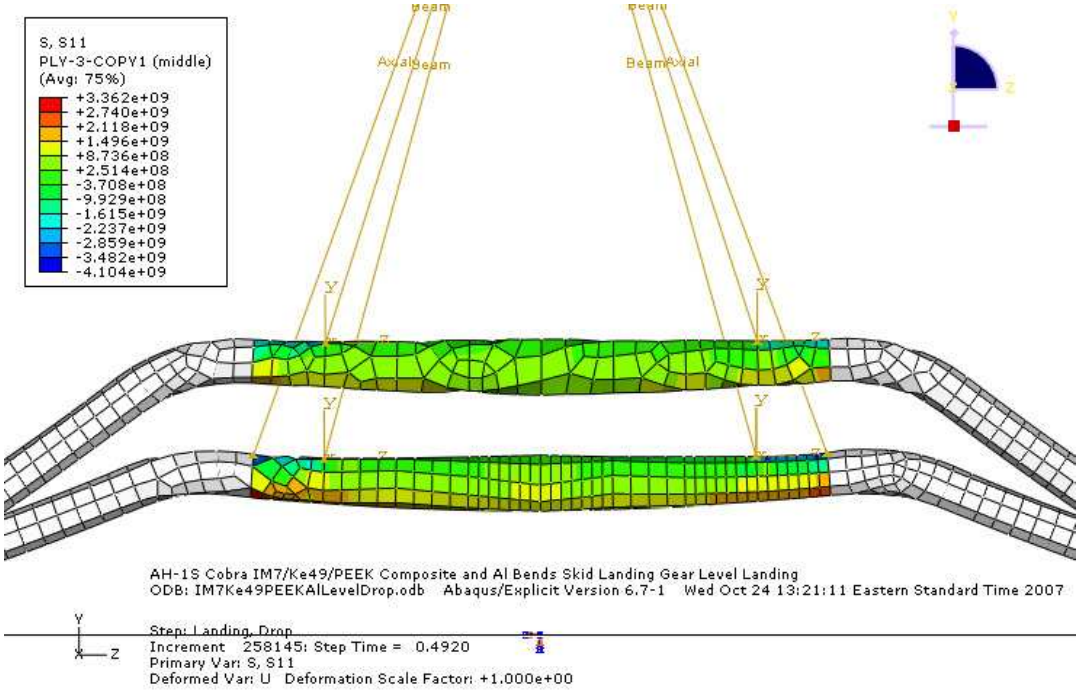

Figure 30. Ply 46 (0º) σ_{11} – Ke49/IM7/PEEK/ Al Bends

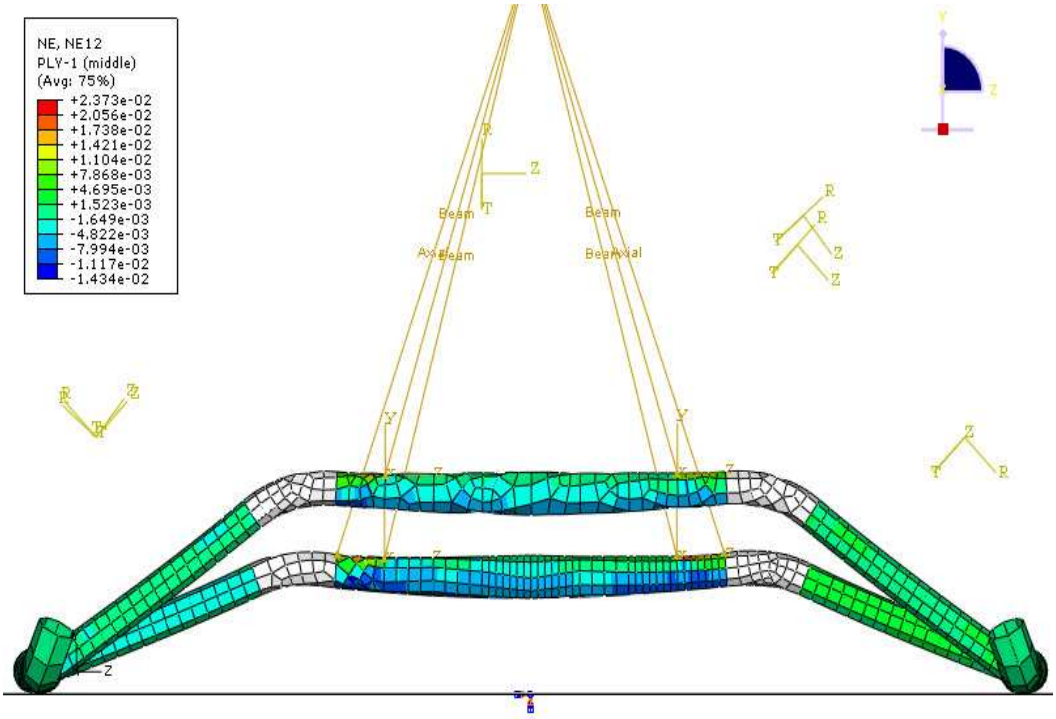

Figure 31. Ply 48 (45º) γ_{12} – Ke49/IM7/PEEK/Al Bends

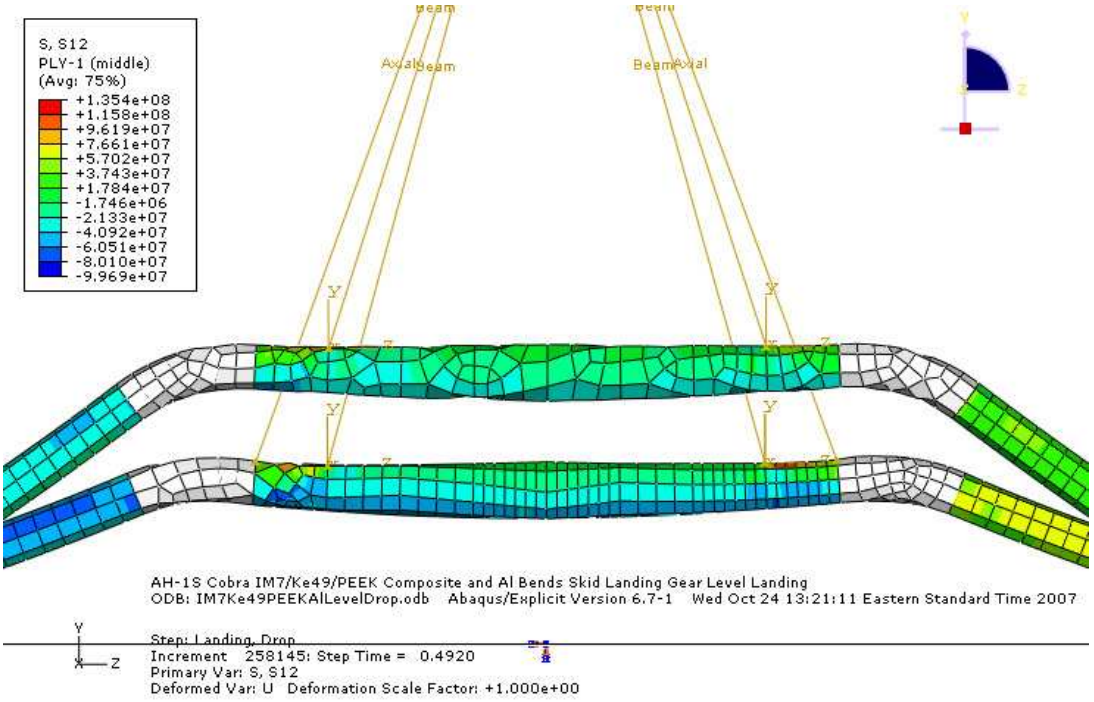

Figure 32. Ply 48 (45°) σ_{12} – Ke49/IM7/PEEK/Al Bends

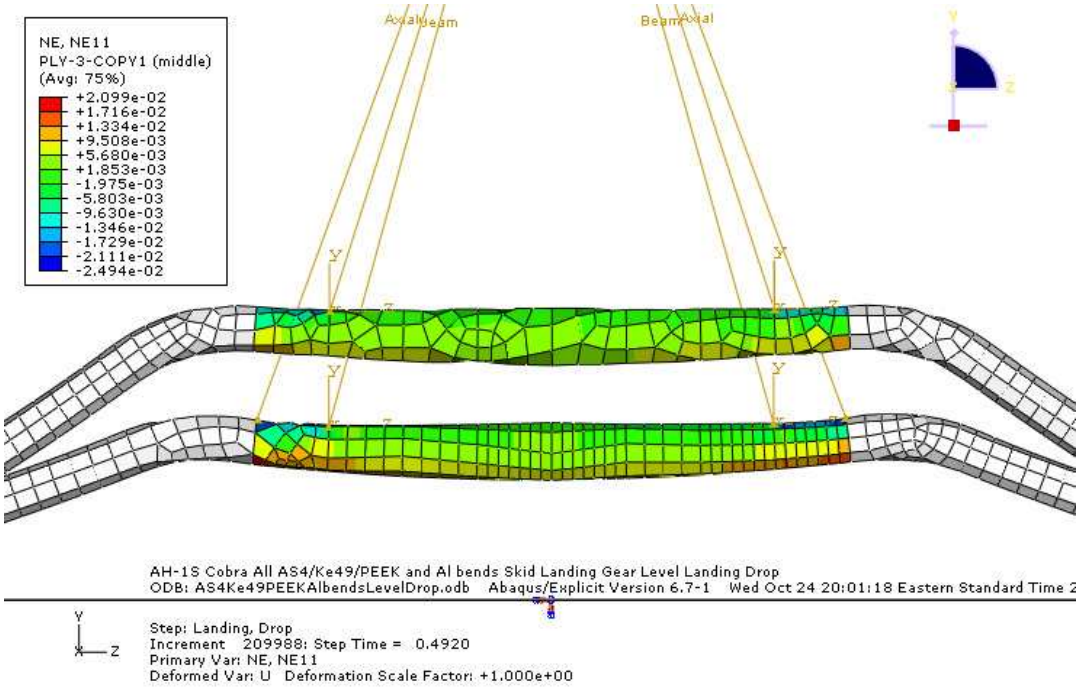

Figure 33. Ply 46 (0°) ε_{11} – Ke49/AS4/PEEK/ Al Bends

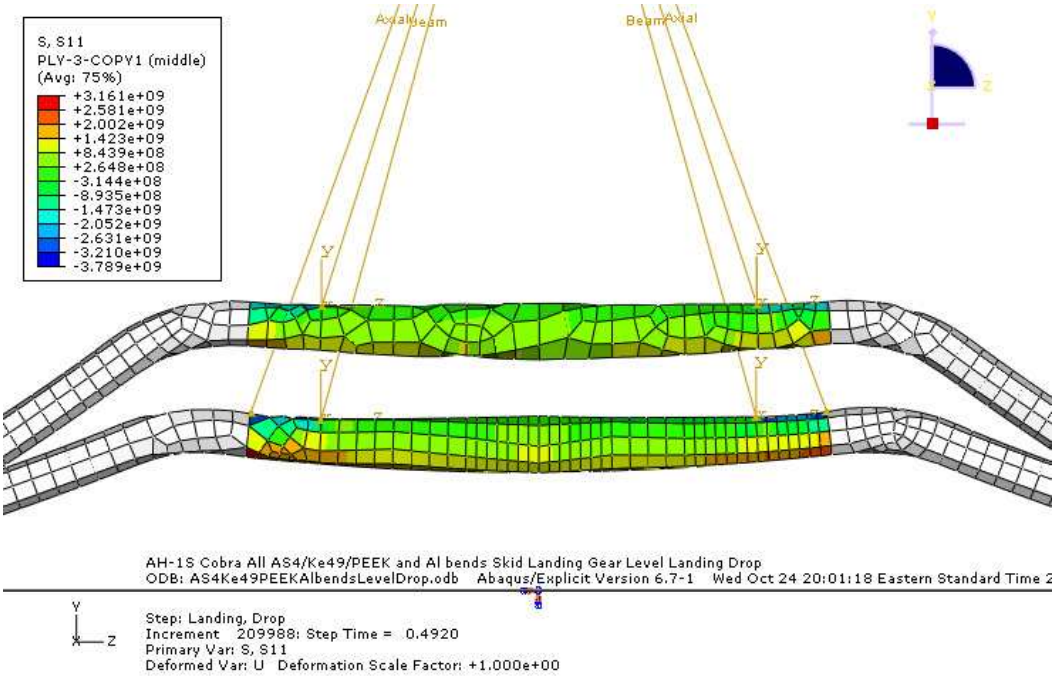

Figure 34. Ply 46 (0°) σ_{11}– Ke49/AS4/PEEK/ Al Bends

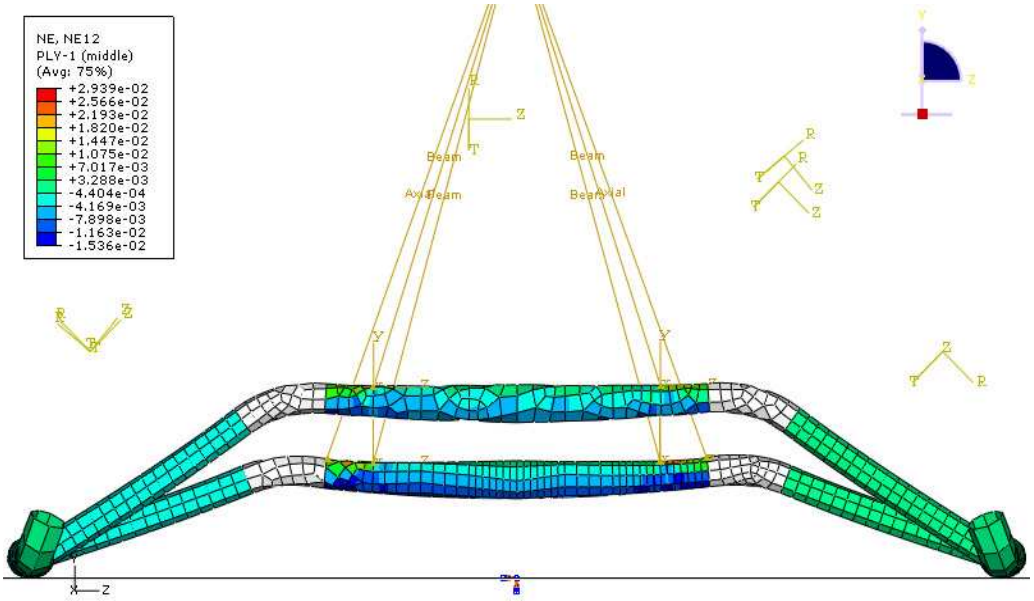

Figure 35. Ply 48 (45°) γ_{12} – Ke49/AS4/PEEK/Al Bends

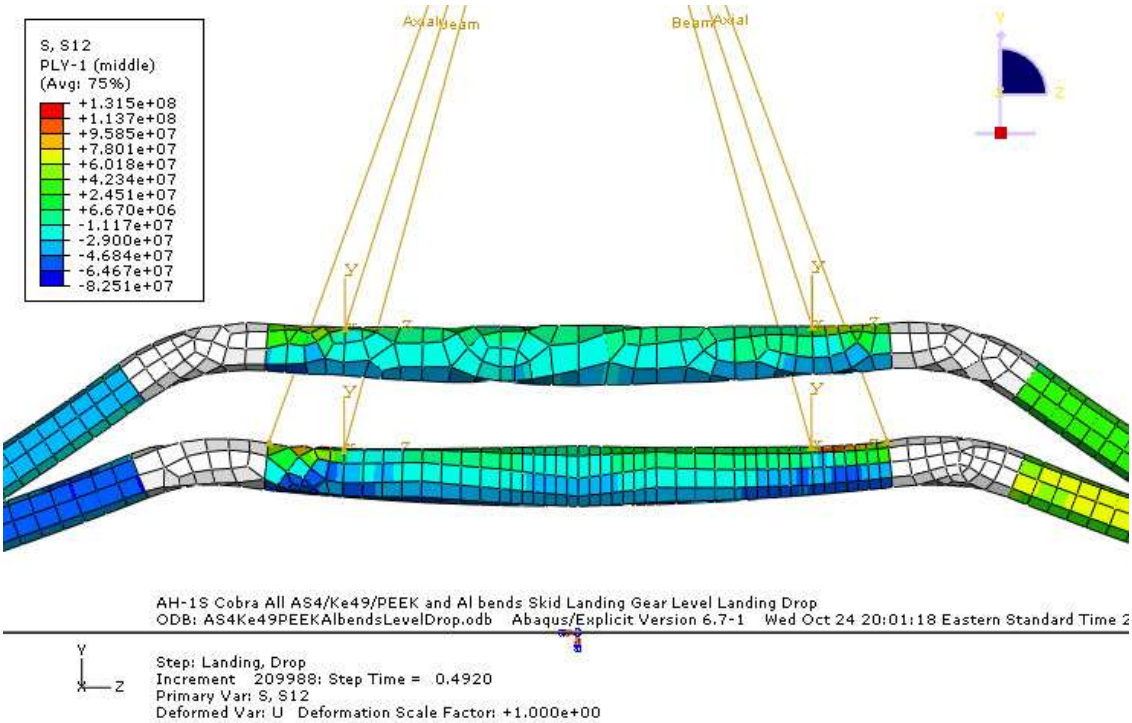

Figure 36. Ply 48 (45°) σ_{12} – Ke49/AS4/PEEK/Al Bends

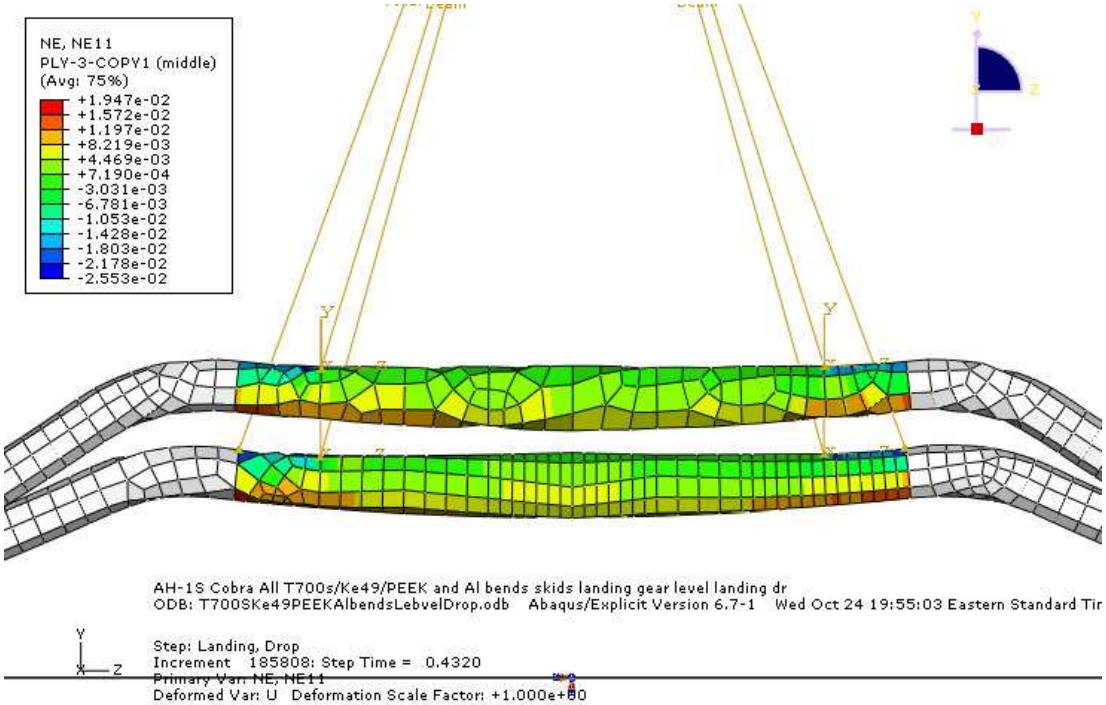

Figure 37. Ply 46 (0°) ε_{11} – Ke49/T700S/PEEK/Al Bends

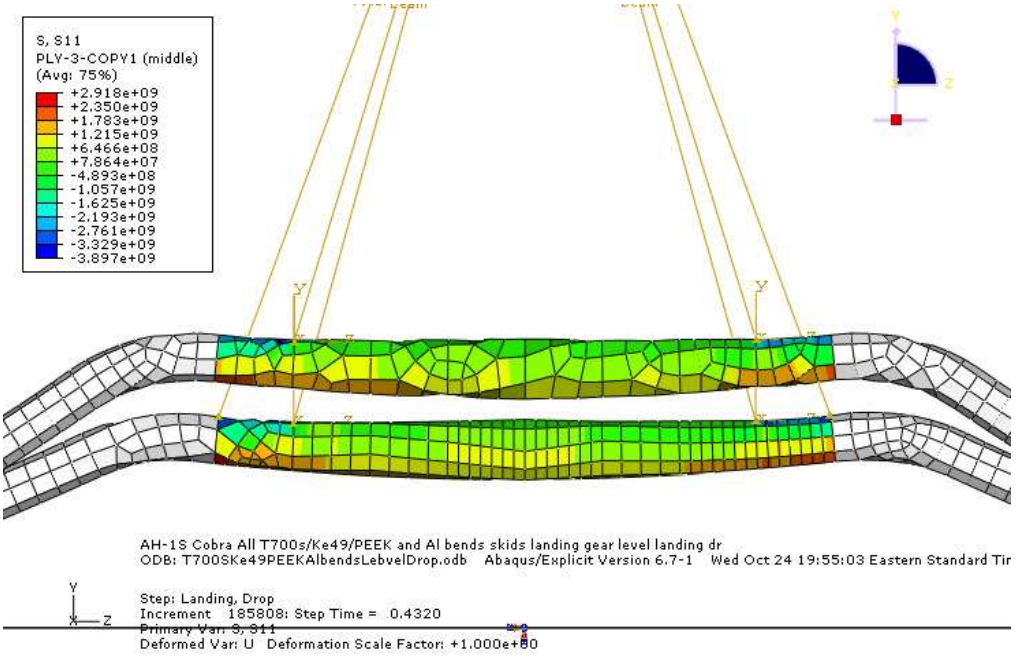

Figure 38. Ply 46 (0°) σ_{11} – Ke49/T700S/PEEK/Al Bends

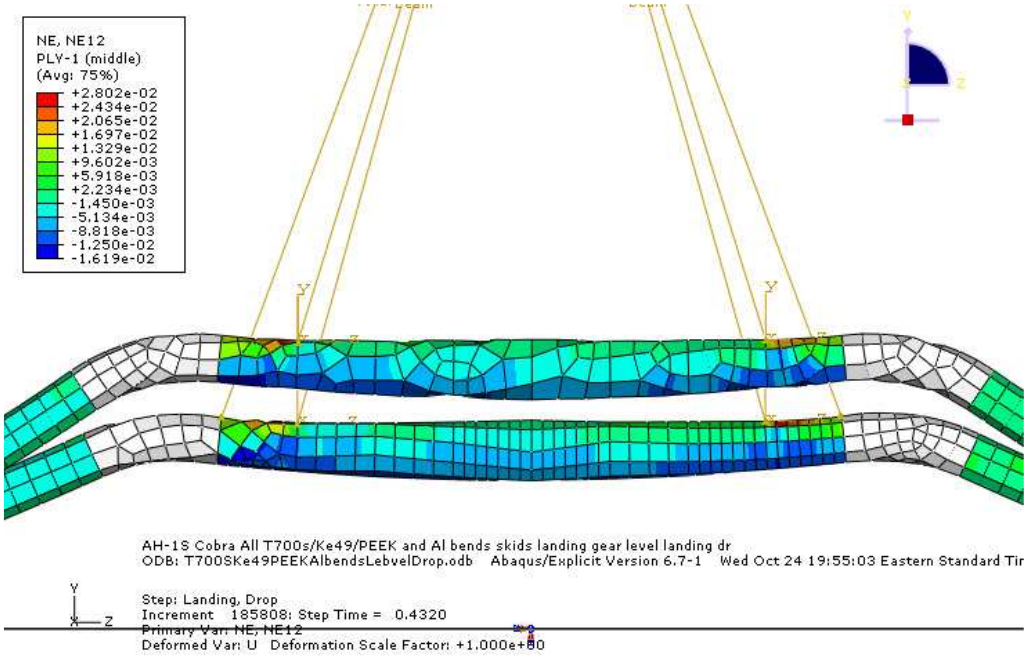

Figure 39. Ply 48 (45°) γ_{12} – Ke49/T700S/PEEK/Al Bends

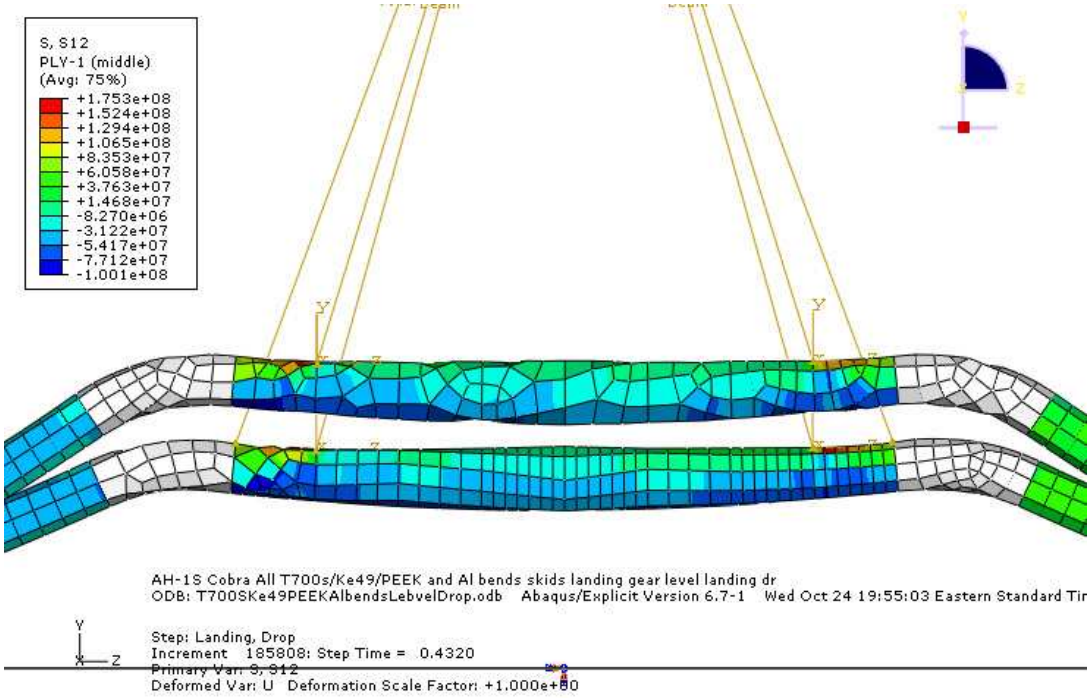

Figure 40. Ply 48 (45º) σ_{12} – Ke49/T700S/PEEK/Al Bends

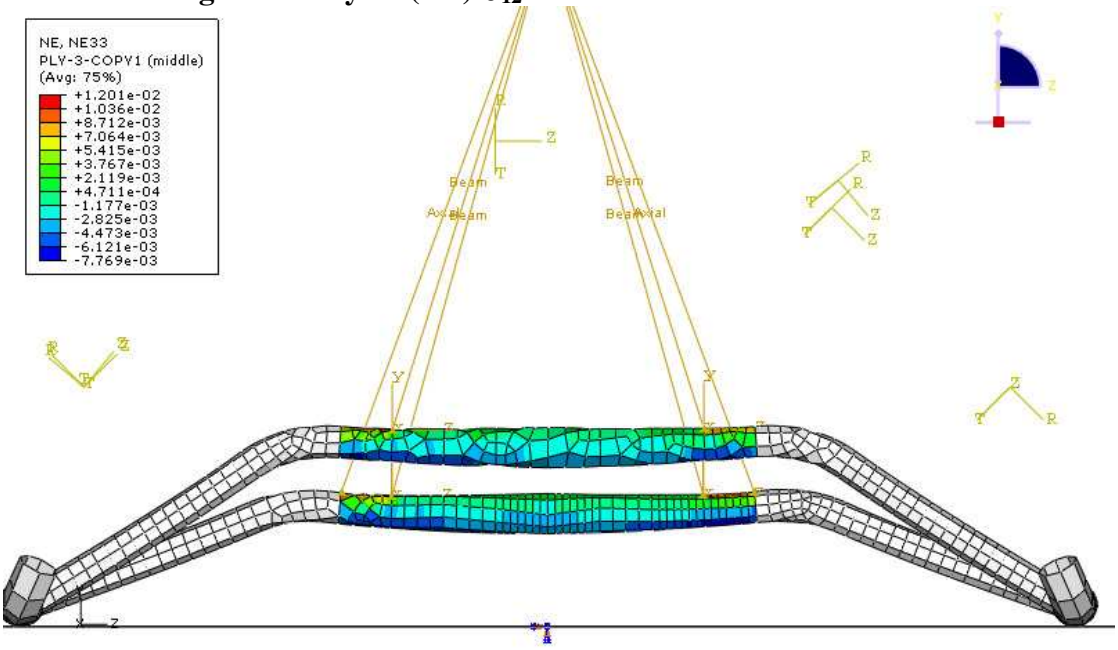

Figure 41. Out-of-Plane Strain Ply 46 (0º) – Ke49/IM7/PEEK/Al Bends

Level Landing with Drag (run-on) – IM7/977-3 Skid Landing Gear

Figure 42 depicts CG displacements and acceleration plots. The impact surface and landing gear are to be tilted at 26.6º with respect to the horizontal. This was simulated by imposing resolved components of the gravity load and lift, while maintaining the horizontal attitude of the landing gear and impact surface. An initial forward velocity equaling half the level landing drop velocity at impact was simulated for drag. The drop height to achieve these velocities at impact is 0.633 m (~25”). Figure 43 shows the ply strains in the 46th ply (0º) fiber direction, again high in localized regions along the rear cross member tapered beam. Load Factor obtained for this case is 4.74.

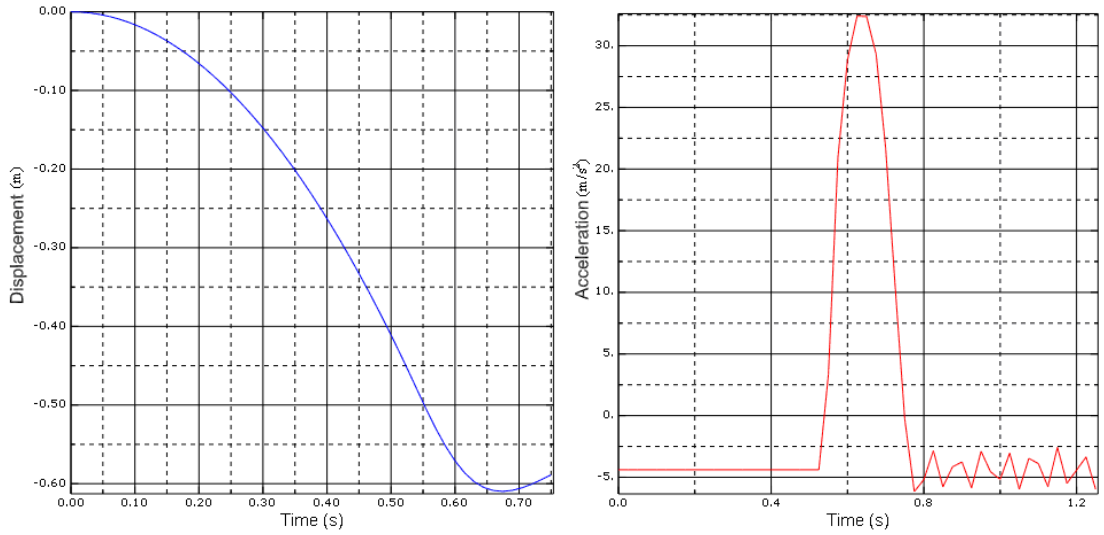

Figure 42. CG Vertical Displacement and Acceleration – Level Landing with Drag

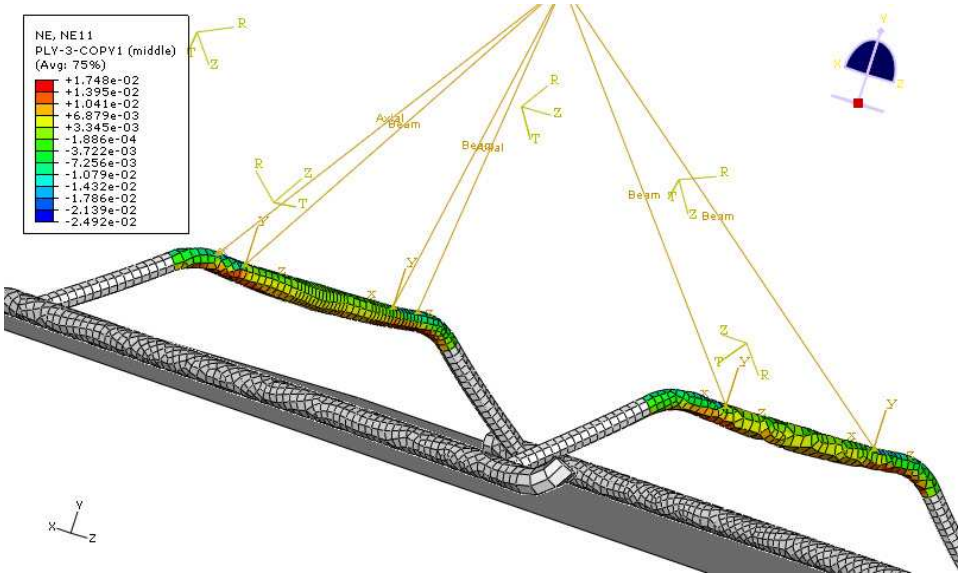

Figure 43. Ply 46 (0^o) ε_{11} – IM7/977-3

Rolled Attitude Landing – IM7/977-3 Skid Landing Gear

Rolled attitude landing impact has been simulated as the critical rolling condition reported by Sareen et al. Sink speed of 3.04 m/s (10 ft/s) with a rolled attitude angle of 6.4º has been simulated by inclining the landing gear assembly at 6.4º to the horizontal with drop height equaling 0.471 m (18.6”). Figure 44 depicts CG displacement and maximum acceleration. Load factor obtained is 4.54. This is lower than that for level landing and level landing with drag (run-on) conditions, and in agreement with published trend. Load factor is lower due to larger CG displacement (141 mm). Ply strains are acceptable in regions away from the bend radii as shown in Figure 45. This is another indication that metal plasticity is essential to relieve strains.

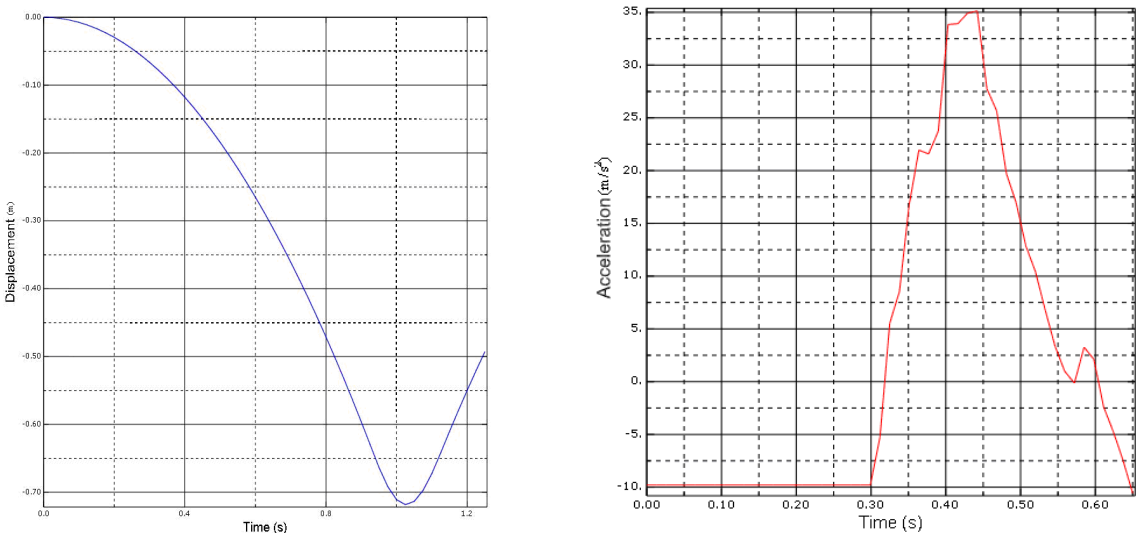

Figure 44: CG Vertical Displacement and Accelerations –Rolled Attitude Landing

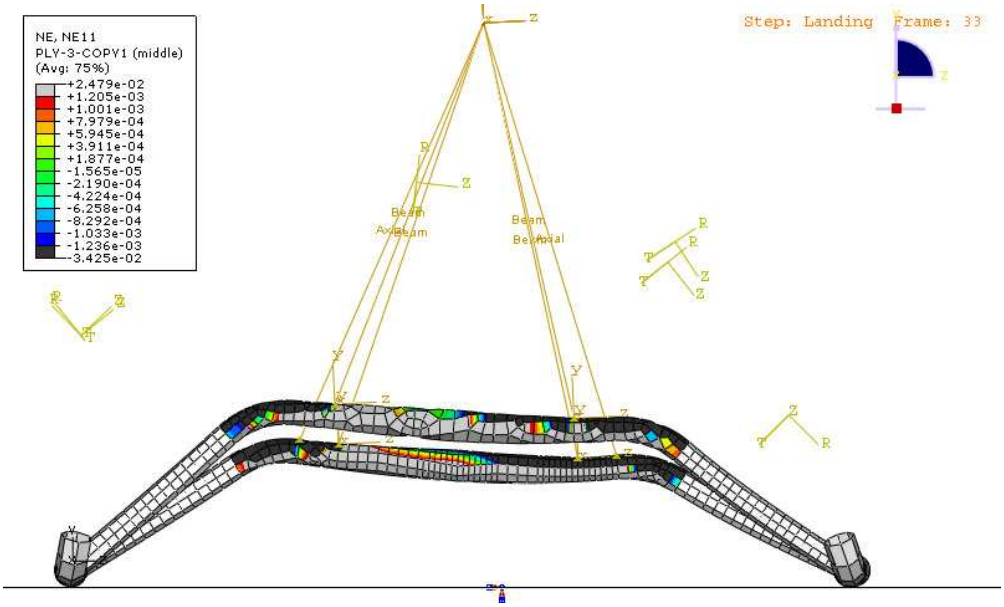

Figure 45. Ply 46 (0º) ε_{11}–Rolled Attitude Landing

5.6 Load Factor and Weight Saving

Table 10 shows load factors and weight saving for various configurations discussed. Designs with Ke49 skids, Al cross member bends and the rest with composite/PEEK (or composite/977-3) show desired load factors.

Table 10. Load Factors and Weight Saving

Design Configuration	Weight Saving	n_j (g's)
Level Landing		
Al 7075	---	**3.59**
IM7/977-3	42.21 %	**5.73**
IM7/PEEK	42.21 %	5.75
T700S/977-3	42.21 %	5.34
AS4/977-3	42.21 %	5.19
Al Bends & Skids Rest IM7/977-3	13.73 %	4.40
Al Bends Rest IM7/977-3	41.77 %	4.14
Ke49/PEEK skids Rest IM7/PEEK	49%	5.73
Ke49/PEEK Skids Al Bends Rest IM7/PEEK	49%	**4.08**
Ke49/PEEK Skids Al Bends Rest T700S/PEEK	49%	3.99
Ke49/PEEK Skids Al Bends Rest AS4/PEEK	49%	4.13
Level Landing with Drag (Run-On)		
IM7/977-3	42.21	4.74
Rolled Attitude Landing		
IM7/977-3	42.21	4.54

5.7 Summary

Composites show higher load factors as expected but result in weight saving up to 40%. High strains are observed in the all composite landing gear in localized regions along the cross member tapered beams. The highest strains are observed in-plane and in compression along the 0º fiber orientations (ply 45). Out-of-plane strains are within 15000 με in compression and 20000 με in tension for all composite configurations and 7000 με for hybridized designs. Focht[37] et al report the allowable strains for IM7/977-3 unidirectional, cross ply and angle ply laminates to be as high as 18000 με for the unidirectional laminate in the fiber direction to up to 30000 με for cross plies, under high strain rate compressive impact loading. Out-of plane strains reported are as high as 35000 με. Reinforcements such as short I-beam sections or stiffeners integrated within the composite tube at critical locations may result in increased localized stiffness without

significant weight addition and load factor increase. Hybridization of aluminum with composites results in lower strains along all fiber directions in the composite sections with maximum Mises stresses in the aluminum regions being as high as 549 MPa. The difference between aluminum bends only skid landing gear and aluminum bends-skids landing gear indicates that not much benefit is obtained by making the skid tubes out of aluminum. Larger bend region out of aluminum may be useful instead for benefits of plastic bending and further strain reduction in the composite regions. The hybridized landing gear performances were evaluated only under level landing conditions.

5.8 Conclusions

The following conclusions can be drawn from the design feasibility study:

1. An all composite skid landing gear is feasible by locally stiffening the hot spots on the cross member beams or by increasing the number of plies.
2. Increasing number of plies increases load factors but reduces weight saving.
3. Hybridization of aluminum and composite is feasible and achieves more acceptable load factors than an all composite skid landing gear does.
4. Plastic bending in metals is highly desired in the cross member regions.
5. Weight savings of 20-40% can be obtained despite hybridization.
6. Failure criteria need to be established based on testing under limit and crash conditions and will be a basis for further work.
7. Crashworthiness of both the configurations needs to be determined.

CHAPTER 6

COMPOSITE SKID LANDING GEAR PERFORMANCE AND LAMINATE TAILORING FOR LOAD FACTOR OPTIMIZATION UNDER LIMIT LOADS

6.1 Skid Landing Gear Modifications

The cross member bend radii were modified to simulate large radii on the AH-1S Cobra skid landing gear, unlike the smaller radii used in previous research. Figure 46 depicts the modified skid landing gear design meshed with 4487 S4R shell elements. To eliminate coupon testing, 977-3 epoxy from the previous analyses was substituted by a similar 356^{o} F cure 8552 epoxy resin matrix. Strength based failure allowable published for both IM7/8552 and AS4/8552 laminates were used. Table 11 shows strengths[25,38] for IM7/8552 and AS4/8552, as longitudinal tensile strength (X_T), transverse unidirectional tensile strength (Y_T), longitudinal compressive strength (X_C), transverse compressive strength (Y_C), in-plane shear strength (S_L).

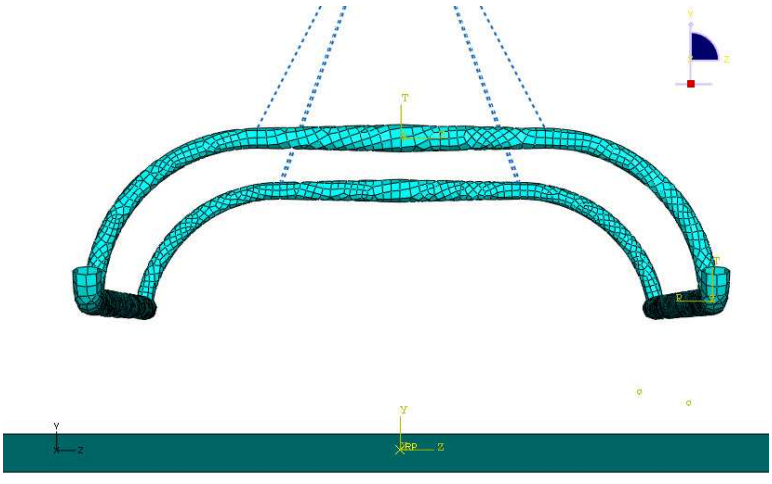

Figure 46. Modified Skid Landing Gear

Table 11. Laminate Strength Allowable

Allowable (MPa)	Composite Laminate	
	IM7/8552	**AS4/8552**
X_T	2724	2207
X_C	1690	1531
Y_T	111	81
Y_C	199.8	244
S_L	130.2	114

6.2 Strength based Failure Criteria

Tsai-Wu failure criterion was implemented in ABAQUS by requesting the output variable CFAILURE. The fail stress option was activated and strength based allowable mentioned above in Table 11 were inputted in the property card. As per ABAQUS convention, a value of $R \geq 1$ indicates failure. Stress states in the plies reported to have failed were extracted from ABAQUS and used with LaRC04 physics based failure criteria for fracture mode prediction. Equations 3-10 show criteria for the different fracture modes.

Matrix cracking under transverse tension ($\sigma_{22} \geq 0$) and in-plane shear

$$(1-g)\frac{\sigma_{22}}{Y_T} + g\left(\frac{\sigma_{22}}{Y_T}\right)^2 + \left(\frac{\sigma_{12}}{S_L}\right)^2 - 1 \leq 0 \tag{3}$$

$$(1-g)\frac{\sigma_{22}^{(m)}}{Y_T} + g\left(\frac{\sigma_{22}^{(m)}}{Y_T}\right)^2 + \left(\frac{\sigma_{12}^{(m)}}{S_L}\right)^2 - 1 \leq 0 \tag{4}$$

$$\sigma_{11} < 0, \, |\sigma_{11}| < X_C/2$$

In equations 3 and 4, g is the ratio of the fracture toughness of modes I and II. G_{Ic} and G_{IIc} values used are 277.4 J/m^2 and 787.9 J/m^2 respectively. The stress state with superscript m is in a reference frame transformed to align with the fiber misalignment angle. Details can be found in Camanho and Lambert's[25] work.

Matrix cracking under transverse compression (σ_{22} <0) and in-plane shear

$$(\frac{\tau_e^T}{S_T})^2 + (\frac{\tau_e^L}{S_L})^2 - 1 \le 0 \text{ , } \sigma_{11} \ge -Y_C \tag{5}$$

$$(\frac{\tau_e^{(m)T}}{S_T})^2 + (\frac{\tau_e^{(m)L}}{S_L})^2 - 1 \le 0 \text{ , } \sigma_{11} \le -Y_C \tag{6}$$

The subscript e implies effective shear stress, defined with respect to the angle between the plane perpendicular to the laminate mid-plane and the fracture plane. Details can be found in Camanho and Lambert's[25] work.

Fiber longitudinal failure in tension ($\sigma_{11} \ge 0$)

$$\frac{\sigma_{11}}{X_T} - 1 \le 0 \tag{7}$$

Fiber longitudinal failure in compression ($\sigma_{11} < 0$) and in-plane shear (fiber kinking)

$$\left\langle \frac{\left|\sigma_{12}^{(m)}\right| + \eta_L \sigma_{22}^{(m)}}{S_L} \right\rangle - 1 \le 0 \text{ , } \sigma_{22}{}^{(m)} < 0 \tag{8}$$

$$(1-g)\frac{\sigma_{22}^{(m)}}{Y_T} + g(\frac{\sigma_{22}^{(m)}}{Y_T})^2 + (\frac{\sigma_{12}^{(m)}}{S_L})^2 - 1 \le 0 \tag{9}$$

$$\sigma_{22}{}^{(m)} \ge 0, \left|\sigma_{11}\right| \ge X_C/2$$

The parameter η_L in equation 8 is the coefficient of influence and relates the in-plane shear strength to the longitudinal compressive strength. Details can be found in work done by Camanho et al[25]. It is to be noted that the equations 3-9 are functions of the fracture toughness ratio (g) for mode I and II crack propagation. The reason is as follows. Camanho et al[46] report that in-situ strengths of plies under transverse tension and in-plane shear are much higher as shown by experiment than the unidirectional strength of that ply. This is attributed to increase in strength when a ply is embedded between multiple of

plies of different fiber orientations. A fracture energy approach was suggested for prediction of matrix cracking under transverse tension and in-plane shear. The failure criterion as shown previously in equations 3-9, was based off experimental results obtained by Wu and Reuter[47] and a stress intensity factor based equation proposed by Hahn[48]. The equations when written in terms of the components of the stress tensor were shown in equations 3-9.

6.3 Level Landing Results

Level Landing Drop Test analysis shows that the regions of failure as well as the number of plies which are reported to have failed are larger in the AS4/8552 design. The IM7/8552 design shows desired performance with the exception that multiple plies, predominantly in the 45^{o}/-45^{o} fiber directions have undergone failure in specific elements along the metal-composite joint cross member region. Figure 47 and Figure 48 depict graphical results. Elements showing an R value $\geq$ to 1 in the IM7/8552 design are less in number compared to that in the AS4/8552 design. Hence, IM7 fiber is the final selection. PEEK matrix is suggested due to high fracture toughness. Matrix cracking under transverse compression and in-plane shear and fiber kinking under in-plane shear and longitudinal compression are the dominant modes of fracture. Figure 51 shows the acceleration plot. The difference is negligible despite lower stiffness of AS4 fiber. This is attributed to larger bends and increased plasticity. Load factors for IM7/8552 and AS4/8552 are 4.18 and 4.27. Despite increasing the aluminum radius to represent the actual AH-1S Cobra skid landing gear, 37% weight saving is obtained as shown in Table 12. Table 13 lists failed plies in the stacking sequence, ply orientations, element id's in which they were observed and the fracture mode that LaRC04 failure criteria report.

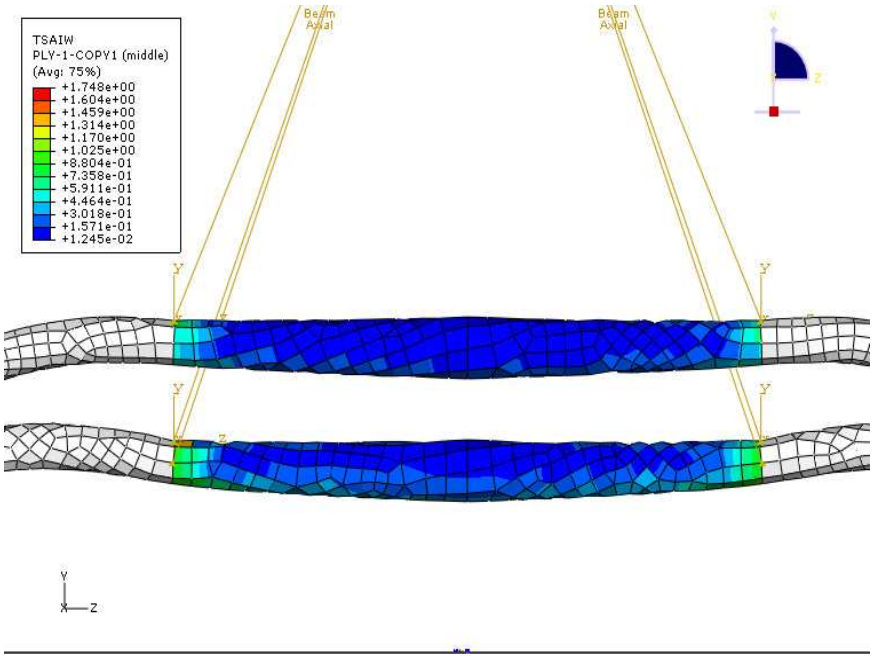

Figure 47. Tsai-Wu R Values– IM7/8552 Design

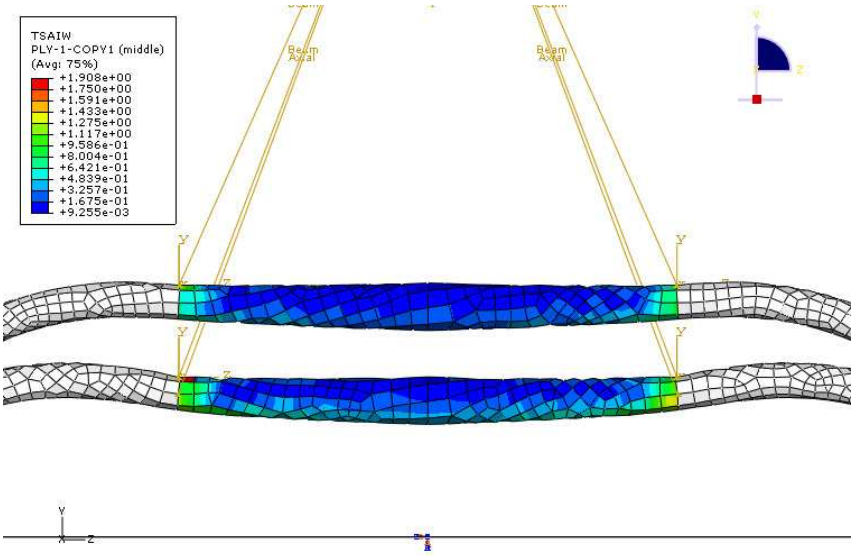

Figure 48. Tsai-Wu R Values – AS4/8552 Design

Testing will be essential to ascertain if results correlate well. The failed elements lie along the metal-composite joint. Thus, failure would be dictated by the bond and/or mechanical strength of the joint. Fracture mode predictions in this region will not be accurate. It is to be noted that corrosion concerns between IM7 carbon fiber and

Aluminum at the joint region may arise upon fabrication. It is to be noted that the color gradation in the figures as plotted by ABAQUS can mislead into interpreting the mid-span of the cross member beams as being under uniform stress. Figure 49 and Figure 50 show graphically and numerically, the normal stress values in ply 48 (45º) along the fiber direction. The first 12 elements are along the three column of elements highlighted on the rear cross member. The last 8 elements are those highlighted on the front cross member. As can be seen from the numerical output, the stress values are not uniform and also follow the correct pattern of bending with compressive stress in the elements on the top side of the beams and tensile stress in the elements on the bottom side. Thus, the results for the R ratio shown graphically in previous figures are not to be misinterpreted for uniformity along regions where the color distribution appears same.

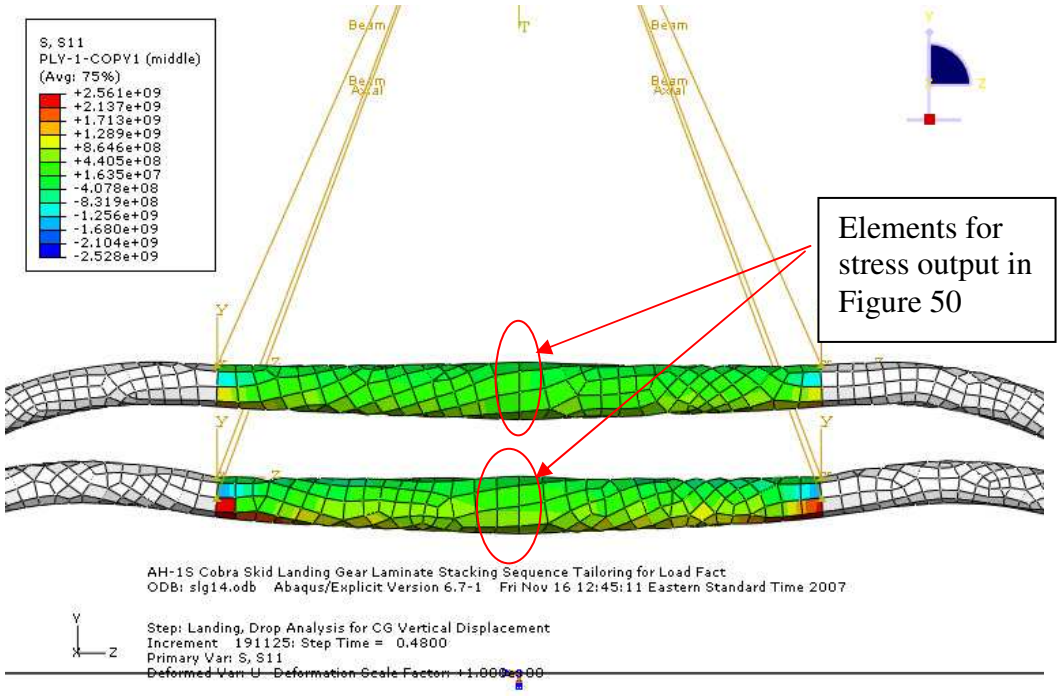

Figure 49. Cross Member Tapered Beam in Bending

```
******************************************************************************
Probe Values Report, written on Mon Apr 07 12:27:33 2008

Source
-------

   ODB: D:/ABAQUSTemp/slg14.odb
   Step: Landing
   Frame: Increment    191125: Step Time =   0.4800

Loc 1 : Integration point values at shell < composite #1 > < elset = ASSEMBLY_NEW
ASSEMBLY-1_CROSS BEAMS-1 > : fraction = 0.979167, Layer = 48

Probe values reported at integration points

  Part Instance  Element ID        Type        Int. Pt.          S: S11
------------------------------------------------------------------------------
  NEW ASSEMBLY-1         213         S4R               1    -312.279E+06
  NEW ASSEMBLY-1          37         S4R               1    -276.727E+06
  NEW ASSEMBLY-1          46         S4R               1    -211.969E+06
  NEW ASSEMBLY-1         223         S4R               1     19.2479E+06
  NEW ASSEMBLY-1          26         S4R               1     111.672E+06
  NEW ASSEMBLY-1          27         S4R               1     199.235E+06
  NEW ASSEMBLY-1         234         S4R               1     556.935E+06
  NEW ASSEMBLY-1           9         S4R               1      581.91E+06
  NEW ASSEMBLY-1          11         S4R               1     676.211E+06
  NEW ASSEMBLY-1         252         S4R               1     904.882E+06
  NEW ASSEMBLY-1          10         S4R               1     914.054E+06
  NEW ASSEMBLY-1          21         S4R               1      1.0113E+09
  NEW ASSEMBLY-1        3471         S4R               1    -236.234E+06
  NEW ASSEMBLY-1        3324         S4R               1    -214.788E+06
  NEW ASSEMBLY-1        3477         S4R               1     14.9453E+06
  NEW ASSEMBLY-1        3323         S4R               1     75.1798E+06
  NEW ASSEMBLY-1        3547         S4R               1     347.009E+06
  NEW ASSEMBLY-1        3322         S4R               1     367.887E+06
  NEW ASSEMBLY-1        3546         S4R               1     537.776E+06
  NEW ASSEMBLY-1        3315         S4R               1     517.403E+06


  Minimum                                          1    -312.279E+06
  at Element                                     213
  in Part Instance                        NEW ASSEMBLY-1

  Maximum                                          1      1.0113E+09
  at Element                                      21
  in Part Instance                        NEW ASSEMBLY-1
```

Figure 50. Cross Member Beam Element Stress Output

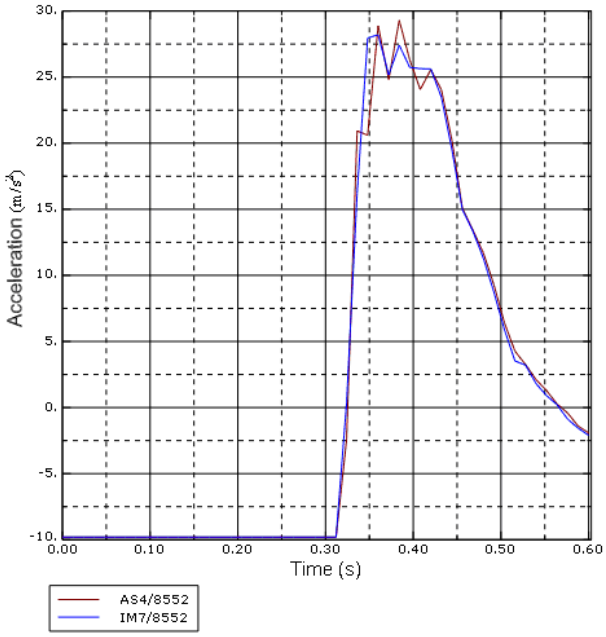

Figure 51. Load Factor Comparison

Table 12. Weight Saving

Design	Mass (kg)	Weight Saving
Aluminum 7075	52.74	---
IM7/8552	32.94	37.54%

Table 13. IM7/8552 Failures – Level Landing

Element	Ply	θ	Fracture Mode
32	41	90º	**A**
	43	-45º	No Failure
	48	45º	
48	37	90º	**A**
	41	90º	
	45	90º	
	47	-45º	No Failure
	48	45º	
55	2	-45º	
	6	-45º	
	10	-45º	
	42	0º	**A**
	46	0º	
68	40	45º	
	44	45º	
	48	45º	
72	39	-45º	
	43	-45º	**B & C**
	45	90º	

	47	-45º	
89	1	45º	**A**
	3	45º	No failure
	5	45º	**B & C**
	7	45º	**C**
	9	45º	
	11	45º	
	13	45º	
	15	45º	
	17	45º	
	19	45º	
	21	45º	
	23	45º	**B & C**
	26	45º	
	30	45º	No failure
	34	45º	**C**
	38	45º	**A**
	42	45º	
	44	45º	**C**
	46	45º	**A**
	47	45º	No failure
	48	45º	**D**
209	41	90º	**A**
	45	90º	
216	2	-45º	**B & C**
	3	0º	
	6	-45º	
	7	0º	
	10	-45º	
	11	0º	
	14	-45º	
216	15	0º	**B & C**
	18	-45º	
	19	0º	
	22	-45º	
	23	0º	
	26	0º	
	27	-45º	
	30	0º	**C**
	31	-45º	**B & C**
	34	0º	**C**
	35	-45º	
	38	0º	**A**
	39	90º	**C**
	42	0º	**A**
	43	-45º	**C**
	44	45º	No failure
	46	0º	**A**
	47	-45º	**D**

	48	45º	No failure
227	36	45º	**C**
	40	45º	
	41	90º	**B & C**
	44	45º	**C**
	45	90º	**B & C**
	48	45º	
240	43	-45º	**A**
	47	-45º	
3302	30	0º	**C**
	34	0º	
	38	0º	**A**
	42	0º	
	46	0º	

A - Fiber Kinking, In-Plane Shear
B - Matrix Cracking, In-Plane Shear / Compression
C - Fiber Kinking, Longitudinal Compression
D - Matrix Cracking, Transverse Tension

6.4 Load Factor Optimization

The IM7/8552 design was used for laminate stacking sequence tailoring with load factor under limit loads being the objective function. In lieu of conducting a landing analysis, a drop mass to total mass ratio of 0.9075 (W_e = 3300 kg) was used. Only level landing drop analyses were conducted. Five laminate families, namely, $[0/90/\theta/-\theta]_{6s}$, $[0_2/\theta/-\theta]_{6s}$, $[0_2/90_2/\theta/-\theta]_{4s}$, $[0_2/90_2/(\theta/-\theta)_2]_{3s}$ and $[0/\theta/-\theta]_{8s}$ were considered with θ being a single variable for parameterization. Parametric study was conducted within ABAQUS by creating multiple input files in conjunction with a python script file (.psf). Tsai-Wu criterion was used to impose strength constraints.

6.5 Optimization Results

Table 14 lists load factors computed for all five laminate families. $[0/\theta/-\theta]_{8s}$ results in load factors lower than 4.50 for four θ/−θ values, more than for any other laminate family. Three out of five laminates result in lowest load factor, within that

specific laminate family, with θ/−θ values of 75º/-75º. The second set of lowest load factors result in laminates, in four out of five families, with θ/−θ equaling 45º/-45º. However, all 48 plies undergo failure in the laminates with θ/−θ > 45º/-45º and the damage extends beyond the column of elements along the metal-composite joint. Thus, 6 of the 12 stacking sequences, four of them having lowest load factors (<4.50) within that specific laminate family, were eliminated. While a significant number of plies show failure in laminates with θ/−θ equaling 45º/-45º, the elements and thus the failure region are restricted to the metal-composite joint. Laminates with 15º and 30º orientations show lesser number of ply failures. Most failures occur in the elements in the metal-composite region. Figure 52 and Figure 53 show the cross member failures and commonly reported failed elements. Joining metal-filament wound composites with adhesive bond and mechanical fasteners is suggested. Stresses in these regions would be driven by the bond/fastener strength. Hence, results for the elements in that region were neglected for now. Failure in elements outside this region was considered sufficient to eliminate that specific design case. Figure 54 shows the highest transverse shear stress, in ply 25, as 91 MPa, lower than the interlaminar shear strength (ILSS) of 137 MPa, suggesting that delamination may not occur. Final laminate selected is $[0/90/45/-45]_{6s}$ with optimized load factor 4.17g. Figures 53-57 show load factors for θ/−θ in each laminate family.

Table 14. Laminate Family Load Factors

θ	1	2	3	4	5
0º	4.59	4.57	4.54	4.53	4.62
15º	4.55	4.47	4.46	4.55	**4.33**
30º	4.65	**4.39**	4.68	4.65	4.52
45º	**4.17**	4.42	**4.21**	**4.18**	**4.25**
60º	4.52	4.69	**4.27**	4.51	**4.18**
75º	**4.06**	**4.13**	4.43	**4.07**	**4.26**
90º	4.52	4.54	4.53	4.52	4.62

Note: 1 = $[0/90/\theta/-\theta]_{6s}$

2 = $[0_2/\theta/-\theta]_{6s}$

3 = $[0_2/90_2/\theta/-\theta]_{4s}$

4 = $[0_2/90_2/(\theta/-\theta)_2]_{3s}$

5 = $[0/\theta/-\theta]_{8s}$

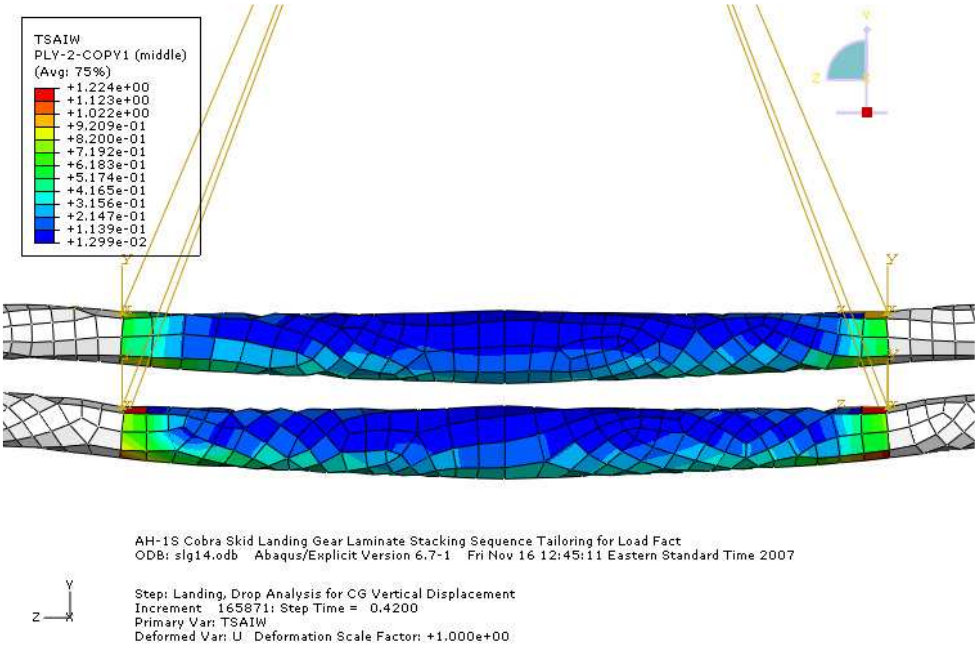

Figure 52. Cross Member Failures

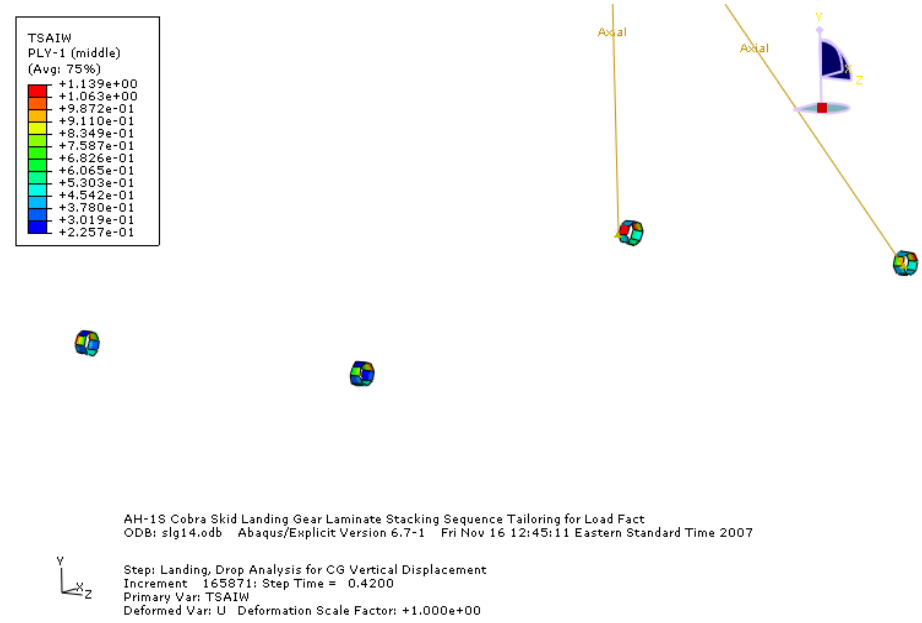

Figure 53. Commonly reported Failed Elements

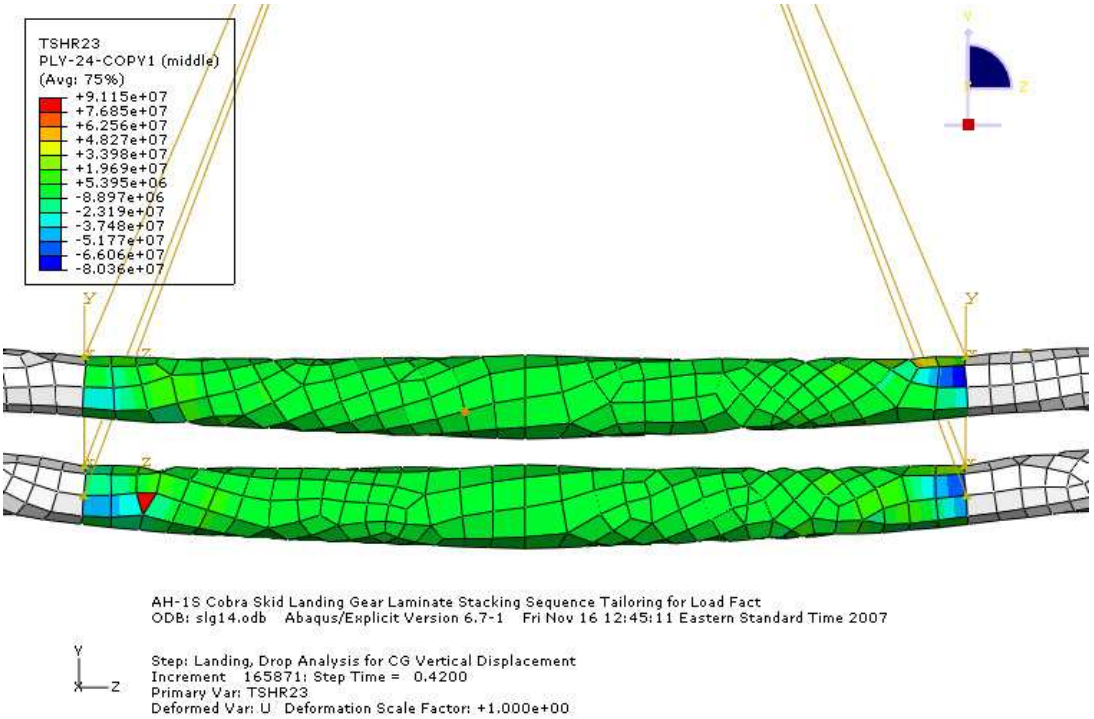

Figure 54. Transverse Shear Stress – Ply 25

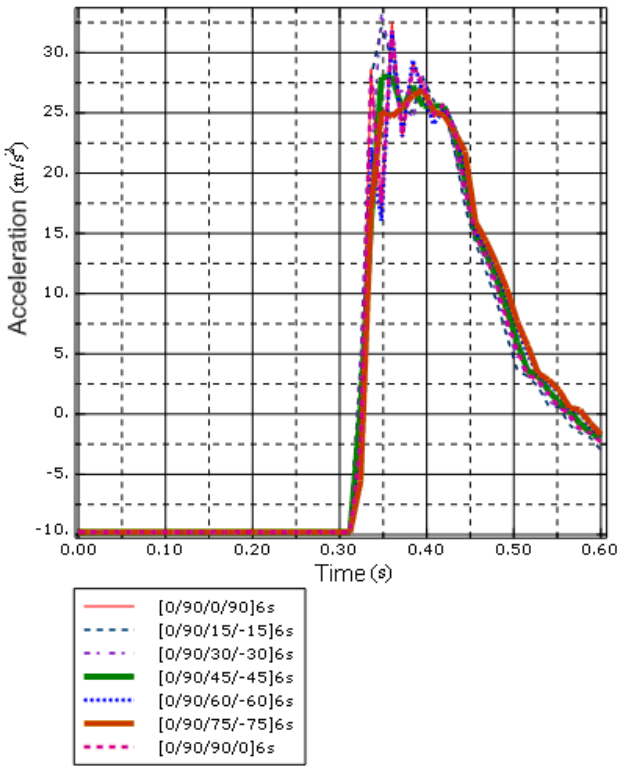

Figure 55. Load Factors – $[0/90/\theta/-\theta]_{6s}$

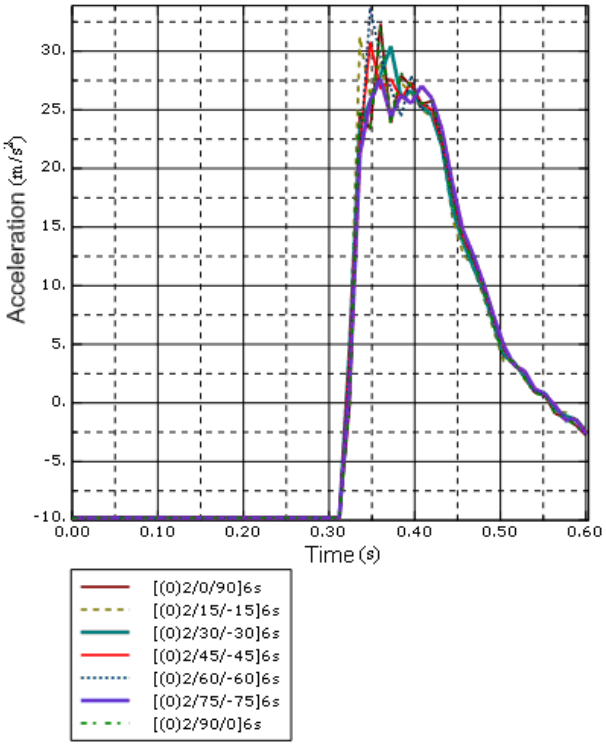

Figure 56. Load Factors – $[0_2/\theta/-\theta]_{6s}$

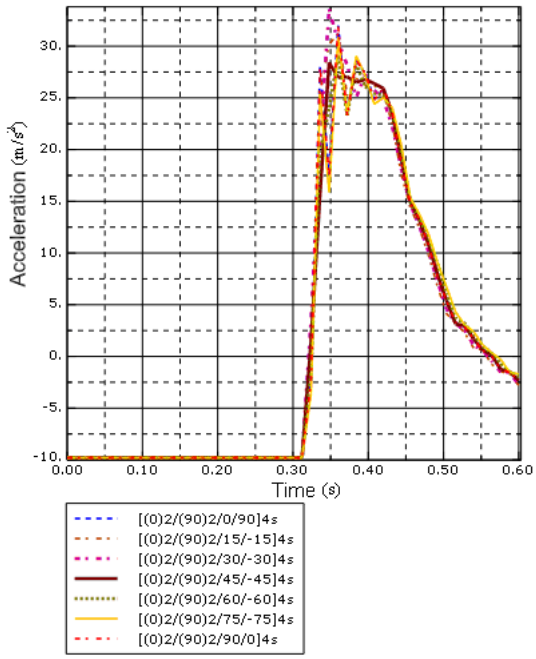

Figure 57. Load Factors – $[0_2/90_2/\theta/-\theta]_{4s}$

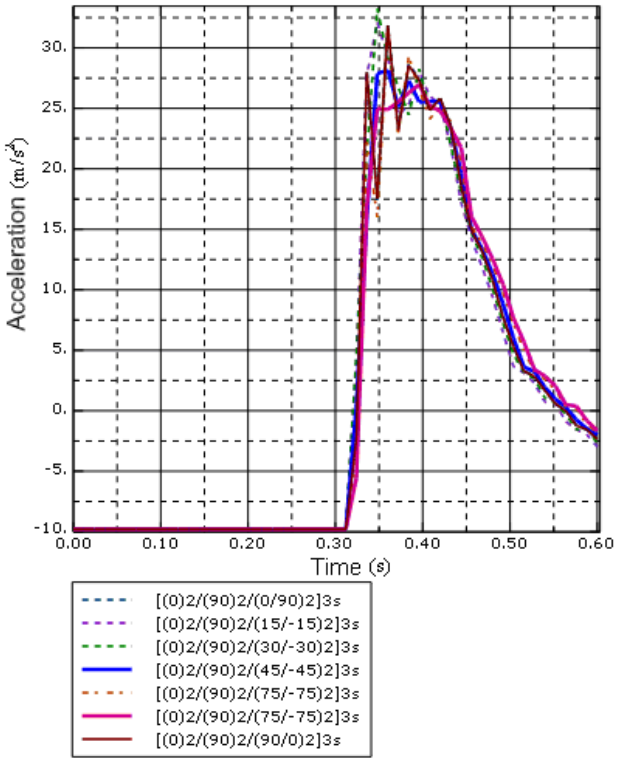

Figure 58. Load Factors – $[0_2/90_2/(\theta/-\theta)_2]_{3s}$

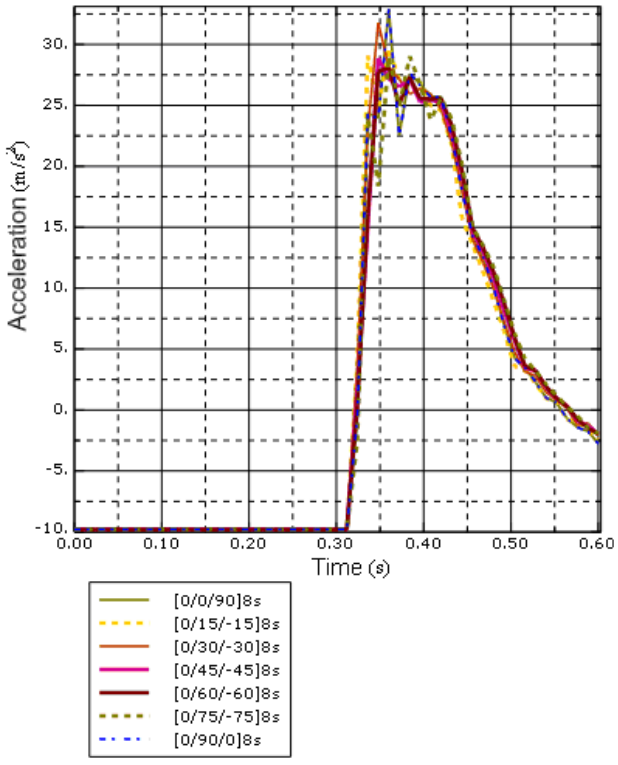

Figure 59. Load Factors – $[0/\theta/-\theta]_{8s}$

6.6 Level Landing with Drag (Run-On) Condition

Level landing with drag (run-on) condition analysis was conducted with the tailored laminate to investigate the resulting load factor and strength performance. Figure 60 shows the acceleration plot. The final load factor is 3.70. The number of failures is lower than that for level landing scenario and rolled attitude landing scenarios. Figure 61 shows the failure region. Figure 62 shows the highest transverse shear stress observed, in ply 21, and equals 72 MPa lower than the allowable ILSS of 137 MPa.

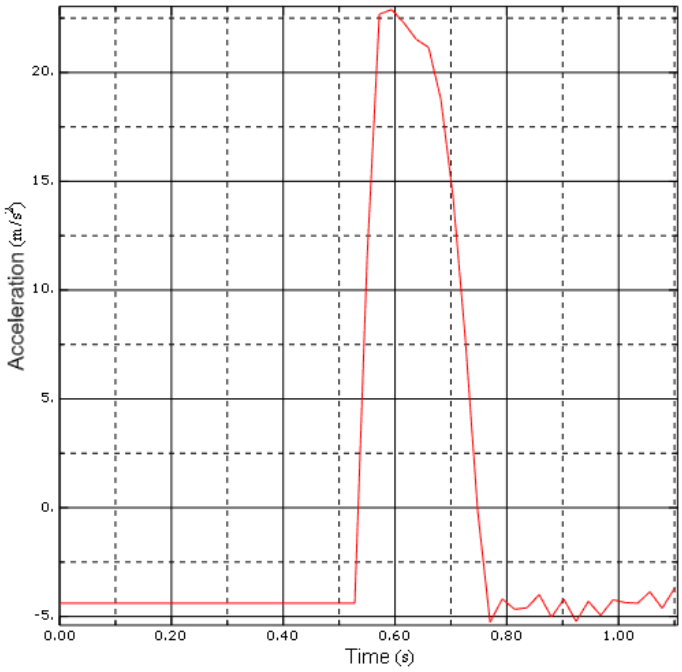

Figure 60. Level Landing with Drag (Run-On) Condition Acceleration

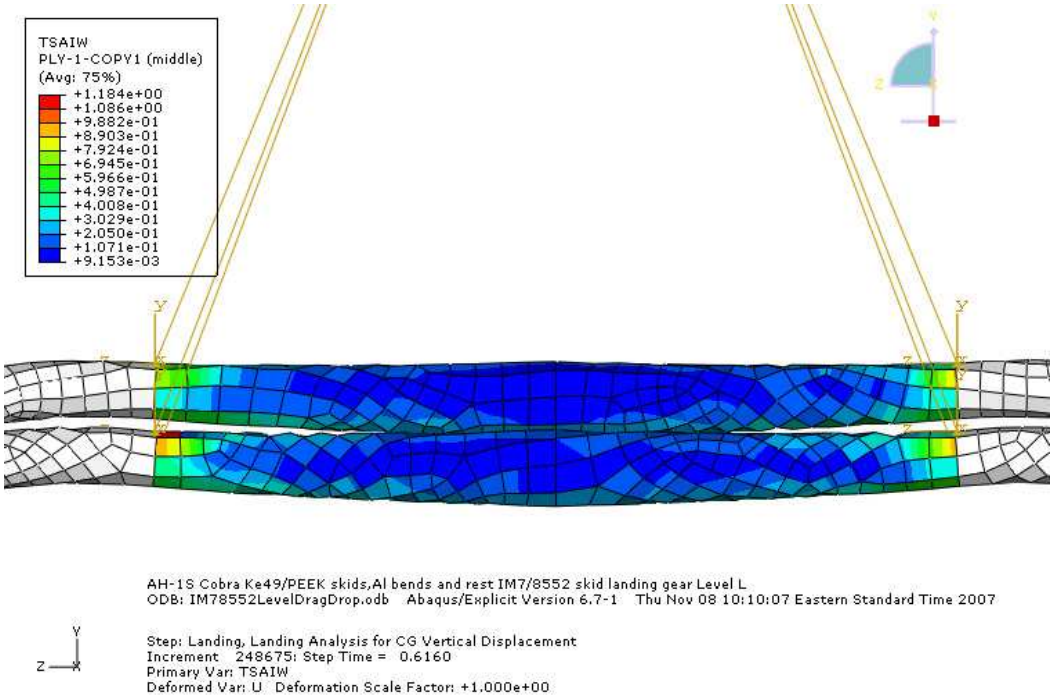

Figure 61. Failures for Level Landing with Drag

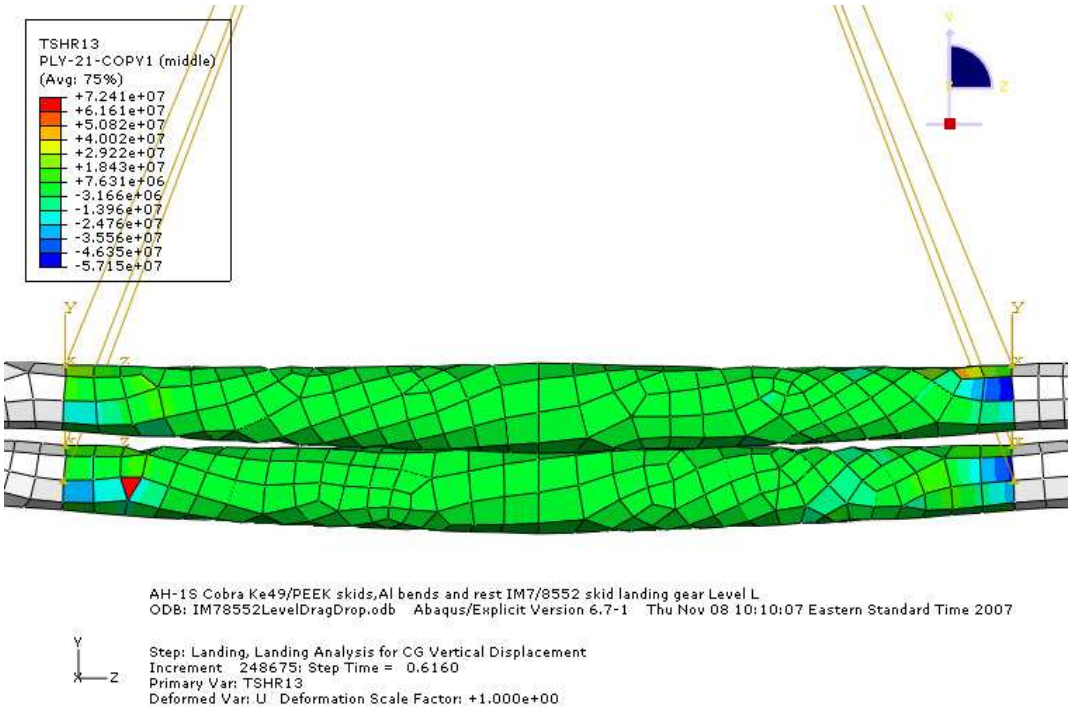

Figure 62. Transverse Shear Stress – Ply 21

6.7 Rolled Attitude Landing

Figure 63 shows the acceleration plot. Load factor obtained is 3.51. The number of failures is lower than for level landing but higher than that for level landing with drag (run-on) condition. Figure 64 shows the failure region. Highest transverse shear stress, in ply 24, shown in Figure 65, is 79 MPa and lower than ILSS of 137 MPa.

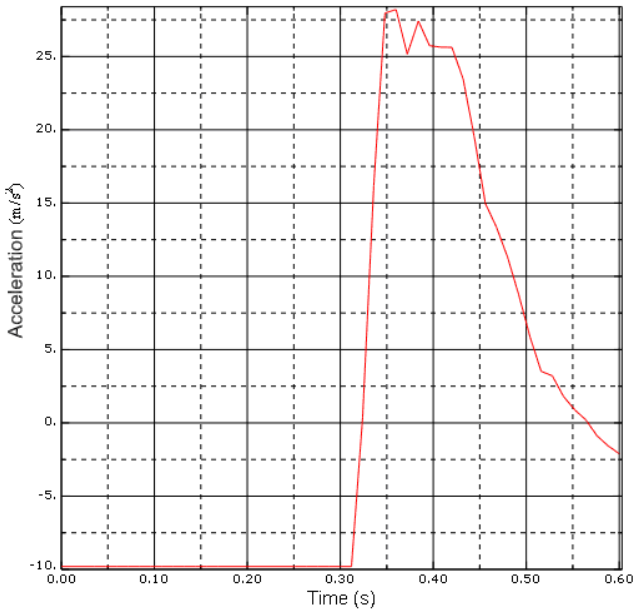

Figure 63. Rolled Attitude Landing Acceleration

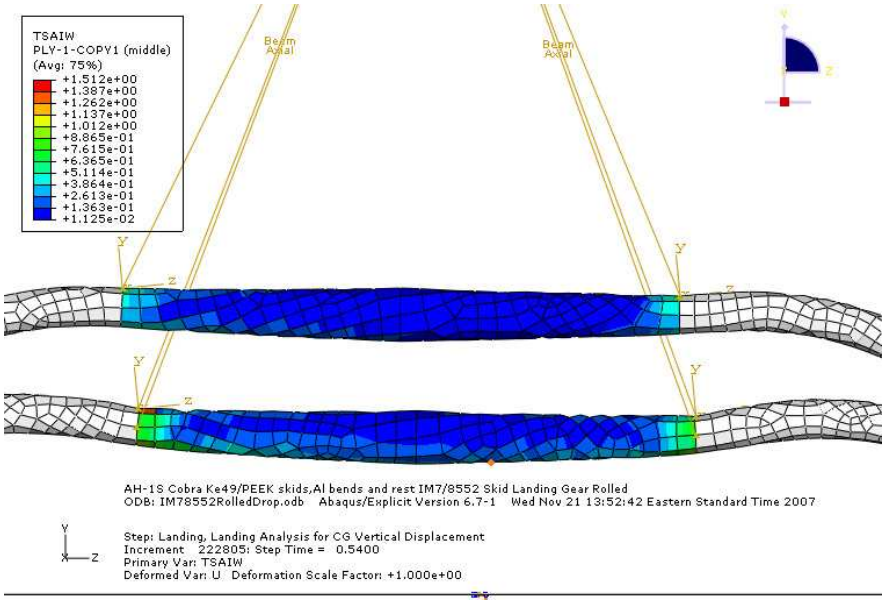

Figure 64. Failures for Rolled Attitude Landing

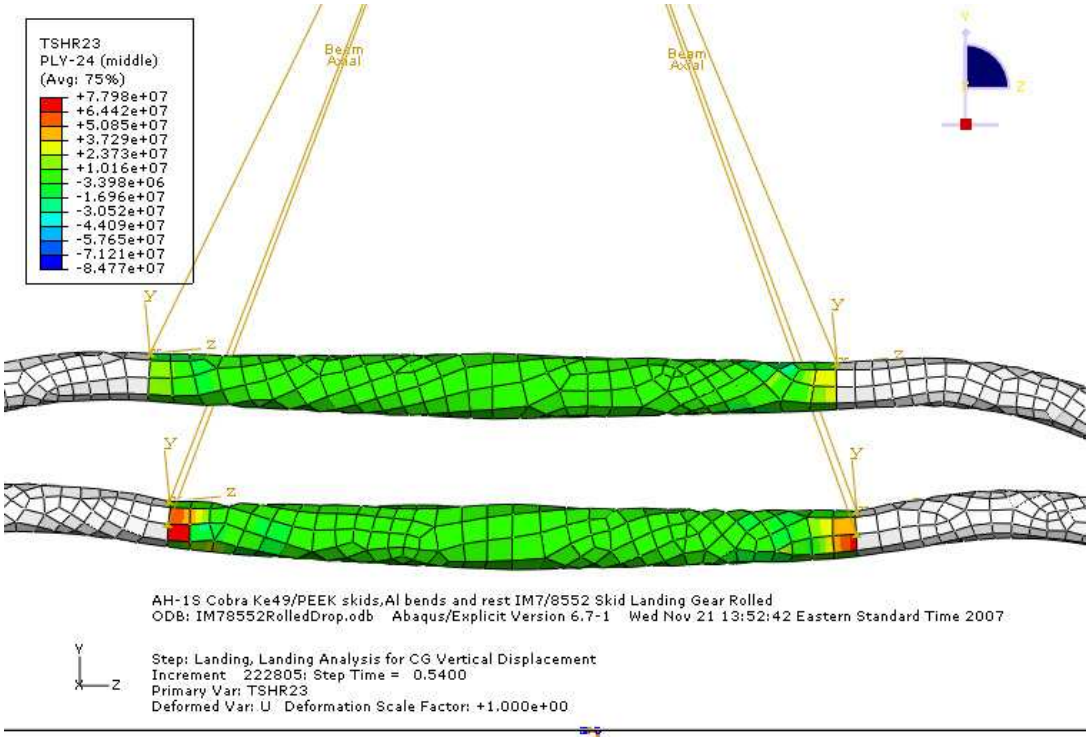

Figure 65. Transverse Shear Stress – Ply 25

6.8 Hybrid Metal-Composite Joining

The motivation for the different joining methods comes from crash and energy dissipation mechanisms during crash landing. It is desired to trigger crush during bending in the composite regions and investigate the magnitude of energy dissipation. In order for the fracture, regardless of the mechanism, to propagate through the composite beams and thus dissipate energy in the form of damage, the metal-composite joint will have to be adequately strong as well as stiff. A failure of this joint, even under crash loading, will not be permissible as it will cause the skid and metal cross member radii to slide out and fall apart without dissipating any energy. Mamalis et al[2] have shown through experiment that crushing during bending occurs in composite beams, clamped at one end and also simply supported along the span, when subjected to moments/torques. Hence, one method analyzed was inclusion of an epoxy adhesive bond between an aluminum metal

plug and the tapered composite beams. Figure 66 shows an FE model of this joint with 3485 shell (S4R), 80 solid (C3D8R) and 80 cohesive (COH3D8) elements

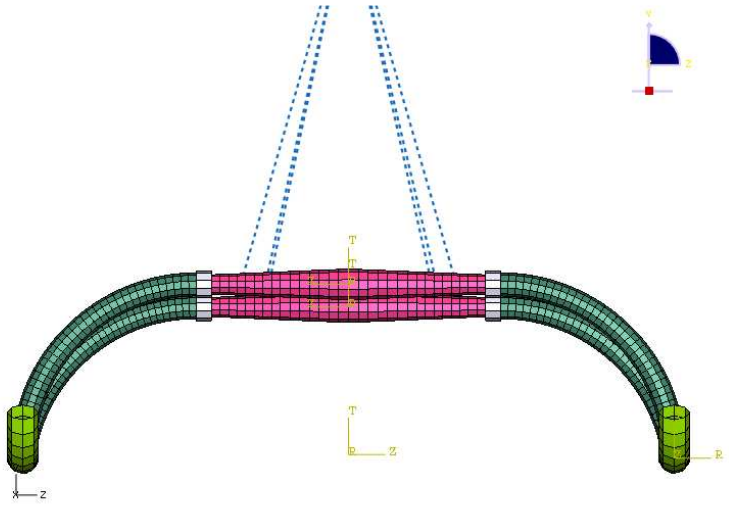

Figure 66. Adhesively Bonded Hybrid Joint

A second method suggested is filament winding the metal and composite regions together. The advantage in this would lie in the stiffness provided to the region. Gray and Moser[39] state that beyond 5000 με, fiber stiffening up to 10% can occur in filament wound composites. The key in this joining method would again lie in ensuring that metal and composite interface, which would have resin matrix and an injected bonding material, do not catastrophically fail.

A third method suggested includes internal or external threading on the metal plug which is filament wound with the composite tube. This threaded region would mate with the corresponding threaded region of the aluminum cross member bend radii. Finally, the most practical method suggested is that of filament winding the metal and composite regions together with an injected adhesive and then bolting this piece onto the metal cross member bend radii. Adequate bolt strength will have to be exhibited to ensure that the

beam ends do not fail and fracture in the composite can propagate over the beam. Finite element analysis for two of these methods was done and is discussed next.

6.9 Finite Element Model Modifications

A single skid tube and cross member radii bend part created by merging instances of the skid tubes and radii, and tapered cross member beam parts, was meshed with part dependency to create an orphan mesh part. All the geometry was modeled using S4R shell elements. The shell element ends of the cross member radii, which connect to the composite tapered cross member beams, were then offsetted to form 2 layers of C3D8R solid elements. This region, seen in Figure 66 in grey color, represents the aluminum plug within which the composite beam would be adhesively bonded. A single layer of finite thickness cohesive elements (COH3D8) was created by offsetting the solid elements. The geometric thickness of these elements was modeled as 33 microns, same as the actual adhesive bond line constitutive thickness. Node sharing and multi-point constraints (MPC) in the form of Tie constraints were prescribed between the aluminum shell radii and aluminum solid plug, the aluminum solid plug and the adhesive cohesive elements and the composite shell tapered beams and the cohesive elements respectively. The adhesive was modeled using the Continuum approach with linear elastic isotropic properties prescribed. An elasto-plastic law was also inputted and was based on work done by Charalambides et al[40]. For the filament wound metal-composite analysis, no adhesive bond was simulated. Node sharing and Tie constraints between the aluminum plug and the composite were prescribed. Composite shells were modeled as bottom surfaces for this case and top surfaces for the adhesive bond analysis.

6.10 Adhesive Bond Failure Criteria

Equivalent Mises stress and the six stress components were extracted from ABAQUS using MISESMAX and S output variables. The adhesive bond in the first model was modeled with an elasto-plastic law. Charalambides et al[40] have shown that polymeric materials are not well represented by the classic Von Mises yield criterion as their yield strengths vary in tension and compression. Thus, Bauschinger effect would need to be accounted for by including a user defined yield criterion in ABAQUS, in the future. Equivalent stress (MISESMAX) in excess of 65 MPa was considered as failure stress for bond strength.

6.11 Results

Adhesive Bond Joint

Level landing drop test was simulated with TIE multi-point constraints (MPC) between the following connections; solid aluminum plug elements (C3D8R) and solid cohesive bond elements (COH3D8), cohesive bond elements and composite shell elements (S4R), solid Al elements and shell Al cross member radii elements.

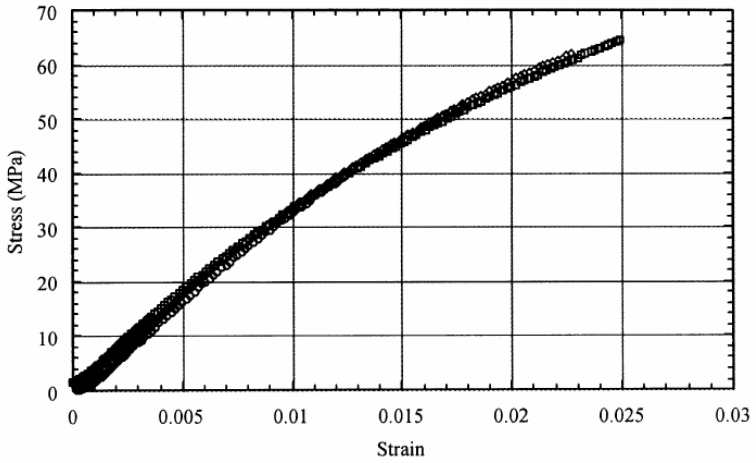

Figure 67. Redux 319 Stress Strain Curve[40]

Figure 67 shows the stress strain plot for Redux 319 as published by Camanho and Matthews[41] and taken from Charalambides et al's[40] work. Elasto-plastic law was inputted based on this plot. Redux 319 isotropic properties are shown in Table 15. Figure 68 shows the MISESMAX equivalent stress which has exceeded 65 MPa in most of the cohesive elements. Figures 67-69 show the individual stress components. It can be inferred that failure occurs in the cohesive bond primarily in tension. Though Charalambides et al[40] have quoted experimental shear strength allowable of 60 MPa, lap shear strength greater than 35-40 MPa is generally not available as concluded from literature survey. Thus, failure in lap shear is also a concern, considering that the highest shear stress reached is 38 MPa. Progressive damage modeling of the composite and/or adhesive may alleviate these stresses significantly. Implications of progressive damage in composites, such as loss of landing gear rebound and the time at which the landing gear would reach zero velocity and come to rest after progressive damage are unknowns. Under limit loads, complete fracture is not permissible. In progressive damage modeling, so long as the elements have residual strength and gravity continues to act through the time step, the analysis shall continue. The landing gear will deform and result in stressing of the bondline and subsequent failure. Thus, bond failure prediction by progressive damage modeling would need test data regarding the time duration after which the landing gear settles into static equilibrium, in order evaluate bond strength, at that time step. A polymeric material yield criterion incorporating Bauschinger effect should alleviate stresses due to higher yield stress in compression. This may eliminate lap shear strength concerns. Tensile stress still may be of concern. Simply bonding the composite and metal plug may be insufficient. Filament winding would be essential.

Table 15. Redux 319 Epoxy Adhesive

E (GPa)	ν	σ^T_y (MPa)	σ^T_c (MPa)
3.78	0.4	34.7	45.1

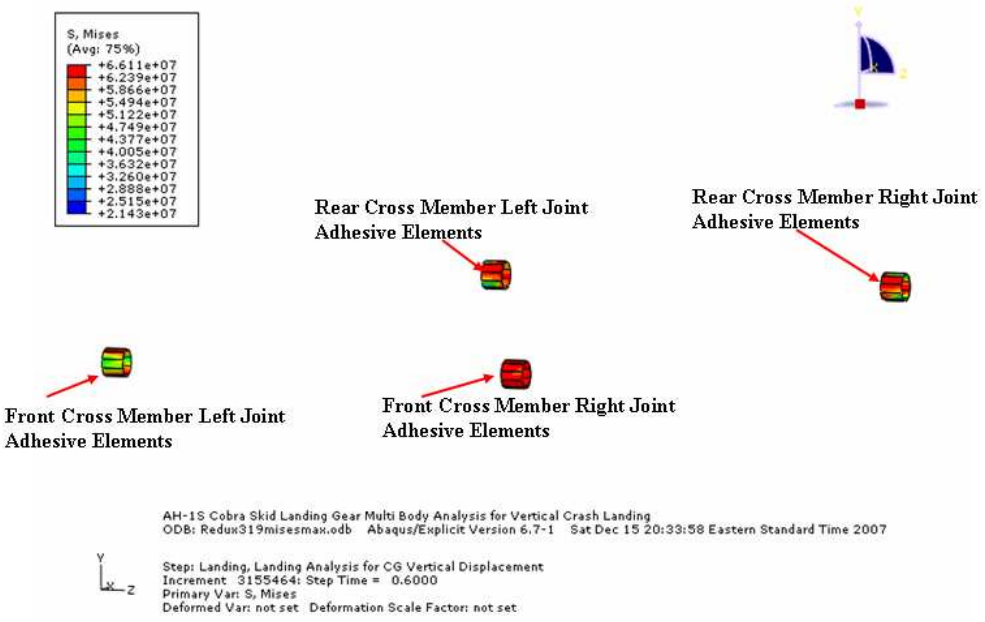

Figure 68. MISESMAX Equivalent Stress

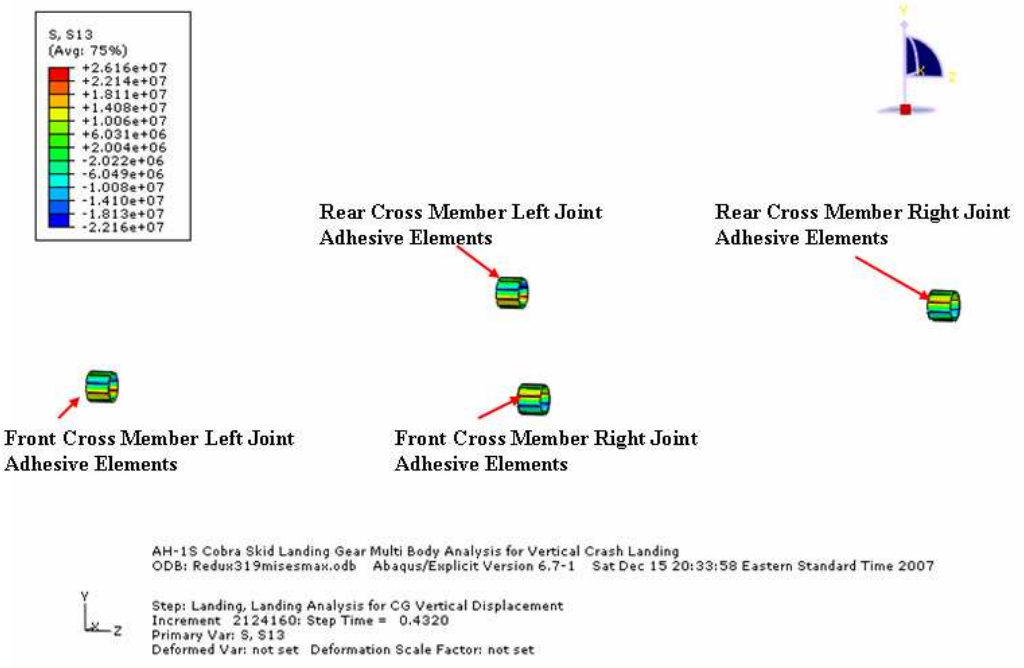

Figure 69. Shear Stress (τ_{13})

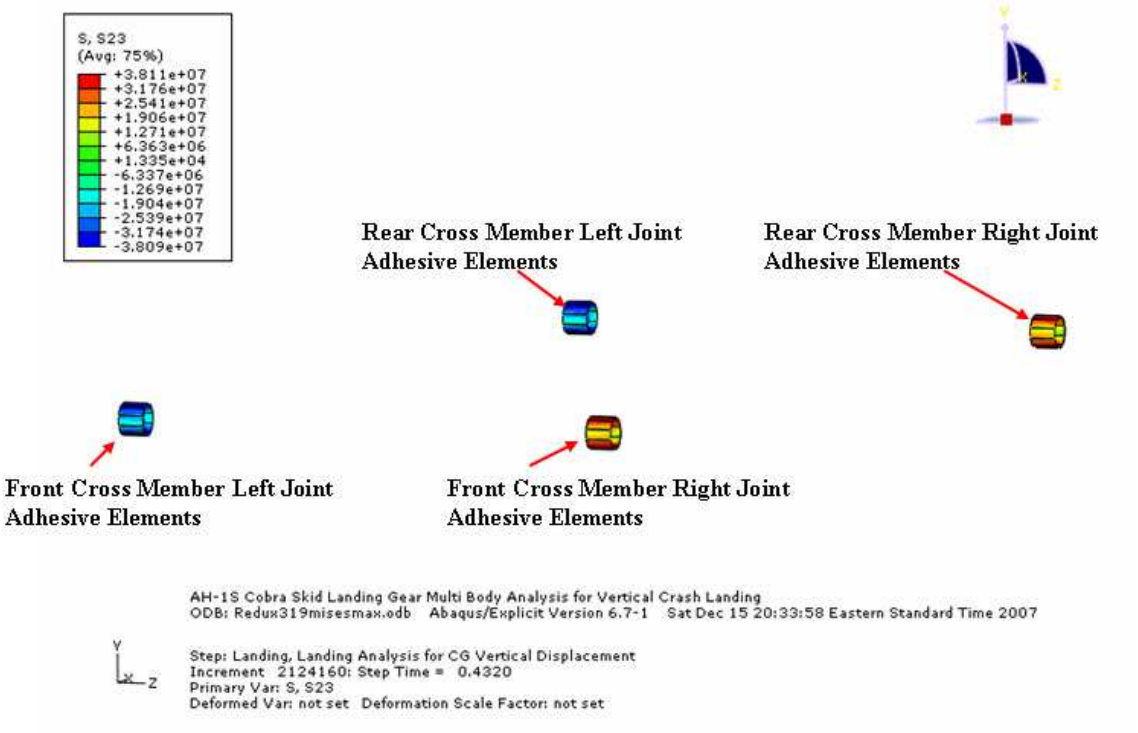

Figure 70. Shear Stress (τ_{23})

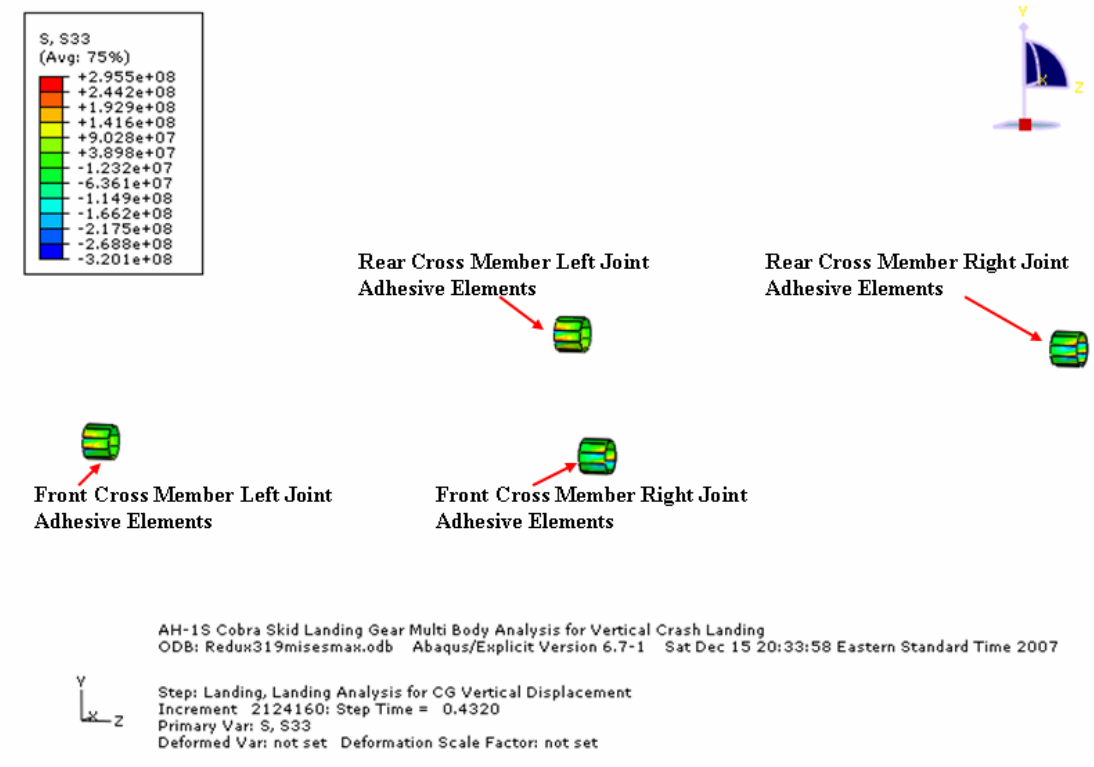

Figure 71. Tensile Stress (σ_{33})

Filament Wound Joint

Filament winding was simulated by approximating the properties in the form of laminate theory. Every θ/−θ winding shall be overlapped by a -θ/θ winding and thus balance and symmetry can be assumed. The adhesive was not simulated in this analysis. The solid aluminum plug elements (C3D8R) and composite shell elements (S4R) were tied together. The aluminum plug is modeled inside the filament wound composite. Mechanical fasteners were not modeled at this stage. Figure 72 shows the mesh of 5484 elements, solids and shells combined. Figure 73 shows Tsai-Wu failure criterion R values in ply 48 over the composite tapered cross member beams. **No failure** is reported in any plies, during level landing. Figure 74 shows the acceleration plot with load factor computed as 3.60g. Further analysis was conducted on this configuration for level landing with drag (run-on) condition and rolled attitude landing scenarios. Figure 75 shows the transverse shear stress values have exceeded 137 MPa in several elements. This is an indication of the onset of delamination in laminates. However, delamination allowable for filament wound composites may be different than that for the IM7/8552 composite laminate. Also, fiber stiffening with increase in strain was not accounted for as a material non-linearity in the analysis. Thus, delamination may not actually occur.

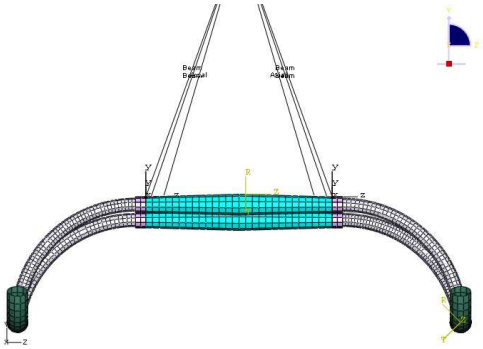

Figure 72. Filament Wound Hybrid Joint

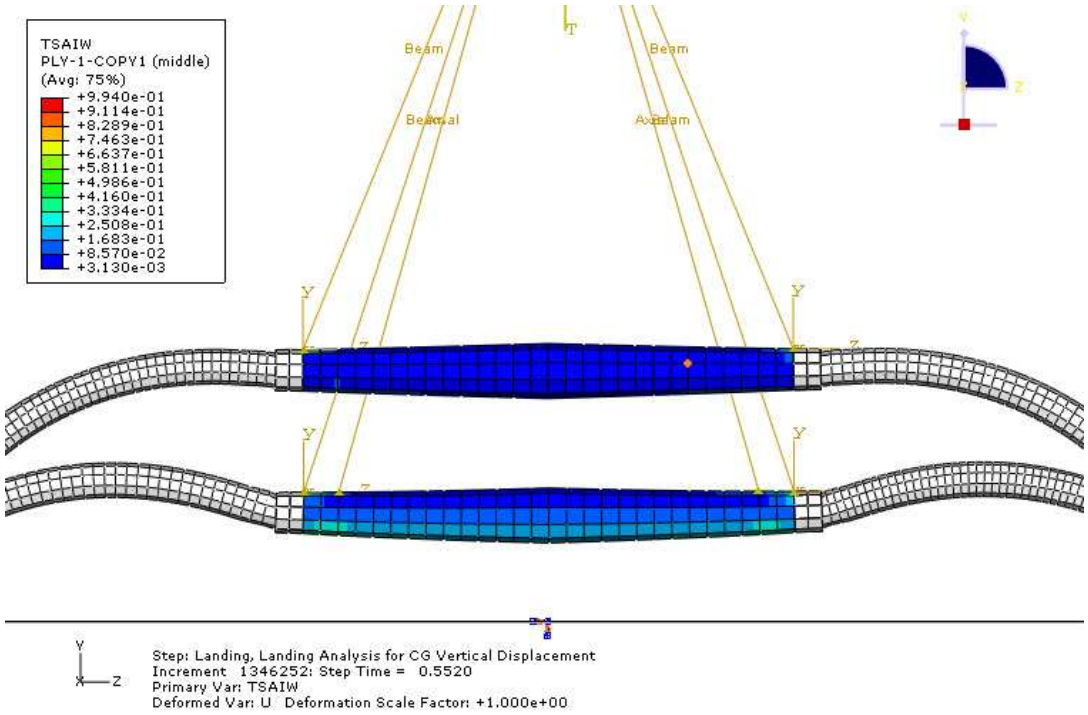

Figure 73. Tsai-Wu R values – Ply 48 (45º)

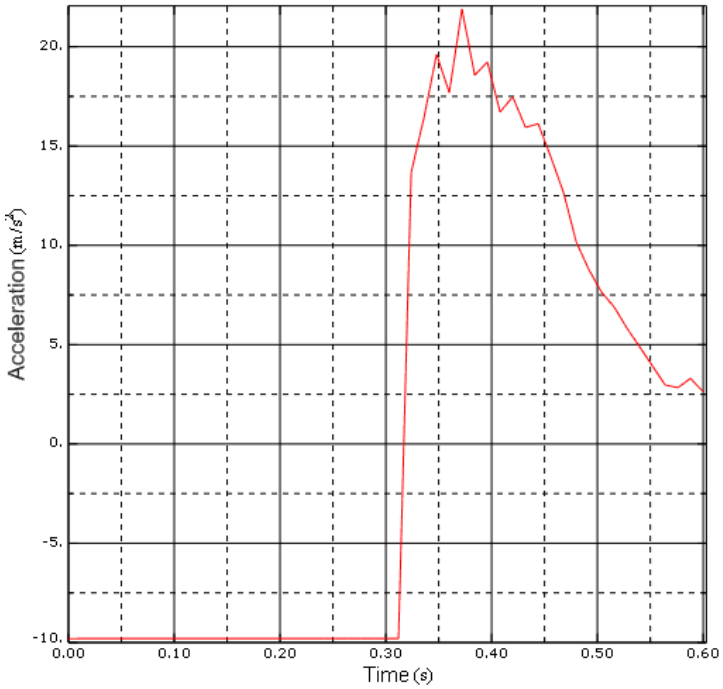

Figure 74. Level Landing Acceleration Plot

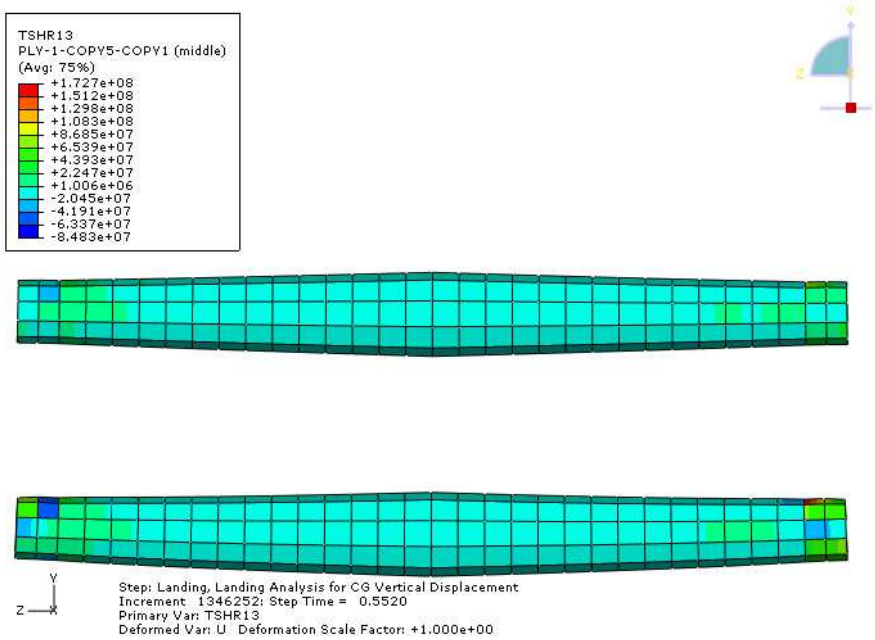

Figure 75. Transverse Shear Stress – Ply 24

6.12 Level Landing with Drag (Run-On) Condition

Figure 76 shows R values for ply 48. No failure is reported in any plies during this analysis. Figure 77 shows the acceleration plot with load factor as 3.37g. Figure 78 shows transverse shear stress, in ply 24, as 141 MPa which exceeds ILSS of 137 MPa.

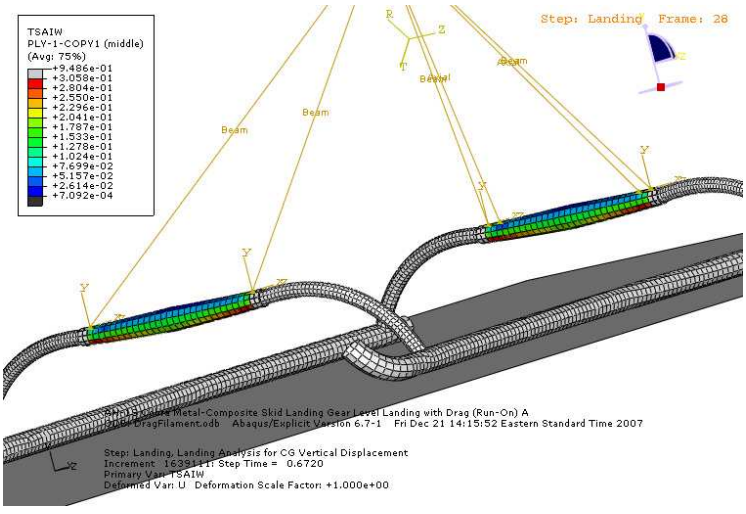

Figure 76. Tsai-Wu R values for Level Landing with Drag (Run-On) Condition

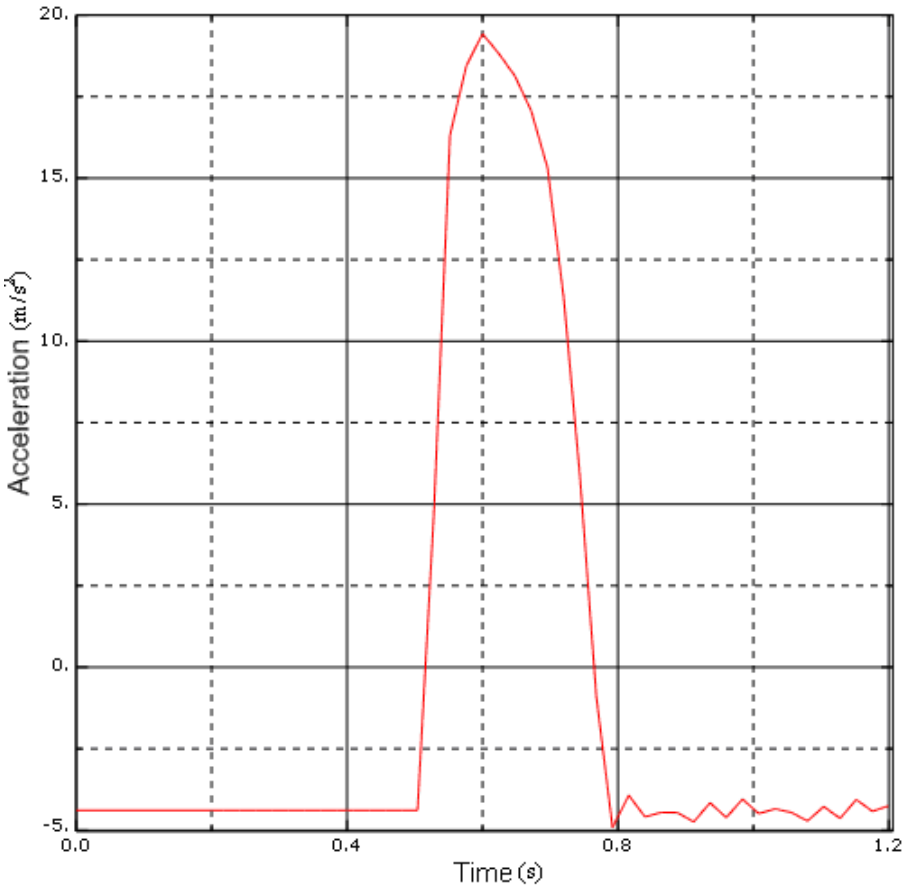

Figure 77. Level Landing with Drag Acceleration

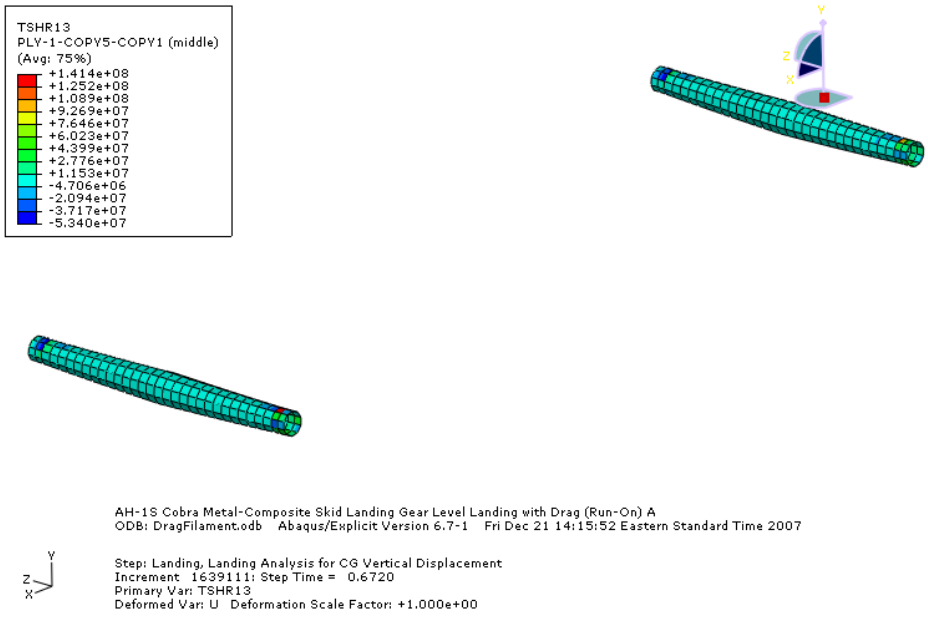

Figure 78. Transverse Shear Stress

6.13 Rolled Attitude Landing

Very few element failures were reported in this case. Figure 79 shows R values for ply 48. Figure 80 shows the highest transverse shear stress, in ply 24, as 102 MPa. Figure 81 shows the acceleration plot. The load factor obtained is 3.14g.

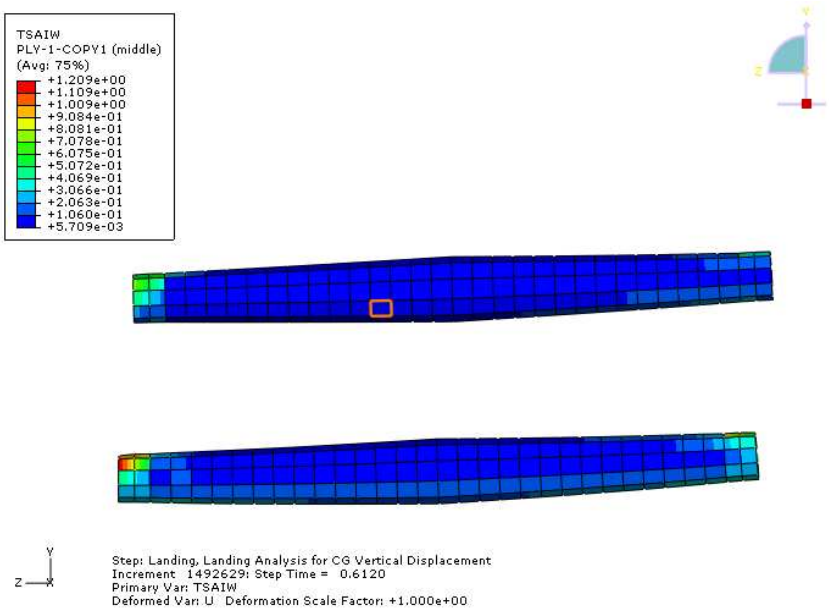

Figure 79. Tsai-Wu R values

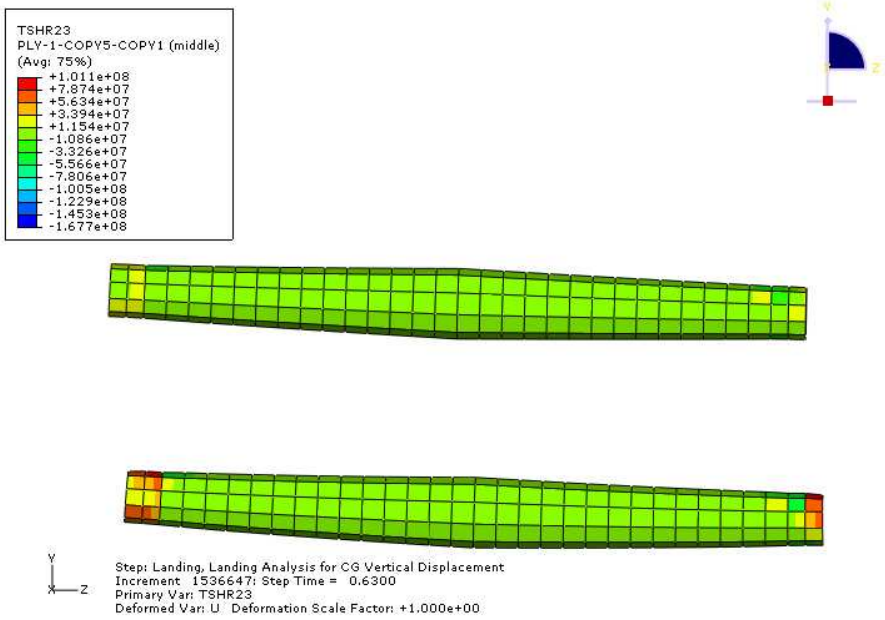

Figure 80. Transverse Shear Stress

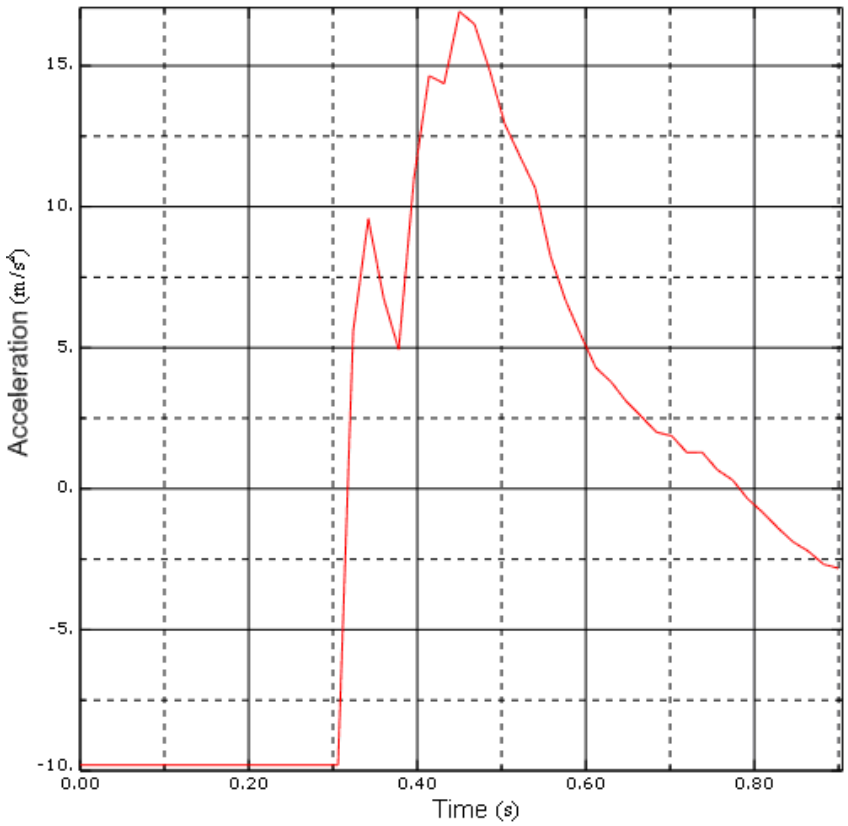

Figure 81. Rolled Attitude Landing Acceleration

6.14 Summary

IM7/8552 shows better performance than AS4/8552. Tsai-Wu failure criterion predicts failed plies mostly within the metal-composite joint region. LaRC04 failure criteria predict the dominant fracture modes to be matrix cracking in compression and in-plane shear and fiber kinking under in-plane shear as well as longitudinal compression. Incorporation of load factor optimization based on single variable parameterization with strength based constraints resulted in an optimized load factor value of 4.17g for quasi-isotropic $[0/90/45/-45]_{6s}$ laminate. Inclusion of 75° orientation in the stacking sequence results in lowest load factors but with increased amount of damage. $[0/\theta/-\theta]_{8s}$ laminate family is promising for low load factors for multiple values of θ. Despite increasing the

size of the aluminum radius bend, which in the modified form represents the actual AH-1S Cobra skid landing gear more accurately, 37% weight saving is still obtained. Failures being in the metal-composite junction, it would be necessary to test and model the type of mechanical connection before predicting the stresses.

A single piece metal plug at the end of the aluminum radius with adhesive bonding between the plug and tapered composite cross member beams was suggested. The perceived advantage of this is as follows. Mamalis et al[2] have shown through experiment that a beam clamped at one end and supported at a spanwise location, when subjected to moments/torques, can fail in crushing mode. Thus, a metal plug, either one piece with the aluminum radius or welded to the end of the aluminum radius can suit as the clamped end when the tapered cross member is adhesively bonded to it. The fuselage connection point on the tapered cross member would then serve as the second spanwise support. It is a hypothesis that such an arrangement may be helpful for producing crush in the composite tapered beam under crash loads, provided the bond strength is adequate and fracture can sufficiently propagate through the composite beam. A second method suggested is mechanically fastening the aluminum bend region and metal-composite filament wound beam by bolts. The composite fracture would propagate provided the bolts do not fail. This could provide damage dissipation energy in addition to the metal plastic dissipation and enhance crashworthiness. Thus, the joining method would dictate failure in this region.

Adhesive bond between the composite tapered cross member beams and aluminum, analyzed with Redux 319 epoxy adhesive, did not show sufficient strength even under limit loads. Filament wound metal-composite joint shows adequate strength

and is hence recommended. An adhesive can be injected when filament winding the metal and composite pieces together. The joint will be more complex than a regular adhesive bond with substrates on either side. Thus, prediction of this joint strength will have to be done based upon testing and detailed modeling. It may even be possible to include threading on the interior of the metal plug which is filament wound and have external threads on the cross member bend radii. Thus, a tight fit can be obtained while simplifying assembly.

Epoxy adhesive and thermoset adhesives were the only bonding materials found in literature with relatively high strengths, particularly in lap shear. Despite including a typical elasto-plastic constitutive law for the adhesive, tensile failure commenced prior to the landing gear's settling down. Filament winding of the metal-composite with bolt fasteners appears to be the most suitable methodology for the metal-composite joint. The bolt strengths, damage propagation during crash and energy dissipation due to plastic dissipation as well as damage will need to be addressed to ensure that the landing gear is crashworthy.

6.15 Conclusions

The following conclusions were drawn:

1. IM7 is the final selection for fiber material
2. The limit load design configuration incorporates a 48 ply IM7/8552 (or IM7/PEEK) quasi-isotropic laminate in the cross member beams, Ke49/PEEK laminate in the skids and Al 7075 in the bend radii.
3. Tsai-Wu failure criterion predicts failure mostly along the metal-composite joint.

4. LaRC04 failure criteria predict matrix cracking under compression and in-plane shear and fiber kinking under in-plane shear and longitudinal compression as the predominant fracture modes.
5. Lowest load factors in four of the five laminate families result from laminates with θ/−θ values of 75º/-75º.
6. θ/−θ equaling 45º/-45º produce load factors less than 4.50 while having lesser failures.
7. The optimized load factor is 4.17 for quasi-isotropic laminate.
8. 37% weight saving is obtained even with increased aluminum cross member radii.
9. Simply adhesive bonding of metal-composite may not provide sufficient strength.
10. Hybrid filament wound metal-composite bolted to metal bends is recommended for the metal-composite joint.
11. Crashworthiness needs to be addressed.

CHAPTER 7

COMPOSITE SKID LANDING GEAR PERFORMANCE UNDER CRASH LOADS

7.1 Skid Landing Gear Modifications

Composite skid *inner* diameters and cross members have been sized for a ¼" wall thickness. Inner diameters of the skid tubes and cross members were modified to 101.6 mm (4") and 76.2 mm (3") with maximum taper at the mid-span of the cross member, resulting in 101.6 mm (4") diameter. Figure 82 depicts the modified skid landing gear design meshed with 5314 S4R and 6 S3R shell elements and 164 C3D8R solid elements.

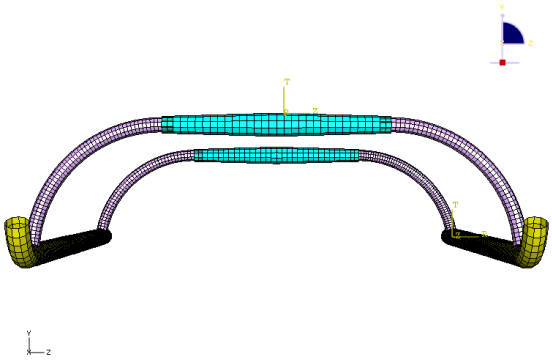

Figure 82. Filament Wound Metal-Composite Joint Skid Landing Gear

7.2 MIL STD 1290 A(AV)

Light Fixed and Rotary-Winged Aircraft Crash Resistance requirements state that the landing gear must be capable of dissipating energy equivalent of 20 ft/sec (6.096 m/s) of aircraft velocity. With the mass of 3636.36 kg of the chosen rotorcraft, this translates to a kinetic energy equivalent of 67.6 kJ. This is necessary for the following crash impact design conditions, with landing gear extended.

Table 16. Crash impact design conditions, with the landing gear extended

Impact direction (aircraft axes)	Object Impact	Δv (ft/sec)
Longitudinal cockpit	Rigid vertical barriers	20
Longitudinal cabin		40
Vertical	Rigid horizontal. surface	42
Lateral, Type I		25
Lateral, Type II		30
Combined high angle Vertical		42
Horizontal		27
Combined low angle Vertical	Plowed Soil	14
Horizontal		100

7.3 Finite Element Analysis Modifications

Dynamic Explicit FEA was conducted using ABAQUS/EXPLICIT V 6.7-1 for four landing scenarios, namely; level crash, rolled crash at -10º, nose-up crash at 15º and nose-down crash at -5º respectively. Figure 83 shows the envelope in roll and pitch within which crashworthiness demonstration is a requirement. Skid tubes and cross members were modeled using S4R shell elements. Master-Slave contact interaction was specified with the ground as the Master surface and the skid landing gear as the contacting Slave surface. General, All with Self, contact interaction was used when no multi-point constraints (MPC) had to be prescribed. The reference aluminum skid landing gear, which was modeled with 5555 S4R and S3R shell elements, analysis included this contact formulation. Total step time was typically 0.075 seconds.

Crash analysis was conducted by prescribing a predefined velocity of 12.8016 m/s (42 ft/sec) with 1 Design Gross Weight (DGW) lift imposed on the fuselage. The landing gear was in near-contact with the ground for this analysis. For the aluminum skid landing

gear, a single continuous mesh was prescribed with a homogeneous shell section property. For the hybrid metal-composite skid landing gear, a single ply laminate with equivalent properties as listed in Table 4 was used for both the cross member tapered beams as well as the skid tubes. The cross member bend radii were modeled with shell elements and the shell-solid connection of was done by node sharing between the appropriate elements amongst 164 solid C3D8R elements and the composite shell elements. The parameters of concern are the energies dissipated and not stresses and strains. Hence, a single equivalent laminate with fracture energies for IM7/8552 in the longitudinal and transverse directions in tension and compression, as shown in Table 17, was modeled. Since filament winding was modeled without fiber angles and with a smeared property assumption, laminate strengths were used for this analysis. For an actual detailed analysis, strengths of a filament wound beam under bending and fiber winding angle variation with stiffness increment with increase in strain should be accounted for. Skid shells were modeled as outer surfaces while the cross member beam composite as well as metal shells were modeled as bottom surfaces. Composite lay-up was modeled as a conventional shell with local cylindrical co-ordinates.

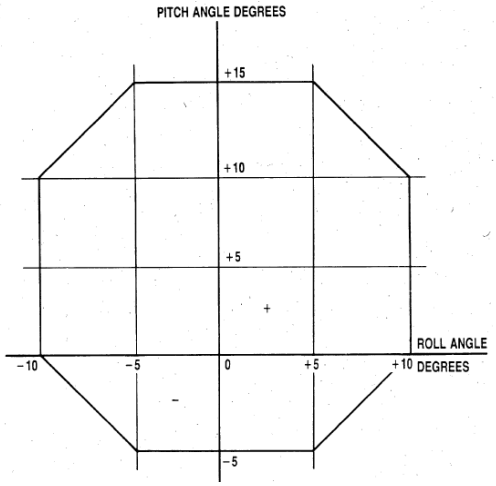

Figure 83. Roll and Pitch Envelope

Table 17. Laminate Allowable

Allowable	IM7/8552
X_T (MPa)	2724
X_C (MPa)	1690
Y_T (MPa)	111
Y_C (MPa)	199.8
S_L (MPa)	130.2
G_{IC} tension (J/m^2)	81500
G_{IC} compression (J/m^2)	101600
G_{IIC} tension (J/m^2)	277.4
G_{IIC} compression (J/m^2)	787.9

7.4 Aluminum Skid Landing Gear Results

Vertical- ¼" wall thickness

The all aluminum configuration was analyzed first with a ¼" wall thickness in accordance with previous research done for limit load design. Plastic dissipation and frictional dissipation were the two energies extracted from ABAQUS at the time step at which one or both of the cross member tapered beams touch the rigid ground. Continuation of analysis beyond this point would not be meaningful as in reality the fuselage would be resting on top of the damaged beams. Figure 84 shows the deformed and damaged skid landing gear in vertical crash. Plastic dissipation is 42.68 kJ and friction energy dissipation is 9.40 kJ. Thus 52.28 kJ, less than the required 67.6 kJ, is dissipated. Hence, wall thickness was increased to 3/8". Figure 85 shows the dissipated energies as a function of time. It is to be noted that the friction dissipation plot shows a discontinuous jump at t = 0.0465 seconds. This is attributed to a software error as discussed ahead.

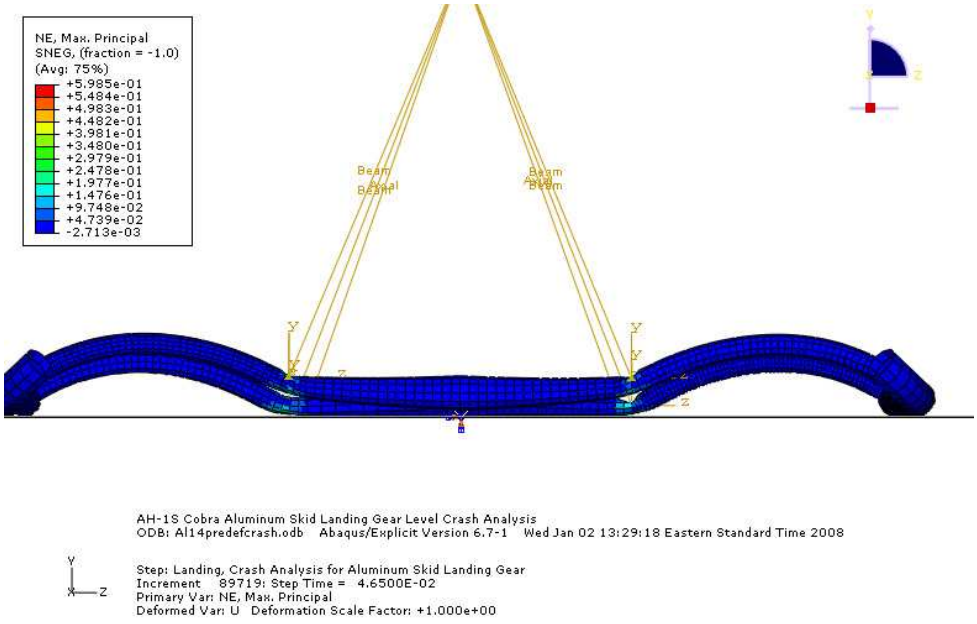

Figure 84. Al 7075 ¼" wall – Vertical Crash

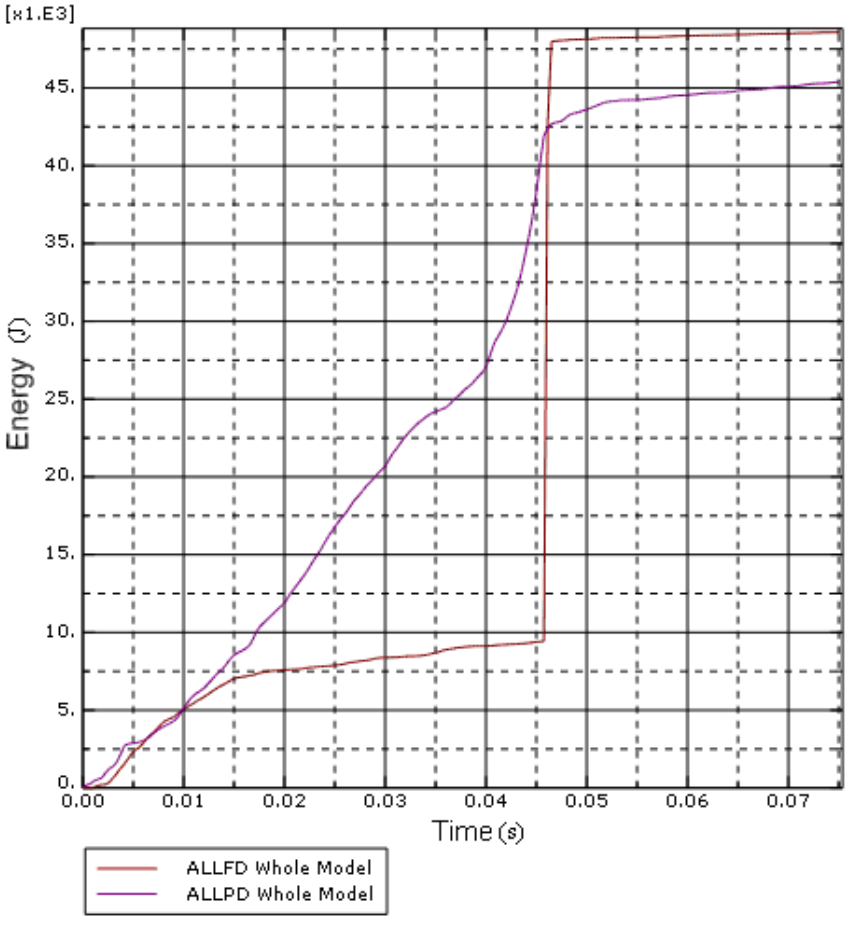

Figure 85. Al 7075 ¼" Energy Dissipation – Vertical Crash

Vertical- 3/8" wall thickness

Plastic energy dissipation is 68.7 kJ while friction energy dissipation is 14.93 kJ. Finally, the total energy dissipated is 83 kJ which meets the requirements. Figure 86 shows energy dissipation plots. Further analysis with three crash scenarios was done with the 3/8" wall thickness configuration only.

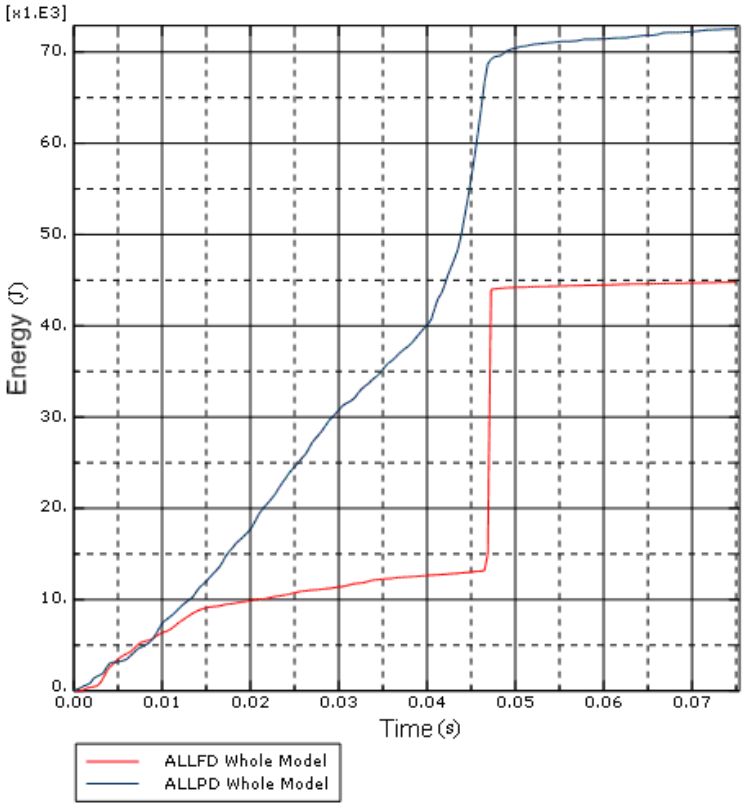

Figure 86. Al 7075 3/8" Energy Dissipation – Vertical Crash

Rolled attitude – 3/8" wall thickness

Rolled attitude crash analysis was conducted from the same drop height with respect to the lowest point on the skid landing gear, closest to the ground. The fuselage attitude was maintained at -10º and the impact velocity was again 42 ft/sec (12.8016 m/s). Figure 87 shows the deformed and damaged skid landing gear. Plastic energy dissipation

obtained was a healthy 91.29 kJ and friction dissipation 10.03 kJ resulting in a net energy dissipation of 101.32 kJ which is well over the required 67.6 kJ. Figure 88 shows the energies plotted versus time.

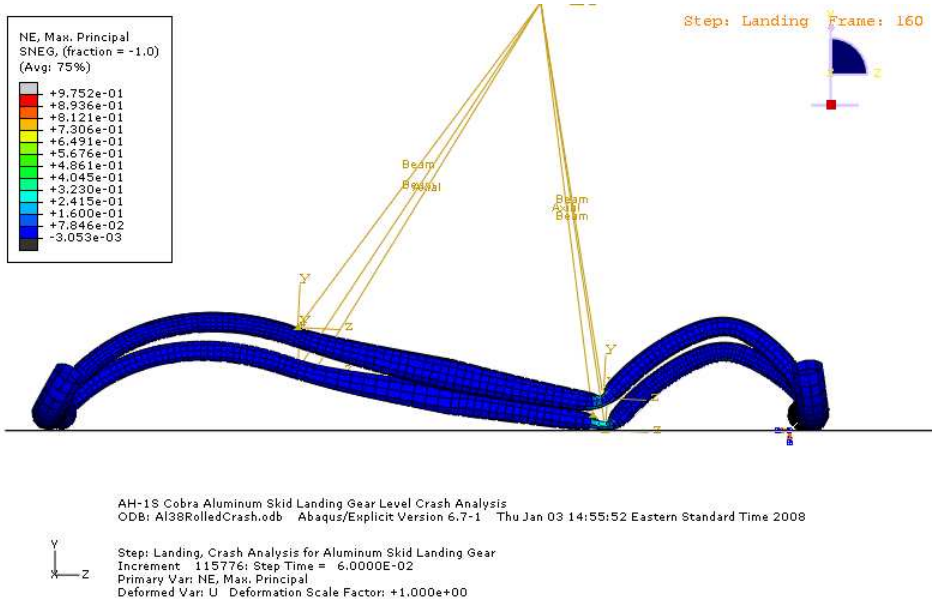

Figure 87. Al 7075 ½" Rolled Attitude Crash

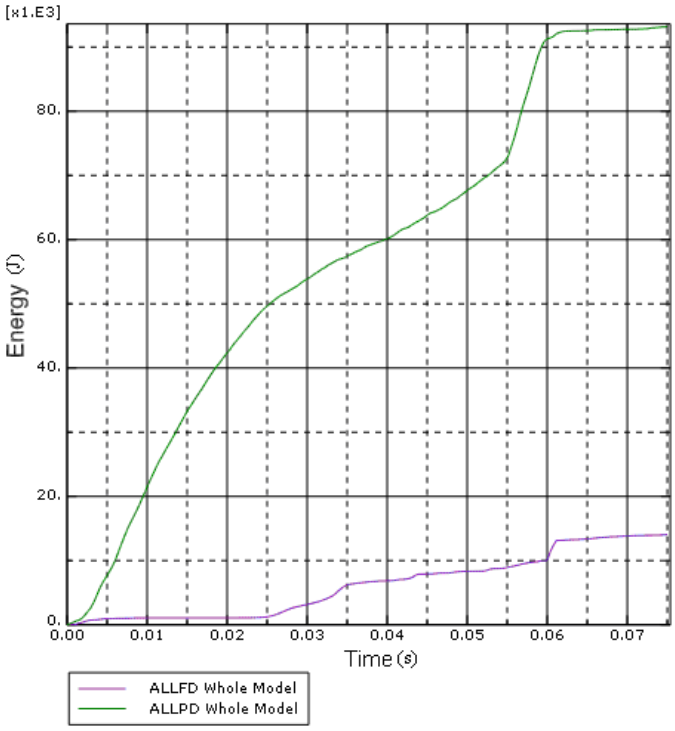

Figure 88. Al 7075 3/8" Energy Dissipation – Rolled Attitude Crash

Nose-Up attitude -3/8" wall thickness

Nose-Up attitude crash analysis was conducted from the same drop height with respect to the lowest point on the skid landing gear, closest to the ground. The fuselage attitude was maintained at + 15º and the impact velocity was again 42 ft/sec (12.8016 m/s). Figure 89 shows the deformed and damaged skid landing gear. Plastic energy dissipation obtained was a healthy 48.61 kJ and friction dissipation 7.86 kJ resulting in a net energy dissipation of 56.47 kJ which is less than the required 67.6 kJ. Figure 90 shows energies versus time.

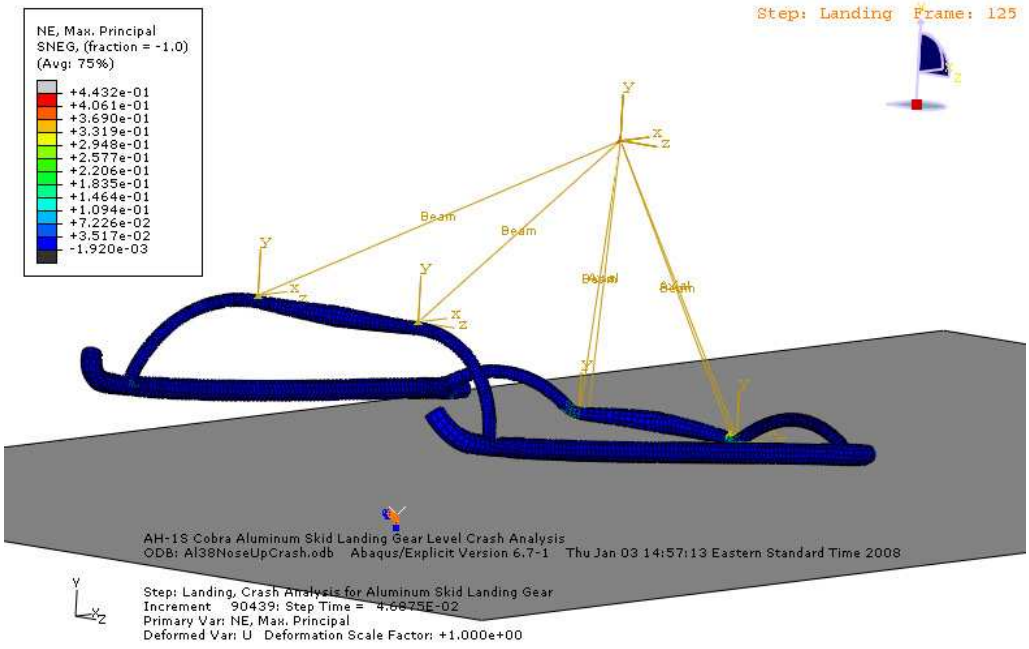

Figure 89. Al 7075 3/8" Nose-Up Attitude Crash

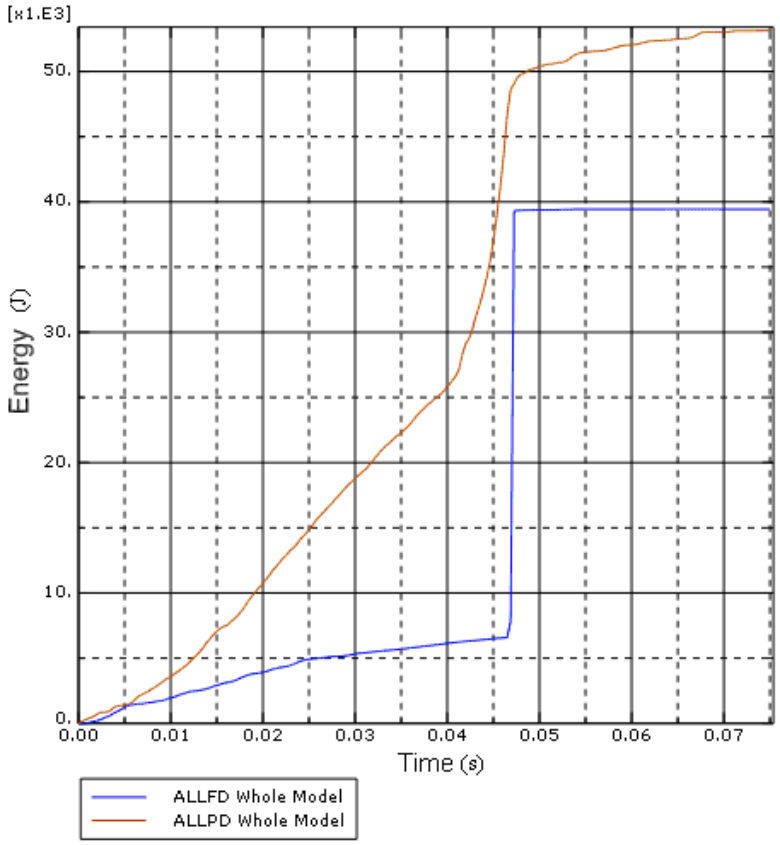

Figure 90. Al 7075 3/8" Energy Dissipation - Nose-Up Attitude

Nose-Down attitude -3/8" wall thickness

Nose-Down attitude crash analysis was conducted from the same drop height with respect to the lowest point on the skid landing gear, closest to the ground. The fuselage attitude was maintained at - 5º and the impact velocity was again 42 ft/sec (12.8016 m/s). Figure 91 shows the deformed and damaged skid landing gear. Plastic energy dissipation obtained was 95.87 kJ and friction dissipation 25.72 kJ resulting in a net energy dissipation of 121.59 kJ which is over the required 67.6 kJ. Figure 92 shows energies plotted versus time. Friction dissipation computed was higher than in other scenarios.

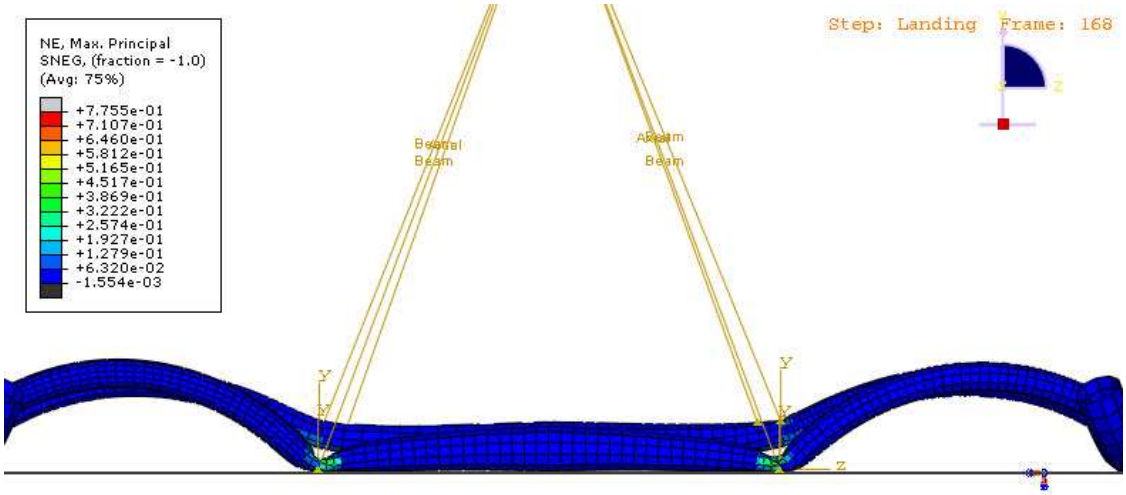

Figure 91. Al 7075 3/8" Nose-Down Attitude Crash

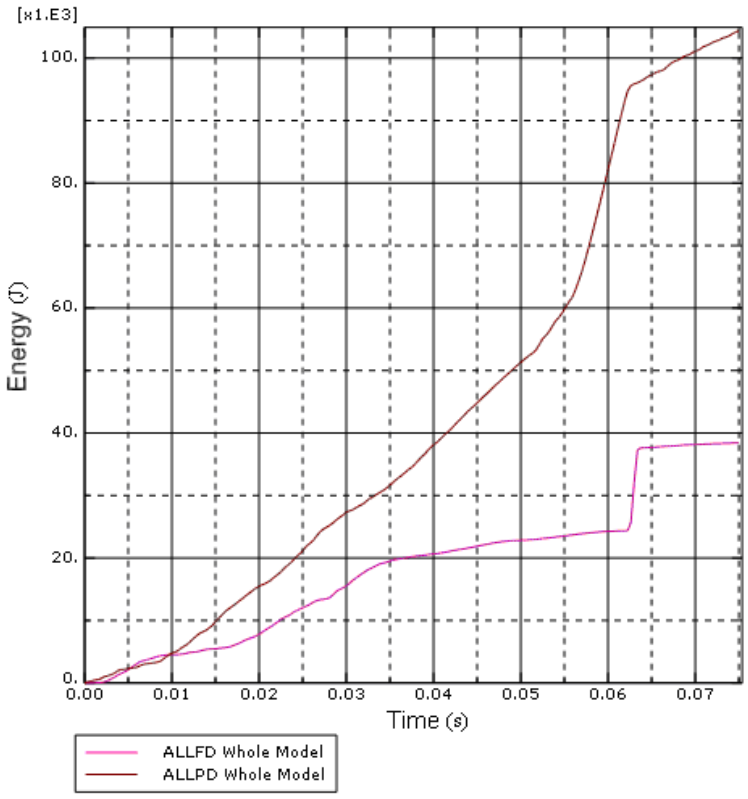

Figure 92. Al 7075 3/8" Energy Dissipation – Nose-Down Attitude

7.5 Metal-Composite Skid Landing Gear Results

Vertical

Plastic energy, friction energy and damage energy were the three energies which contributed to energy dissipation. Progressive damage with Hashin's damage model in ABAQUS with an energy based damage evolution law and damage stabilization was prescribed. Figure 93 shows the damaged skid landing gear in vertical crash. It is to be noted that the metal plug-composite filament wound region bolted to the cross member radii was not simulated. Plastic dissipation computed is 54.45 kJ, friction energy dissipation is 7.06 kJ and damage energy dissipation is 20.45 kJ, resulting in total energy dissipation of 81.96 kJ as is shown in Figure 94. This meets the crash requirements. It is to be noted that the aluminum bend radii have a wall thickness of ¼" and the skids and cross member tapered beam composites are nearly of the same wall thickness with 48 plies (0.000127 mm = 5 mils each). Thus, with a ¼" wall thickness, the reference aluminum skid landing gear seems to have lower energy dissipation than the hybrid metal-composite skid landing gear. In other words, if the wall thickness of the metal cross member bend radii was increased to 3/8" in the hybrid design, the energy dissipation should increase significantly and be comparably higher than the 3/8" wall thickness reference aluminum skid landing gear and importantly, meet the crash requirements. This would have to be experimentally proven as well.

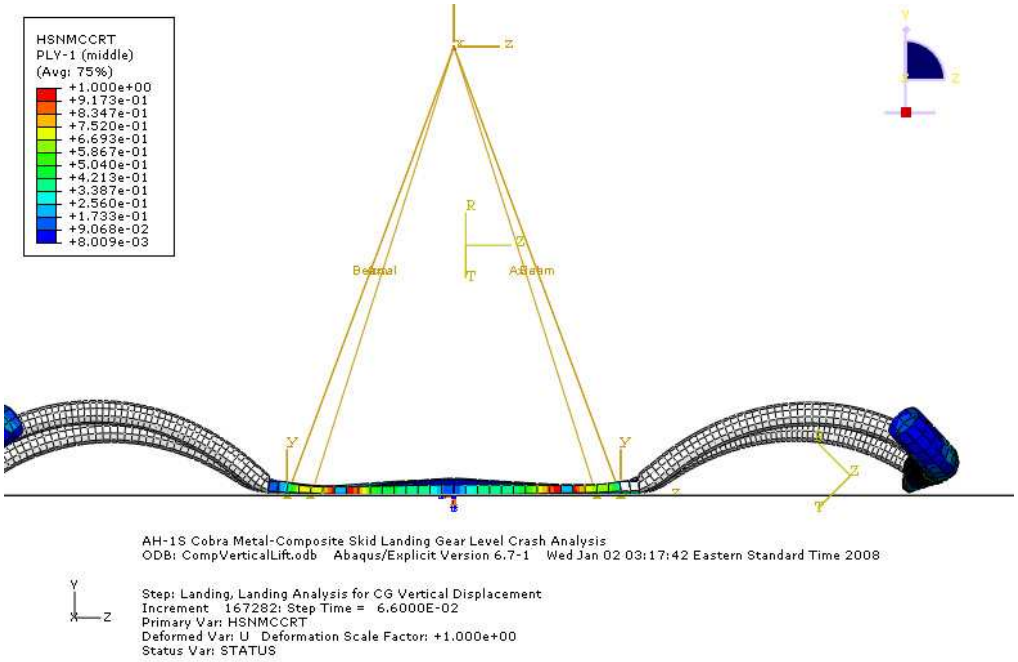

Figure 93. Metal-Composite– Vertical Crash

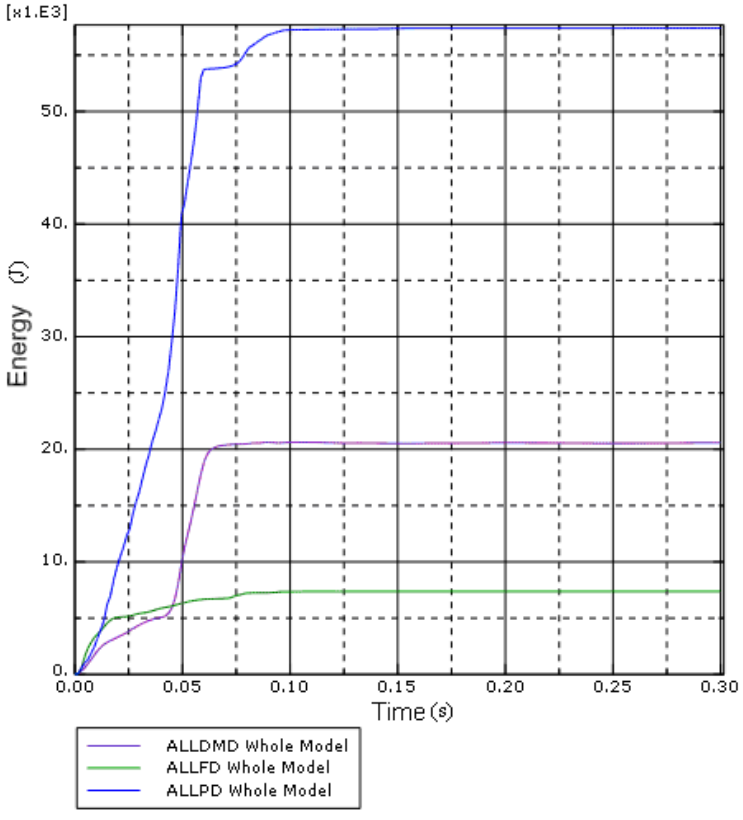

Figure 94. Metal-Composite Energy Dissipation- Vertical Crash

Rolled attitude

Figure 95 shows the deformed and damaged skid landing gear. Plastic energy dissipation obtained was 45.54 kJ, friction dissipation 6.67 kJ and damage dissipation 16.33 kJ, resulting in net energy dissipation of 68.54 kJ which meets the required 67.6 kJ. Figure 96 shows the energies plotted versus time.

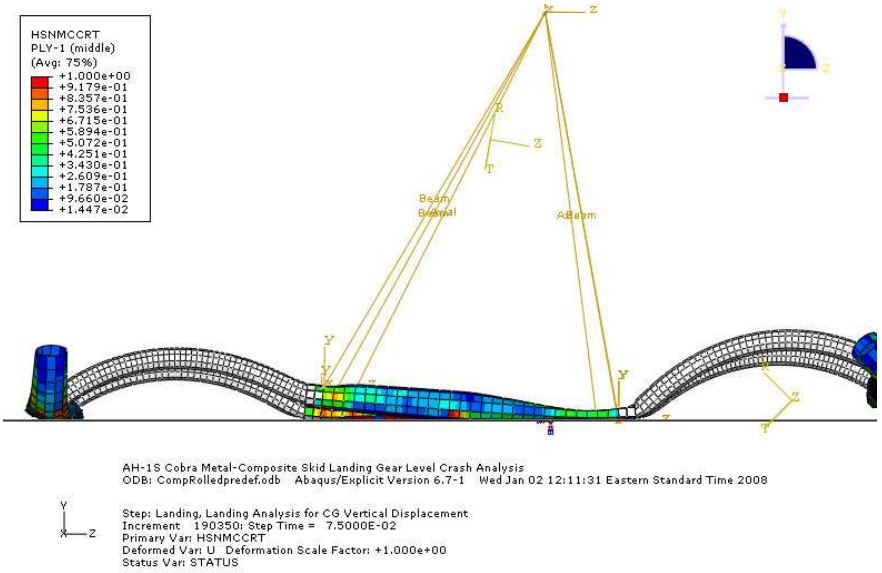

Figure 95. Metal-Composite - Rolled Crash

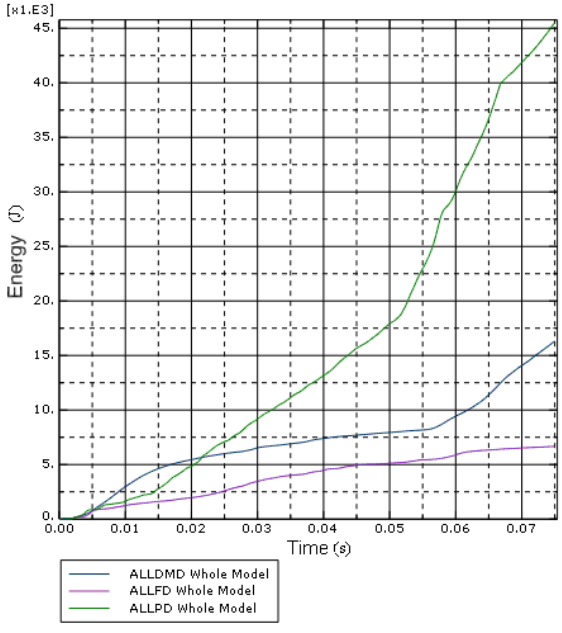

Figure 96. Metal-Composite Energy Dissipation – Rolled Attitude Crash

Nose-Up attitude

Figure 97 shows the deformed and damaged skid landing gear. Plastic energy dissipation obtained was a only 27.03 kJ, friction dissipation was 3.57 kJ and damage dissipation 13.74 kJ, resulting in a net energy dissipation of 44.31 kJ which is less than the required 67.6 kJ. Figure 98 shows the energies plotted versus time. It is perceived that the energy dissipated is less in this scenario, in both the reference and hybrid designs, as the forward cross member does not undergo as much deformation as it does in the other crash scenarios.

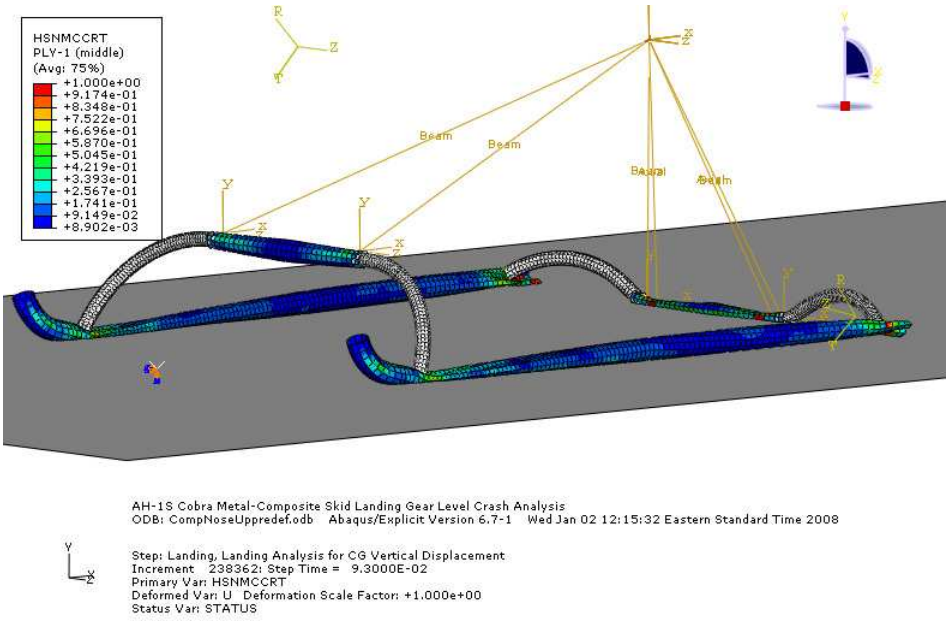

Figure 97. Metal-Composite - Nose-Up Crash

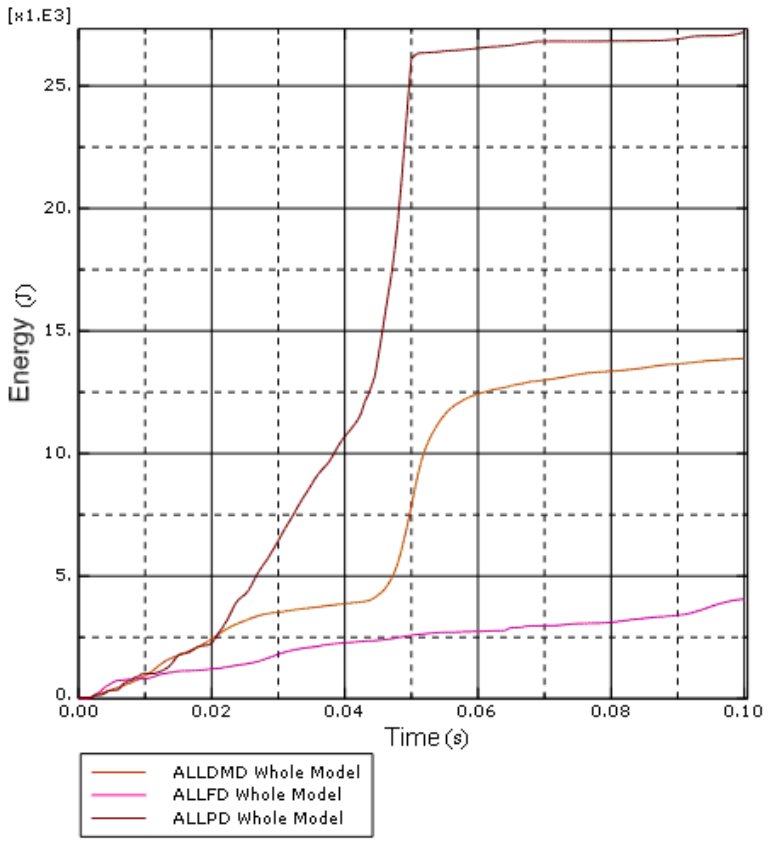

Figure 98. Metal-Composite Energy Dissipation - Nose-Up Attitude

Nose-Down attitude

Figure 99 shows the deformed and damaged skid landing gear Plastic energy dissipation obtained was 54.28 kJ, friction dissipation was 6.77 kJ and damage dissipation 20.30 kJ, resulting in a net energy dissipation of 81.35 kJ which is over the required 67.5 kJ. Figure 100 shows energies versus time.

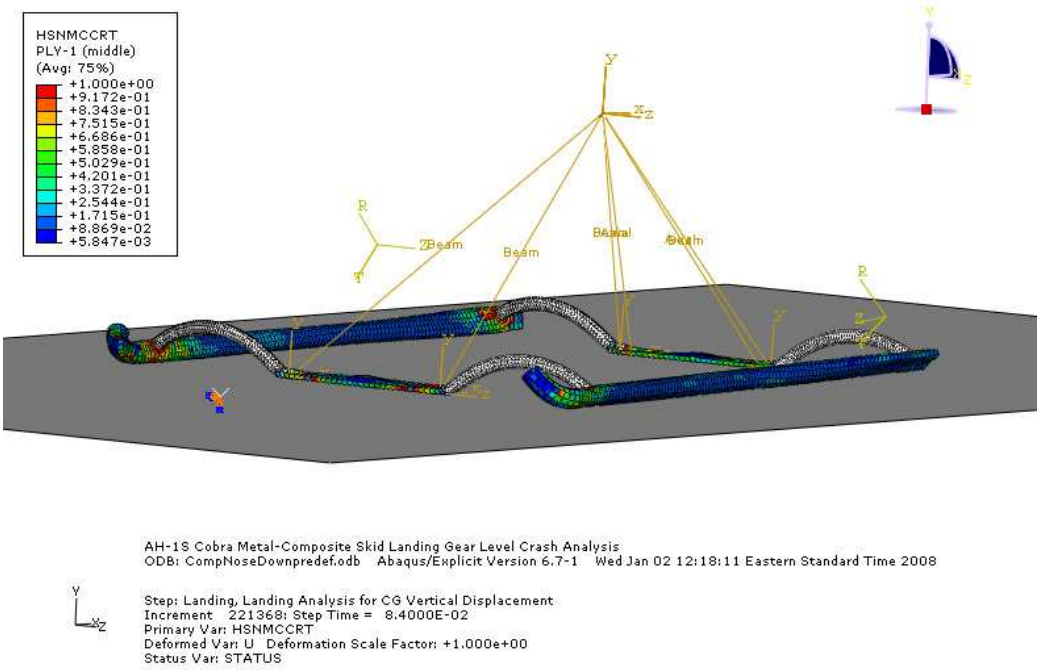

Figure 99. Metal-Composite – Nose-Down Crash

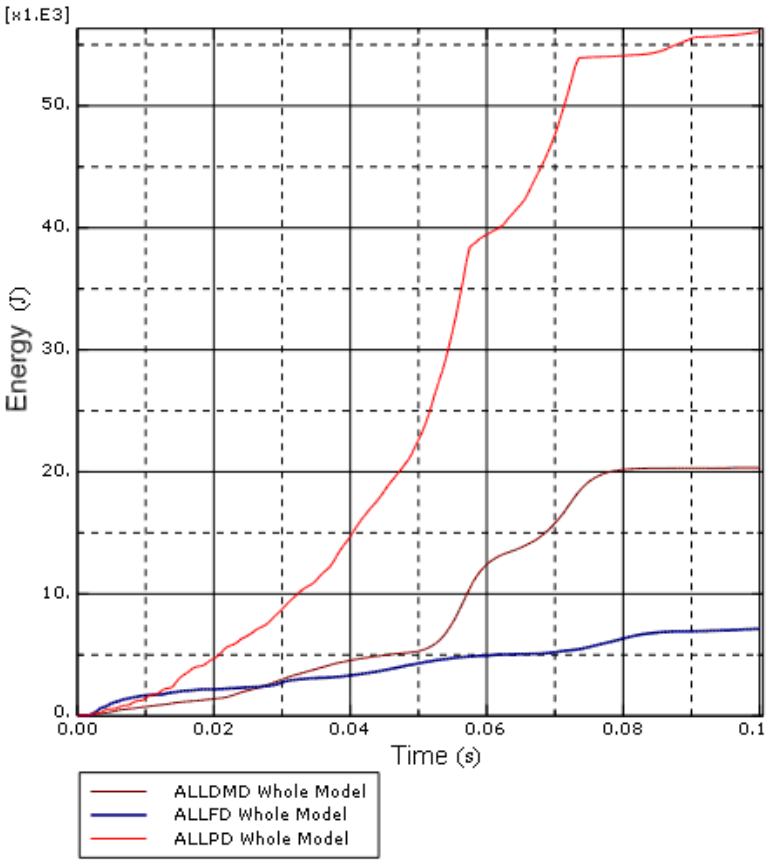

Figure 100. Metal-Composite Energy Dissipation - Nose-Down Attitude

Table 18 shows a comparison of weight saving with the ¼" and 3/8" wall thickness reference landing gears and the hybrid composite design with ¼" aluminum wall thickness and 48 ply composite laminate cross members and skids respectively. Up to 49 % can be saved with the hybrid design.

Table 18. Weight Saving

Design	Mass (kg)	Weight Saving
Al 7075 ¼"	52.74	---
Hybrid w/ filament winding with respect to ¼" Al	37.54	**28.82 %**
Al 7075 3/8"	64.94	--
Hybrid w/ filament winding with respect to 3/8" Al	37.54	**49.28 %**

Friction Energy Discontinuity

As was seen in the energy dissipation plots for the metal skid landing gear, a discontinuity is observed in the friction energy dissipation at the time instant when part or whole of the landing gear has completely flattened out. This is not observed in the energy dissipation plots for any of the composite design crash analyses. All analyses were run with the landing gear in near-contact with the impact surface and crash velocity imposed as a predefined field input. Separate analysis was run by dropping the landing gear at 1g gravity load from 8.383 meters, thus subjected to 42 ft/sec impact velocity. The drop height being 8.353 m the analysis would take weeks to run with lift included. Hence rotor lift was neglected. Figure 101 and Figure 102 show energy dissipation plots. The discontinuity is absent only in the composite analysis. With and without rotor lift, friction energy jumps to an unrealistic value only for metal landing gear analysis. This is being attributed to a software glitch. The fact that the energy increases to beyond the value of plastic energy dissipation further bolsters the fact that it must be unrealistic.

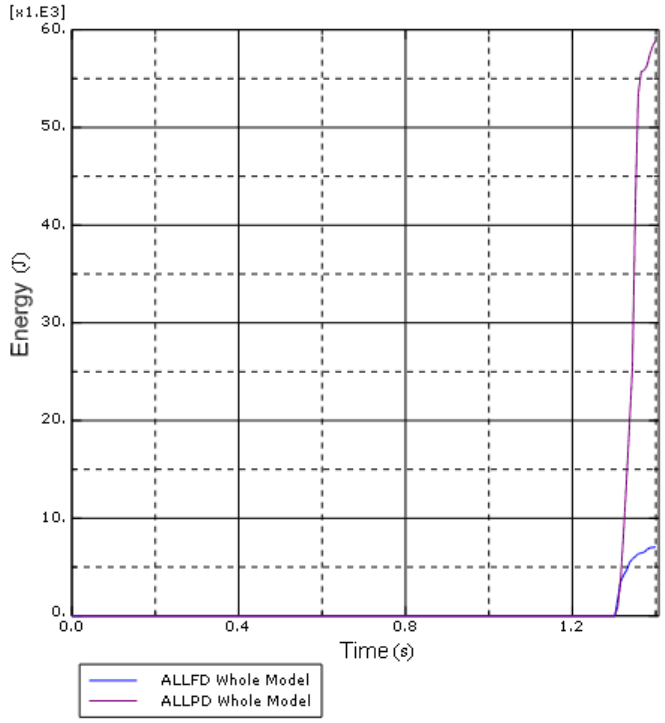

Figure 101. Composite Skid Landing Gear Vertical Crash without 1 DGW Lift

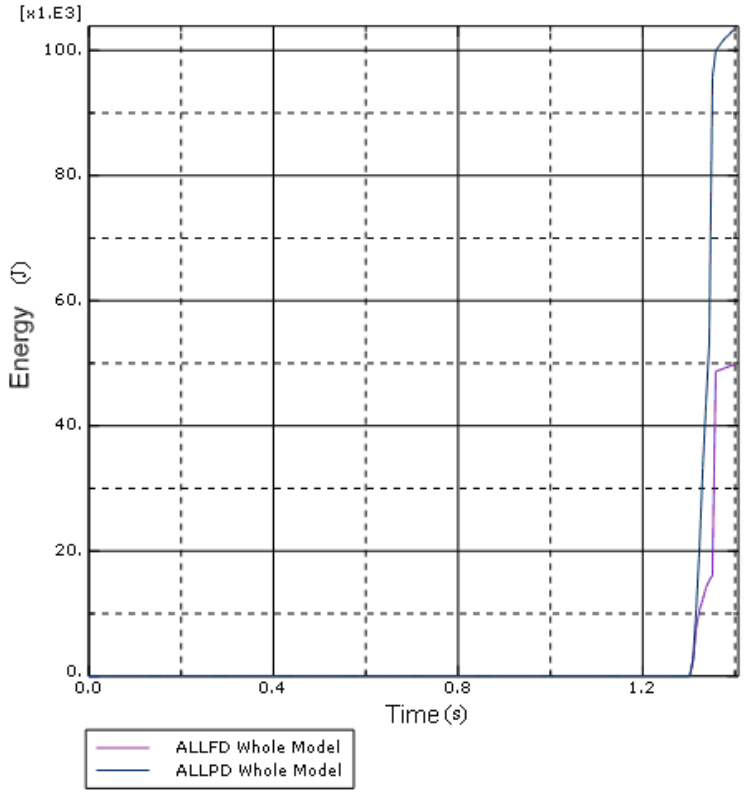

Figure 102. Metal Skid Landing Gear Vertical Crash without 1 DGW Lift

7.6 Summary

The reference aluminum skid landing gear with a ¼" wall thickness had shown acceptable performance under limit loads. Under crash loads, not only does failure strain get produced in the cross member bend radii sooner than it should but the energy dissipation obtained computationally does not meet the 67.6 kJ requirements. Increasing wall thickness to 3/8", results in energy dissipation that alleviates this concern. In contrast, the hybrid metal-composite design dissipated over 80 kJ energy, in most crash scenarios, in the form of plastic, friction and damage dissipation, even with the ¼" wall thickness for the aluminum cross member bend radii. Nose-up attitude was the only scenario during which the landing gear did not yield sufficient energy dissipation for the metal as well as hybrid metal-composite design. Fracture strains are observed as the fuselage is about to touch the ground. Excluding the last few time steps from the plastic energy dissipation should not decrease energy dissipation radically and the requirement shall still be met. The composite should still get crushed under the fuselage weight. Hence, the damage energy has been accounted right till the time step at which the composite beams completely flatten out. It is to be noted that the bolt strengths will play the most significant role in the crash sequence and energy dissipation. Thus, even though fracture strains are observed in the metal cross member bends which are connected to the aluminum plug solid elements, the actual fractures should occur around the bolt regions.

Finally, increasing the wall thickness of the cross member bend radii to 3/8" in the hybrid design should still yields significant weight savings. The energy dissipation will further increase due to increased plastic energy dissipation. Experimental testing of composite beams and prototype landing gear will be necessary to validate these analyses.

7.7 Conclusions

The following conclusions were drawn:

1. Hybrid metal-composite skid landing gear meets crash requirements as per MIL STD 1290 A(AV).
2. The reference landing gear meets crash requirements of 67.6 kJ only if the wall thickness of the cross members is increased to 3/8".
3. More than 80 kJ energy dissipation is obtained in the form of damage, friction and plastic dissipation in the hybrid metal-composite design with ¼" Al 7075 bends.
4. More than 90-100 kJ in energy dissipation in the form of plastic and friction energy is obtained with a 3/8" Al 7075 reference skid landing gear cross member wall thickness.
5. Up to 49 % weight savings can be obtained from the hybrid metal-composite design and is contingent upon the Al 7075 wall thickness used.
6. It is imperative that the bolted metal-composite filament wound joint does not fracture before sufficient energy is dissipated in crash.

CHAPTER 8

FUTURE RECOMMENDATIONS

Limit load design was shown to be feasible with filament wound metal-composite beam bolted to the metal cross member bend radii. Crash analysis revealed that less energy is dissipated due to progressive damage propagation as compared to plastic dissipation in metal. Hence, it would be desirable to have a composite material which displays plasticity, such as carbon fiber aluminum matrix composite (CFAMC)[42] in the composite regions. The drawback of CFAMC materials is that their density can be greater than that of Al 7075 and thus, weight saving may not occur if they are used. Low density CFAMC materials research and investigation is recommended.

Low density foam filled Ke49/PEEK tubes for the skids and IM7/8552 cross member tapered beams are recommended for investigation. Foam has excellent energy absorption properties and can aid in crashworthiness. New materials such as Duocel Al foam[43], which can exhibit as high as 10% elasto-plastic strain, could be very useful in energy reduction mechanism for the entire rotorcraft. Jackson et al[44] have used foam sandwiched between hybrid composite materials for crashworthy fuselage research.

It was observed from limit load analysis that the stress distribution along the cross member beams increased in magnitude toward the metal composite hybrid joint. Thus, a taper law that would implement a thicker section closer to the hybrid joints and thinner section along the mid-span is strongly recommended. This may result in further weight savings as well.

For filament wound composites, Hashin's 3-D damage initiation criteria is recommended. Thus, all the modeling in ABAQUS would have to be with 3-D C3D8R

solid elements. A single solid element thick mesh, with the element containing all 48 plies through the thickness, inputted through the property card will be necessary for this. While this will result in a better modeling of through the thickness transverse shear stress and matrix cracking under impact, it may affect computational run time adversely.

Experimental testing of the designed skid landing gear will be required to ascertain all computationally predicted results. Fracture modes, failure mechanisms in composites, measured energy dissipated and possibility of triggering crush using initiators in composite tapered cross member beams are future opportunities. Full scale prototype testing and component dynamic testing under bending is recommended.

With testing supplementing and guiding the computational analysis, it could be worthwhile to further explore the area of light crashworthy composite skid landing gears.

APPENDIX A

MATLAB SCRIPTS FOR LAMINATE PROPERTIES

The following matlab scripts were written in-house by the author.

RULE OF MIXTURES

```
function h = E1(Em,Nuf,Num,Gf,cf)
clc
clear all
close all
disp ('Calculation of effective moduli');
 Em = input('Please enter the matrix Youngs Modulus: ');
 Num = input('Please enter the matrix Poissons Ratio: ');
while (Num < 0 | Num > 1)
       Num = input('Please enter a value between 0 and 1 only')
end
 Gm = (Em)/(2*(1+Num))
 cf = input('Please enter the fiber volume fraction: ');
while (cf < 0 | cf > 1)
       cf = input('Please enter a value between 0 and 1 only')
end
A = sqrt(cf);
B = 1-A;
Nuf = input('Please enter the fiber Poissons Ratio: ');
while (Nuf < 0 | Nuf > 1)
       Nuf = input('Please enter a value between 0 and 1 only')
end
 Gf = input('Please enter the fiber Shear Modulus: ');
choice = input('Please enter 1 if the material is transversely
isotropic or 2 if isotropic: ');
while (choice ~= 1 & choice ~=2)
    choice = input('Please enter 1 or 2 only.');
end
if (choice == 2)
 Ef = input('Please enter the fiber Youngs Modulus: ');
    E1a = A*Ef + B*Em;
    Nu12a = A*Nuf + B*Num;
    G = (A/Gf)+ (B/Gm);
    G12a = 1/G;
    C = (A/Ef) + (B/Em);
    D = (A*B)/(Ef*Em);
    E = (Nuf*Em - Num*Ef)^2;
    F = A*Ef + B*Em;
    EE2a = (C-(D*E/F));
    E2a = 1/EE2a
    Qa =inv([1/E1a -Nu12a/E1a 0; -Nu12a/E1a 1/E2a 0; 0 0 1/G12a]);
    Qb = inv([1/Em -Num/Em 0; -Num/Em 1/Em 0; 0 0 1/Gm]);
    Q = A*Qa + B*Qb;
    E1 = (Q(1,1)*Q(2,2) - (Q(1,2)^2))/Q(2,2)
    E2 = (Q(1,1)*Q(2,2)-(Q(1,2)^2))/Q(1,1)
    Nu12 = Q(1,2)/Q(2,2)
    G12 = Q(3,3)
```

```
    h = [E1,E2,Nu12,G12]
end
if (choice == 1)
    Elong = input('Please enter the fiber longitudinal Youngs Modulus:
');
    Etran = input('Please enter the fiber transverse Youngs Modulus:
');
    E1a = A*Elong + B*Em
    Nu12a = A*Nuf + B*Num
    G = (A/Gf)+ (B/Gm);
    G12a = 1/G
    C = (A/Etran) + (B/Em);
    D = (A*B)/(Elong*Em);
    E = (Nuf*Em - Num*Elong)^2;
    F = A*Elong + B*Em;
    EE2a = (C-(D*E/F));
    E2a = 1/EE2a
    Qa =inv([1/E1a -Nu12a/E1a 0; -Nu12a/E1a 1/E2a 0; 0 0 1/G12a])
    Qb = inv([1/Em -Num/Em 0; -Num/Em 1/Em 0; 0 0 1/Gm])
    Q = A*Qa + B*Qb
    E1 = (Q(1,1)*Q(2,2)-(Q(1,2)^2))/Q(2,2)
    E2 = (Q(1,1)*Q(2,2)-(Q(1,2)^2))/Q(1,1)
    Nu12 = Q(1,2)/Q(2,2)
    G12 = Q(3,3)
    h = [E1,E2,Nu12,G12]
end
```

EQUIVALENT LAMINATE PROPERTIES

```
clc
clear all
close all
disp('            Analysis of Composite Laminates using Equivalent
Laminate Theory            ');
SQmatrices
ABdelta
amatrix = inv(Amatrix);
    E11 = (Amatrix(1,1)*Amatrix(2,2)-
(Amatrix(1,2)^2))/(t*m*Amatrix(2,2))
    E22 = (Amatrix(1,1)*Amatrix(2,2)-
(Amatrix(1,2)^2))/(t*m*Amatrix(1,1))
    Nu12 = (Amatrix(1,2))/(Amatrix(2,2))
    G12 = (Amatrix(3,3))/(m*t)
end
```

SUBROUTINE SQMATRICES

```
E1 = input('Please enter the Youngs Modulus in the longitudinal
direction: ');
E2 = input('Please enter the Youngs Modulus in the transverse
direction: ');
Nu12 = input('Please enter the Poissons Ratio nu12: ');
G12 = input('Please enter the Shear Modulus: ');
```

```
Smatrix = [1/E1 -Nu12/E1 0; -Nu12/E1 1/E2 0; 0 0 1/G12];
Qmatrix = inv(Smatrix);
```

SUBROUTINE ABDELTA

```
A = zeros(3); B = zeros(3); D = zeros(3);
N(:,3) = [0]; M(:,3) = [0];
m = input('Please enter the number of plies in your stacking sequence:
');
    while (m < 0)
    m = input('Please enter a valid positive number only');
    end
    t = input('Please enter the thickness of each ply: ');
    while (t < 0)
    t = input('Please enter a valid positive thickness only');
    end
    zk = (-m*t/2) + t;
    zkminone = zk - t;
for k = 1:m
    ang = input('please enter the orientation of this ply: ');
    while (ang < -360 | ang > 360 )
        ang = input('please enter only between -360 to 360 degrees: ');
    end
    ang = (ang*pi/180);
    Tepsilon = [cos(ang).^2 sin(ang).^2 sin(ang)*cos(ang); sin(ang).^2
cos(ang).^2 -sin(ang)*cos(ang); -sin(2*ang) sin(2*ang) cos(2*ang)];
    Qbar = (Tepsilon)'*(Qmatrix)*(Tepsilon);
    QforA = Qbar*(zk - zkminone);
    QforB = Qbar*((zk)^2 -((zkminone)^2));
    QforD = Qbar*((zk)^3 -((zkminone)^3));
    A = A + QforA;
    B = B + QforB;
    D = D + QforD;
    zkminone = zk;
    zk = zk + t;
end
Amatrix = A;
Bmatrix = (1/2)*B;
Dmatrix = (1/3)*D;
a = inv(Amatrix);
alpha = a + (a*Bmatrix*inv(Dmatrix - Bmatrix*a*Bmatrix)*Bmatrix*a);
beta = -a*Bmatrix*inv(Dmatrix - Bmatrix*a*Bmatrix);
betatrans = (beta)';
delta = inv(Dmatrix - Bmatrix*a*Bmatrix);
d = inv(delta);
```

APPENDIX B
MATLAB SCRIPT FOR LaRC04 FAILURE CRITERIA

```
%%%%%%%%%%      LaRC04 Strength Based Failure Criteria %%%%%%%%
clc
clear all
close all
disp('          LaRC04 Strength Based Failure Criteria         ');
% Lamina Properties
E1 = 174.2e3; E2 = 9.08e3; G12 = 5.29e3; nu12 = 0.32; t = 0.127;
% E1 = input('Please enter the longitudinal Youngs Modulus (MPa): ');
% E2 = input('Please enter the transverse Youngs Modulus (MPa): ');
% G12 = input('Please enter the shear Modulus (MPa): ');
% nu12 = input('Please enter the poisson ratio: ');
nu21 = nu12*E2/E1;
delta22 = 2*(inv(E2) - (nu21^2/(E1)));
% t = input('Please enter the ply thickness in mm: ');

% Allowable Values
XT = 2724; XC = 1690; YTud = 111;  YC = 199.8; SLud = 120;  GIc =
0.2774; GIIc = 0.7879;
% XT = input('Please enter the longitudinal tensile strength (MPa): ');
% XC = input('Please enter the longitudinal compressive strength (MPa):
');
% YTud = input('Please enter the transverse tensile strength (MPa): ');
% YC = input('Please enter the transverse compressive strength (MPa):
');
% SLud = input('Please enter the in-plane shear strength (MPa): ');
% GIc = input('Please enter the mode I fracture toughness (kJ/m^2): ');
% GIIc = input('Please enter the mode II fracture toughness (kJ/m^2):
');
beta = 2.98e-8;     alph0 = 53*(pi/180);     etaT = -inv(tan(2*alph0));
g = (GIc/GIIc);

% Camanho Strength Corrections
disp('1. Thin Outer Ply Correction');
disp('2. Thin Embedded Ply Correction');
disp('3. Thick Ply Correction');
choice = input('Please select from the options above: ');
    if choice == 1
        YT = 1.79*sqrt(GIc/(t*pi*delta22));
        phi = 24*GIIc/(t*pi);
    elseif choice == 2
        YT = sqrt(8*GIc/(t*pi*delta22));
        phi = 48*GIIc/(t*pi);
    elseif choice == 3
        YT = 1.12*sqrt(2)*YTud;
        phi = 12*(SLud^2/G12) + 18*beta*(SLud^4);
    else
        choice = input('please enter 1,2 or 3 only');
    end
SL = sqrt((sqrt(1 + beta*phi*G12^2) - 1)/(3*beta*G12));
ST = YC*cos(alph0)*(sin(alph0) + (cos(alph0)/tan(2*alph0)));

% Fiber misalignment angle corrections
```

```
etaL = -(SL*cos(2*alph0))/(YC*cos(alph0)^2);
omega = (SL/XC) + etaL;
psic = atan((1 - sqrt(1 - 4*omega*(SL/XC)))/(2*omega));

% Stress state
plies = input('Please enter the number of plies do you wish to analyze:
');
    while plies < 1
        plies = input('Please enter a positive integer value only.');
    end
count = 0;
for loop = 1:plies
    sigma11 = input('Please enter the normal stress along the
longitudinal fiber direction in this ply(MPa): ');
    sigma22 = input('Please enter the normal stress along the
transverse matrix direction in this ply(MPa): ');
    sigma12 = input('Please enter the in-plane shear stress in this ply
(MPa): ');
    gam12 = inv(G12)*sigma12 + beta*sigma12^3;
    psi = (abs(sigma12) + (G12 - XC)*psic)/(G12 + sigma11 - sigma22);
    sigman = sigma22*cos(alph0)^2;
    tauT = -sigma22*sin(alph0)*cos(alph0);
    tauL = sigma12*cos(alph0);
    theta = atan(-abs(sigma12)/(sigma22*sin(alph0)));
    sigm11 = sigma11*cos(psi)^2 + sigma22*sin(psi)^2 +
2*abs(sigma12)*cos(psi)*sin(psi);
    sigm22 = sigma22*cos(psi)^2 + sigma11*sin(psi)^2 -
2*abs(sigma12)*cos(psi)*sin(psi);
    sigm12 = -sigma11*sin(psi)*cos(psi) + sigma22*sin(psi)*cos(psi) +
abs(sigma12)*cos(2*psi);
    sigmn = sigm22*cos(alph0)^2;
    taumT = -sigm22*sin(alph0)*cos(alph0);
    taumL = sigm12*cos(alph0);
    taueT = 0.5*(abs(tauT) + etaT*sigman*cos(theta) + abs(abs(tauT) +
etaT*sigman*cos(theta)));
    taueL = 0.5*(abs(tauL) + etaL*sigman*cos(theta) + abs(abs(tauL) +
etaL*sigman*cos(theta)));
    tauemT = 0.5*(abs(taumT) + etaT*sigmn*cos(theta) + abs(abs(taumT) +
etaT*sigmn*cos(theta)));
    tauemL = 0.5*(abs(taumL) + etaL*sigmn*cos(theta) + abs(abs(taumL) +
etaL*sigmn*cos(theta)));
%%% Failure Criteria  %%%
    % Transverse (Matrix) fracture -  Matrix cracking under transverse
compression and in-plane shear
    if sigma22 < 0
        if sigma11 < -YC
            R3 = (tauemT/ST)^2 + (tauemL/SL)^2 - 1;
            if R3 > 0
                disp('Matrix cracking under in-plane shear has occurred
in this ply.');
                count = count + 1;
            end
        else
            R3 = (taueT/ST)^2 + (taueL/SL)^2 - 1;
            if R3 > 0
                disp('Matrix cracking under transverse compression has
occurred in this ply.');
```

```
                count = count + 1;
            end
        end
    else
    % Transverse (Matrix) fracture -  Matrix cracking under transverse
tension and in-plane shear
        if sigma11 < 0 && abs(sigma11) < XC/2
            R1 = (1 - g)*sigma22/YT + g*(sigma22/YT)^2 + (sigma12/SL)^2
- 1;
            R2 = (1 - g)*sigma22/YT + g*(sigma22/YT)^2 + (sigma12/SL)^2
- 1;
            if R1 > 0
                if R2 > 0
                    disp('MATRIX fracture due to transverse tension and
in-plane shear has occurred in this ply.')
                    count = count + 1;
                end
            end
        end
    end
    % Fiber Fracture under Longitudinal Compression and in-plane shear
Fiber kinking
    if sigma11 < 0
        if sigm22 < 0
            R4 = 0.5*(((abs(sigm12) + etaL*sigm22)/SL) + (((abs(sigm12)
+ etaL*sigm22)/SL))) - 1;
            if R4 > 0
                disp('Fiber Kinking failure has occurred in this ply
under longitudinal compression.');
                count = count + 1;
            end
        else
            if abs(sigma11) > XC/2 || abs(sigma11) == XC/2
                R5 = (1 - g)*sigm22/YT + g*(sigm22/YT)^2 +
(sigm12/SL)^2 - 1;
                if R5 > 0
                    disp('Fiber Kinking failure has occurred in this
ply under in-plane shear.');
                    count = count + 1;
                end
            end
        end
    else
    % Longitudnal Fiber Fracture
        R1 = (sigma11/XT) -1;
            if R1 > 0
                disp('Longitudinal fiber TENSILE failure has occurred
in this ply.')
                count = count + 1;
            end
    end
    if count == 0
        disp('LaRC04 Failure Criteria does not predict any fracture
phenomena in the ply.');
    end
END
```

REFERENCES

[1] Code of Federal Regulations (CFR) 14 Part 27

[2] Mamalis A, Manolakos D, Demosthenous G and Ioannidis M, "Crashworthiness of Composite Thin-Walled Structural Components".

[3] Light Fixed and Rotary-Winged Aircraft Crash Resistance, Department of Defense, September 1998

[4] Fasanella E, Jackson K, Sparks C and Sareen A, "Water Impact Test and Simulation of a Composite Energy Absorbing Fuselage Section", American Helicopter Society (AHS) 59th Annual Forum, Phoenix, AZ, May 6-8, 2003

[5] Macy W, Shea M and Morris D, "Titanium Matrix Composite Landing Gear Development", Aerospace Technology Conference and Exposition, Anaheim, CA, 1989

[6] Airoldi A and Janszen G, "Landing Performance of a Helicopter Skid Landing Gear with the Use of a Multi-Body Program", Proceedings of the 3rd KRASH Users' Seminar, Tempe, AZ, 2001

[7] Caprile C, Airoldi A, Biaggi A and Mandelli P, "Multi-Body Simulation of a Helicopter Landing with Skid Landing Gear in Various Attitudes and Soil Conditions", Proceedings of the 25th European Rotorcraft Forum, 1999, Rome, Italy

[8] Airoldi A and Lanzi L, "Design and Optimization of Helicopter Skid Landing Gears with Multi-Body Analyses", Dipartimento di Ingegneria Aerospaziale, Politecnico di Milano

[9] Airoldi A and Lanzi L, "Multi-Objective Genetic Optimization for Helicopter Skid Landing Gears", American Institute of Aeronautics and Astronautics

[10] Airoldi A and Lanzi L, "Design of Skid Landing Gears by Means of Multibody Optimization", Journal of Aircraft, Vol. 43, No.2, March-April 2006

[11] Bruhn F, "Analysis and Design of Flight Vehicles and Structures", S.R. Jacobs and Associates, Indianapolis (USA), 1973

[12] Tsai S and Wu E, "A general theory of strength for Anisotropic Materials", Journal of Composite Materials, Vol. 5, pp 58-80

[13] Hill R, "Elastic Properties of Reinforced Solids: Some Theoretical Principles", Journal of Mech. Phys. Solids, Vol. 11, pp 357-372

[14] Rotem A and Hashin Z, "Failure Modes of Angle Ply Laminates", Journal of Composite Materials, Vol. 9, pp 191-206

[15] Hashin Z, "Failure Criteria for Unidirectional Fiber Composites", ASME Journal of Applied Mechanics, Vol. 54, pp 872-879

[16] Hoffman O, "The Brittle Strength of Orthotropic Materials", Journal of Composite Materials, Vol. 1 pp 200-206

[17] Puck A, "Calculating the Strength of Glass-Fiber/Plastic Laminates under combined loads", Kunststoffe, Vol. 55, pp 18-19

[18] Christensen R, "Tensor Transformations and Failure Criteria for the Analysis of Fiber Composite Materials", Journal of Composite Materials, Vol. 22, pp 874-897

[19] Kim C and Yeh H, "Development of a New Yielding Criterion: The Yeh-Stratton Criterion", Engineering Fracture Mechanics, Vol. 47, pp 569-582

[20] Chang F and Lessard L, "Damage Tolerance of Laminated Composites Containing an Open Hole and Subjected to Compressive Loadings, Part I-Analysis", Journal of Composite Materials, Vol. 25, pp 2-43

[21] Azzi V and Tsai S, "Anisotropic Strength of Composites", Experimental Mechanics, Vol. 5, pp 283-288

[22] Davila C and Camanho P, "Failure Criteria for FRP Laminates in Plane Stress", NASA/TM-2003-212663

[23] Tho C, Sparks C, Sareen S, Smith M and Johnson C, "Efficient Helicopter Skid Landing Gear Dynamic Drop Simulation Using LS-DYNA", American Helicopter Society (AHS) 59th Annual Forum, Phoenix, AZ, May 6-8, 2003

[24] Camanho P and Lambert B, “A design methodology for mechanically fastened joints in laminated composite materials”, Composites Science and Technology, Vol. 66, Issue 15, December 2006, pp. 3004-3020

[25] Fleming D and Vizzini A, ““The Effect of Side Loads on the Energy Absorption of Composite Structures”, Journal of Composite Materials, Vol. 26 No.4/19 pp 486-499

[26] Talbot P, Tinling B, Decker W and Chen R, “A Mathematical Model of a Single Main Rotor Helicopter for Piloted Simulation”, NASA Technical Memorandum 84281, Sep. 1982

[27] Monterrubio L and Sharf I, “Influence of Landing-Gear Design on Helicopter Ground Resonance”, AIAA Modeling and Simulation Technologies Conference and Exhibit, Portland, OR, Aug. 9-11, 1999

[28] HexTow™ IM7 and AS4(6000) Carbon Fiber Product Data Sheets

[29] TORAYCA® T700S Data Sheet

[30] KEVLAR® ARAMID FIBER Technical Guide

[31] Sun C T, “Mechanics of Composites Materials and Laminates”, Chapter 1, pp 5

[32] Goldberg R and Stouffer D, “High Strain Rate Deformation Modeling of a Polymer Matrix Composite”, NASA/TM – 1998-208664

[33] Kulkarni R, “Characterization of Carbon Fibers: Coefficient of Thermal Expansion and Microstructure”, Department of Mechanical Engineering, Texas A & M University, Dec. 2004

[34] Dowling N, “Mechanical Behavior of Materials”, Chapter 4, pp 162-163

[35] Sareen A, Smith M and Howard J, “Helicopter Skid Gear Dynamic Drop Analysis and Test Correlation”, American Helicopter Society (AHS) 54th Annual Forum, Washington DC, 1998

[36] Focht J, Woldsenbet E and Vinson J, "High Strain Rate Properties of IM7/977-3 Graphite/Epoxy Composites", 39th AIAA/ASME/ASCE/ASC Structures, Structural Dynamics and Materials Conference, April 20-23 1998, Long Beach, CA

[37] HexPly® 8552 Epoxy Matrix Product Data

[38] Gray D and Moser D, "Finite Element Analysis of a Composite Overwrapped Pressure Vessel", 40th AIAA/ASME/SAE/ ASEE Joint Propulsion Conference and Exhibit 11-14 July 2004, Fort Lauderdale, FL

[39] Charalambides M, Kinloch A and Matthews F, "Adhesively-bonded Repairs to Fiber-Composite Materials II: Finite Element Modeling", Composites Part A 29A (1998), pp. 1383-1396

[40] Camanho P and Matthews F, "Bonded Metallic Inserts for Bolted Joints in Composite Laminates", Proceedings of the I MECH E Part L Journal of Materials: Design and Applications, Vol. 214, No. 1, 21 February 2000, pp. 33-40(8)

[41] 3M Aluminum Matrix Composites Typical Properties Data Sheet

[42] ERG Materials and Aerospace Corporation, www.ergaerospace.com

[43] Jackson K, Fasanella E, Sparks C and Sareen A, "Water Impact Test and Simulation of a Composite Energy Absorbing Fuselage Section", Presented at the American Helicopter Society (AHS) 59th Annual Forum, Phoenix, AZ, May 6-8 2003

[44] Fox R, "Helicopter Crashworthiness – Part Two", Helicopter Safety, Vol. 16 No. 1 Jan/Feb 1990

[45] Cronkhite J, "Crash Impact Characteristics of Helicopter Composite Structures", Aircraft Crashworthiness, SAE International PT-50, pp 239-254

[46] Camanho P, Davila C, Pinho S, Iannucci L and Robinson P, "Prediction of In-Situ Strengths and Matrix Cracking in Composites under Transverse Tension and In-Plane Shear", Composites Part A: Applied Science and Manufacturing, 37 (2006), 165-176

[47] Wu E and Reuter Jr. R, "Crack Extension in Fiberglass reinforced plastics", Department of Theoretical and Applied Mechanics, University of Illinois, T&AM Report 1965;275

[48] Hahn H, "A mixed-mode fracture criterion for composite materials", Composite Technology Rev 1983; 5:29-9

[49] Kim C, Kang J, Hong and Kim CG, "Optimal Design of Filament Wound Structures under Internal Pressure based on the semi-geodesic path algorithm", Composite Structures, 67 (2005), 443-452

VITA

KSHITIJ SHROTRI

Kshitij Shrotri was born in Pune, Maharashtra, India. He attended public schools in Pune and received a B.E. in Mechanical Engineering from Maharashtra Institute of Technology, University of Pune in 2000 and an M.S. Engr. in Aeronautics and Astronautics Engineering from Purdue University, West Lafayette, IN, in 2003. He came to Georgia Institute of Technology, School of Aerospace Engineering to pursue a doctorate in Aerospace Engineering with Structures as his Major. When he is not working on his research, Mr. Shrotri enjoys training in martial arts and hiking.